# NUCLEAR INSTRUMENTS & METHODS

A JOURNAL ON ACCELERATORS, INSTRUMENTATION AND TECHNIQUES IN NUCLEAR PHYSICS

EDITOR: K. SIEGBAHN - UPPSALA

VOLUME 10

JANUARY 1961 — APRIL 1961

AUTHOR INDEX FOR VOLUMES 1–10

SUBJECT INDEX FOR VOLUMES 1–10

NORTH-HOLLAND PUBLISHING COMPANY — AMSTERDAM

PRINTED IN THE NETHERLANDS
DRUKKERIJ MEIJER N.V. WORMERVEER AND AMSTERDAM

64-06910

# NUCLEAR INSTRUMENTS AND METHODS

Per.
QC
786
N883
v. 10-11

EDITORIAL BOARD:

J. B. ADAMS (CERN)
F. A. ALSINA (Buenos Aires)
E. AMALDI (Rome)
H. L. ANDERSON (Chicago)
K. T. BAINBRIDGE (Cambridge, Mass.)
P. R. BELL (Oak Ridge)
R. E. BELL (Montreal)
A. BERTHELOT (Saclay)
H. BRINKMAN (Groningen)
E. H. COOKE–YARBOROUGH (Harwell)
S. DE BENEDETTI (Pittsburgh)
M. DE HEMPTINNE (Louvain)
A. DE-SHALIT (Rehovoth)
M. DEUTSCH (Cambridge, Mass.)
S. DU TOIT (Pretoria)
B. S. DŽELEPOV (Leningrad)
W. GENTNER (Heidelberg)
P. C. GUGELOT (Amsterdam)
H. HALBAN (Paris)
O. HAXEL (Heidelberg)
P. HUBER (Basel)
S. KIKUCHI (Tokyo)
J. KOCH (Copenhagen)
M. S. KOZODAEV (Moscow)
S. LIVINGSTON (Cambridge, Mass.)
E. M. MCMILLAN (Berkeley)
M. G. MEŠČERJAKOV (Moscow)
P. B. MOON (Birmingham)
M. L. OLIPHANT (Canberra)
W. PAUL (Bonn)
A. S. RAO (Bombay)
G. SALVINI (Rome)
P. SAVIĆ (Belgrade)
P. SCHERRER (Zürich)
CH. SCHMELZER (CERN)
R. TANGEN (Oslo)
D. TAYLOR (Northampton)
V. I. VEKSLER (Moscow)
G. VON DARDEL (CERN)
O. WERNHOLM (Stockholm)
R. R. WILSON (Cornell)
S. D. WINTER (Saclay)

JANUARY 1961 VOLUME 10 (1961) No. 1

GREGG M. SINCLAIR LIBRARY
UNIVERSITY OF HAWAII
8-7-63

# NUCLEAR INSTRUMENTS & METHODS

A JOURNAL ON ACCELERATORS, INSTRUMENTATION AND TECHNIQUES IN NUCLEAR PHYSICS

EDITOR: K. SIEGBAHN – UPPSALA

CONTENTS

MILORAD MLADJENOVIĆ, Gamma-ray measurements by the magnetic analysis of Compton and photo electrons . . . . . 1

Computer service for calculation of the photoelectric $f$ factor . . . . . 24

ALESSANDRO ALBERIGI QUARANTA and BRUNO RIGHINI, Fast transistorized pulse height analyzer . . . . . 25

K. J. VAN OOSTRUM and A. C. MEIJER, Use of $(p,\gamma)$ reactions in the efficiency calibration of a NaI crystal . . . . . 31

P. K. DUTT, Theory of "ion-bunching" in relation to the development of an electrostatic time-of-flight mass spectrometer . . . . . 37

T. WESTERMARK, B. SJÖSTRAND and H. G. FORSBERG, Some experiments on moisture determination with beta-ray transmission . . . 45

H. DANIEL and L. JACKSON LASLETT, Beta-ray spectrometer with curved exit slit . . . . . 48

L. G. KUO, M. PETRAVIĆ and B. TURKO, A $dE/dx$ — $E$ counter telescope for charged particles produced in reactions with 14 MeV neutrons 53

*Letters to the Editor*

K. R. CHAPMAN and S. GOWARIKER, A convenient method of constructing accelerator tubes . . . . . 66

A. N. JAMES and C. M. P. JOHNSON, Wide band detection of small ion beam currents . . . 68

Book Reviews . . . . . 70

News Item . . . . . 72

NORTH-HOLLAND PUBLISHING COMPANY – AMSTERDAM

# NUCLEAR INSTRUMENTS AND METHODS

*A journal on accelerators, instrumentation and techniques in nuclear physics*

EDITOR: K. SIEGBAHN, UPPSALA



EDITORIAL BOARD:

J. B. ADAMS (CERN)
F. A. ALSINA (Buenos Aires)
E. AMALDI (Rome)
H. L. ANDERSON (Chicago)
K. T. BAINBRIDGE (Cambridge, Mass.)
P. R. BELL (Oak Ridge)
R. E. BELL (Montreal)
A. BERTHELOT (Saclay)
H. BRINKMAN (Groningen)
E. H. COOKE-YARBOROUGH (Harwell)
S. DE BENEDETTI (Pittsburgh)
M. DE HEMPTINNE (Louvain)
A. DE-SHALIT (Rehovoth)
M. DEUTSCH (Cambridge, Mass.)
S. DU TOIT (Pretoria)
B. S. DŽELEPOV (Leningrad)
W. GENTNER (Heidelberg)
P. C. GUGELOT (Amsterdam)
H. HALBAN (Paris)
O. HAXEL (Heidelberg)
P. HUBER (Basel)
S. KIKUCHI (Tokyo)
J. KOCH (Copenhagen)
M. S. KOZODAEV (Moscow)
S. LIVINGSTON (Cambridge, Mass.)
E. M. MCMILLAN (Berkeley)
M. G. MEŠČERJAKOW (Moscow)
P. B. MOON (Birmingham)
M. L. OLIPHANT (Canberra)
W. PAUL (Bonn)
A. S. RAO (Bombay)
G. SALVANI (Rome)
P. SAVIĆ (Belgrade)
P. SCHERRER (Zürich)
CH. SCHMELZER (CERN)
R. TANGEN (Oslo)
D. TAYLOR (Northampton)
V. I. VEKSLER (Moscow)
G. VON DARDEL (CERN)
O. WERNHOLM (Stockholm)
R. R. WILSON (Cornell)
S. D. WINTER (Saclay)


INSTRUCTIONS FOR CONTRIBUTORS

Contributions may be sent to the Editor, Professor K. Siegbahn, Institute of Physics, University of Uppsala, Sweden, either directly or through the intermediation of one of the members of the Editorial Board. Contributions may be written in English, French or German but should always, except for very short papers, be supplied with a brief abstract in English. Figures should be in inked original drawings or glossy prints and they should be sufficiently large. Contributors should make sure that important details in drawings and photographs will show up clearly in the diminished copy used by the publisher.

Books for review should be sent to Professor Siegbahn.

Objective and descriptive material on endeavours and product developments from the industry for the section "Spotlight on Industry" should be sent directly to the publishers, North-Holland Publishing Company, P.O. Box 103, Amsterdam.


Nuclear Instruments and Methods is published monthly. The subscription price of a volume of 360 pages is $ 17.00 (130 s), postage free.

Subscriptions should be sent to the publishers, North-Holland Publishing Company, P.O. Box 103, Amsterdam, or to any subscription-agent.



No part of this issue may be reproduced in any form, by print, photoprint, microfilm or any other means without written permission from the publisher.

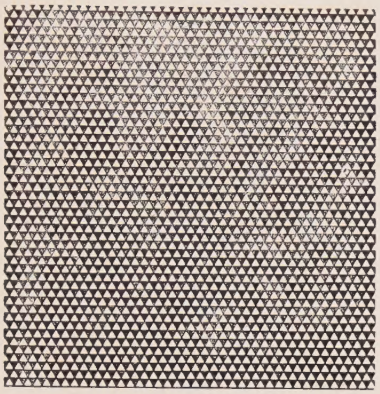

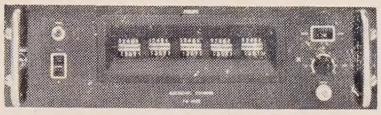

PW 4032

PW 4022

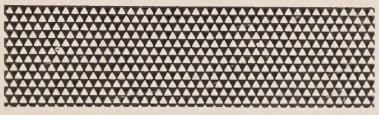

## Scaler for direct connection of scintillation detectors or G.M.-counters

COUNTING CAPACITY: 5 decimal scaling stages; two binary pre-scalers. Total indicated counts: 400 000
RESOLVING TIME: 0.5 μsec (first binary scaler)
INPUT SENSITIVITY: G.M.-counters: 0.5 $V_{p\text{-}p}$.
Scintillation detectors via built-in amplifier with adjustable attenuator: 5 $mV_{p\text{-}p}$
H.V. RANGE: 300-2500 V in steps of 22 V

## Linear count rate meter for direct connection of G.M.-counters, scintillation- or proportional detectors

MEASURING RANGES: 300 - 1000 - 3000 - 10 000 30 000 c.p.m.
ACCURACY: 2% of full scale
TIME CONSTANT: 0.1 -1 -3 -10 -30 -100 sec.
INPUT SENSITIVITY: G.M.-counters: 0.5 $V_{p\text{-}p}$
Scintillation detectors: via built-in amplifier with adjustable attenuator: 5 $mV_{p\text{-}p}$
RECORDING: socket for connection of a strip chart recorder provided, resulting in an improvement of the accuracy to 0.5%

PW 4042

PW 4022

**PHILIPS**
**nuclear equipment**

**N.V. PHILIPS' GLOEILAMPENFABRIEKEN - EINDHOVEN - HOLLAND**

Particle accelerators - Reactor control instrumentation - Health protection and monitoring equipment - Radiation measuring and detection equipment - Geiger-Müller counters - Photomultipliers - Radio-active isotopes.

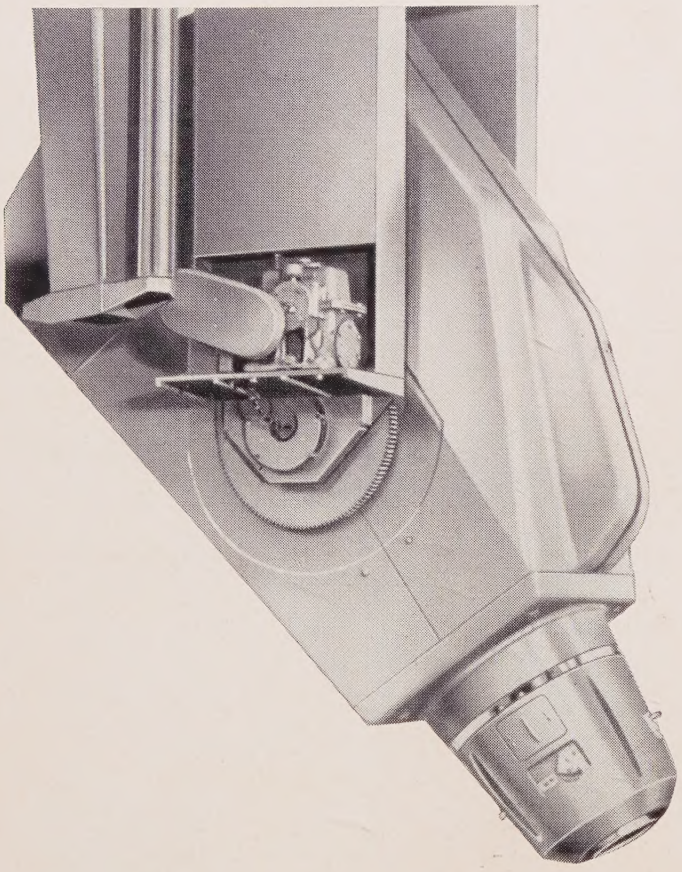

# electron linear accelerators for research, industry and medicine

# by Mullard Equipment Limited

**Electron Linear Accelerators manufactured by Mullard Equipment Ltd. are the logical result of wide and detailed experience in this field. Machines for all types of applications are available, from the standard 4.3 MeV model to equipments specially built to meet individual requirements with electron beam energies up to 50 MeV.**
**The units are designed for continuous operation, ease of control and high reliability.**

**STANDARD MACHINE OPERATING AT 4.3 MeV**

| | |
|---|---|
| Mean power output at 500 pulses per second | 850 W (electrons) |
| Maximum pulse repetition frequency..... | 500 p.p.s. |
| Electron pulse length..... | 1.65 microseconds |
| When used as an X-Ray source maximum X-Ray output is approximately..... | 600 röntgens per minute at 1 metre |

**MULLARD EQUIPMENT LIMITED**

**Mullard House · Torrington Place**
**London W.C.1 · Tel: LANgham 6633**

**RESEARCH** Now regarded as indispensable in many research laboratories Linear Accelerators can be fitted with supplementary heads to provide X-Rays or neutrons. Present day applications include investigation of properties of irradiated materials; preservation of food; basic studies on structure of organic molecules; modification of the properties of plastics.

**INDUSTRIAL RADIOGRAPHY** The compact accelerator design with wide range of movements and precision positioning enables radiographs of complicated heavy metal sections to be taken with minimum setting-up times. The high X-Ray output gives short exposure time and the extremely small (2mm) focal spot gives the highest possible definition. Penetration is sufficient to radiograph steel sections up to 12 inches thick.

**MEDICAL THERAPY** The use of Linear Accelerators for X-Ray and Electron Medical Therapy is well established. These machines give rapid treatment times with precisely defined fields and negligible 'penumbra' effects. Skin and exit dosages are minimised.

ME 664

# he first portable, "desk-top" 400-channel pulse height analyzer

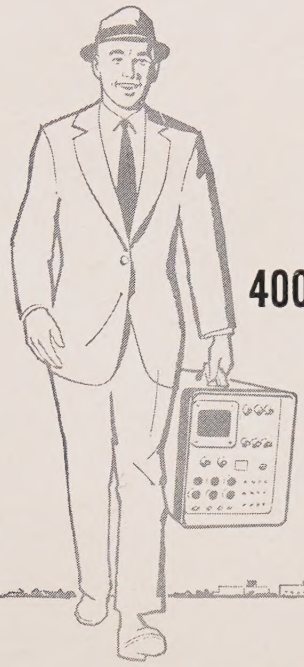

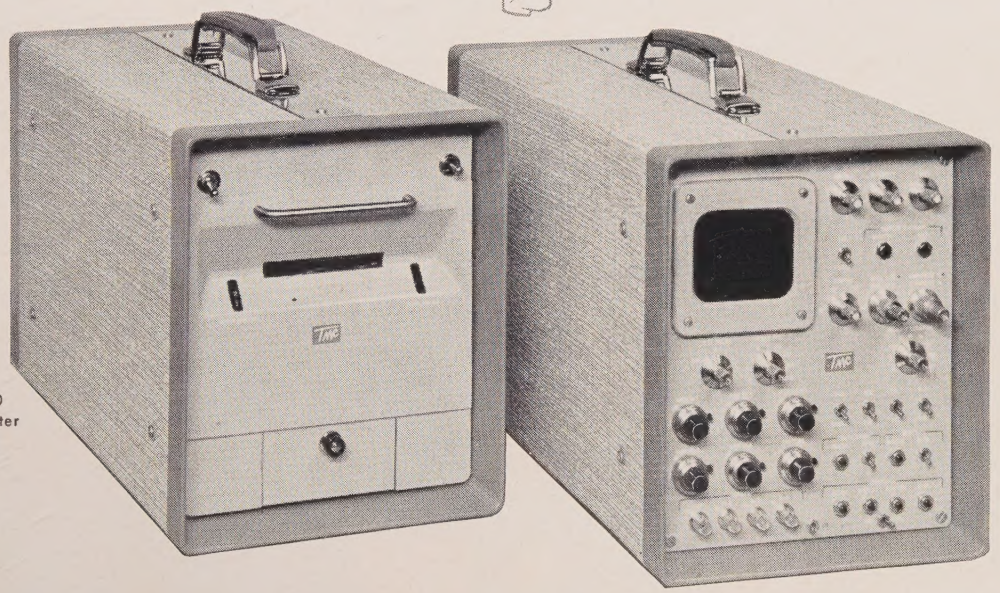

Model 500
decimal printer

Model 404
pulse height analyzer

## — the TMC Model 404

he new TMC Model 404 is the most portable pulse ight analyzer you can own. Take it and use it anywhere. ith its all-transistor, printed circuitry and 400-channel emory in a package just over a cubic foot, this analyzer small enough to operate on your desk. *All* the instru- nts needed for an experiment can be carried easily by e person.

he Model 404 has a magnetic core memory that can be used in sub-groups of two or four; four separate inputs and associated amplifiers; internal pulse routing circuitry pushbutton data transfer and display overlap; very low power requirements and many "system" advantages. And it can be used with the new solid state detectors.

For readout, use its companion unit, the Model 500 Decimal Printer; a high speed paper tape punch; strip chart or X-Y recorders; or an IBM electric typewriter

LITERATURE ON REQUEST

TMC TECHNICAL MEASUREMENT CORPORATION

441 WASHINGTON AVENUE NORTH HAVEN, CONNECTICUT

# SCINTILLATION

**Scintillation Phosphors, Liquids & Crystals** (Bulletins 9, 11, 12, 13, 23 and 25) The NaI(Tl) crystals, (illustrated above) form part of the extensive range of mounted crystals offered by Nuclear Enterprises. CsI(Tl) and LiI(Eu) crystals are also available in mounted form. All three are featured in the crystal-photomultiplier assemblies which afford improved resolution and offer special facilities for counting low level activities. Full details of NE 102 plastic phosphor scintillators, liquid scintillators, loaded liquid scintillators, neutron detectors, scintillation chemicals, crystals and crystal-photomultiplier assemblies will gladly be sent on request.

**Complete Assemblies:** Scanning Scintillation Spectrometer of high performance. Also Liquid Scintillation Spectrometer providing greatly simplified technique for measurement of C14, H3 and Fe55 (with efficiences of 90%, 30% and 20% respectively).

**Probe Units:** Compact probe units for study of gamma rays, low energy X-rays, slow neutrons, fast neutrons and alpha particles. Also special transistorised head units for pulse shape discrimination investigations.

**Special Transistorised Units for Field Investigations:** Four channel Scintillometer for geological and geophysical surveys; Moisture & Density Gauge; Beryllometer. etc.

**Shielded Scinfillation Head Units:** To accommodate photomultipliers, phosphors, and samples. Special units for C14, & H3 analyses.

**Precision Laboratory Instruments:** Non-overloading linear amplifiers, pulse height selectors, EHT units, ratemeters, etc. Also a new range of transistorised instruments of unitised construction.

**Low Level Counting Facilities:** Wide range of human body radiation monitors. Also installations for measuring lean:fat ratios in carcases and live animals.

# NUCLEONIC INSTRUMENTS

Nuclear Enterprises (G.B.) Ltd. offers a complete range of precision nucleonic instruments and a special design and development service to meet individual customer requirements.

**NEW** NE 5550 and NE 5560 series probe units employing pulse shape discrimination techniques for detecting neutrons in a high gamma background.

For full details write for Technical Bulletins & Catalogue to Sales Division, Nuclear Enterprises (G.B.) Ltd., Sighthill, Edinburgh, 11.

ndh 7788

**Nuclear Enterprises (G.B.) Ltd.**

# COUNTING

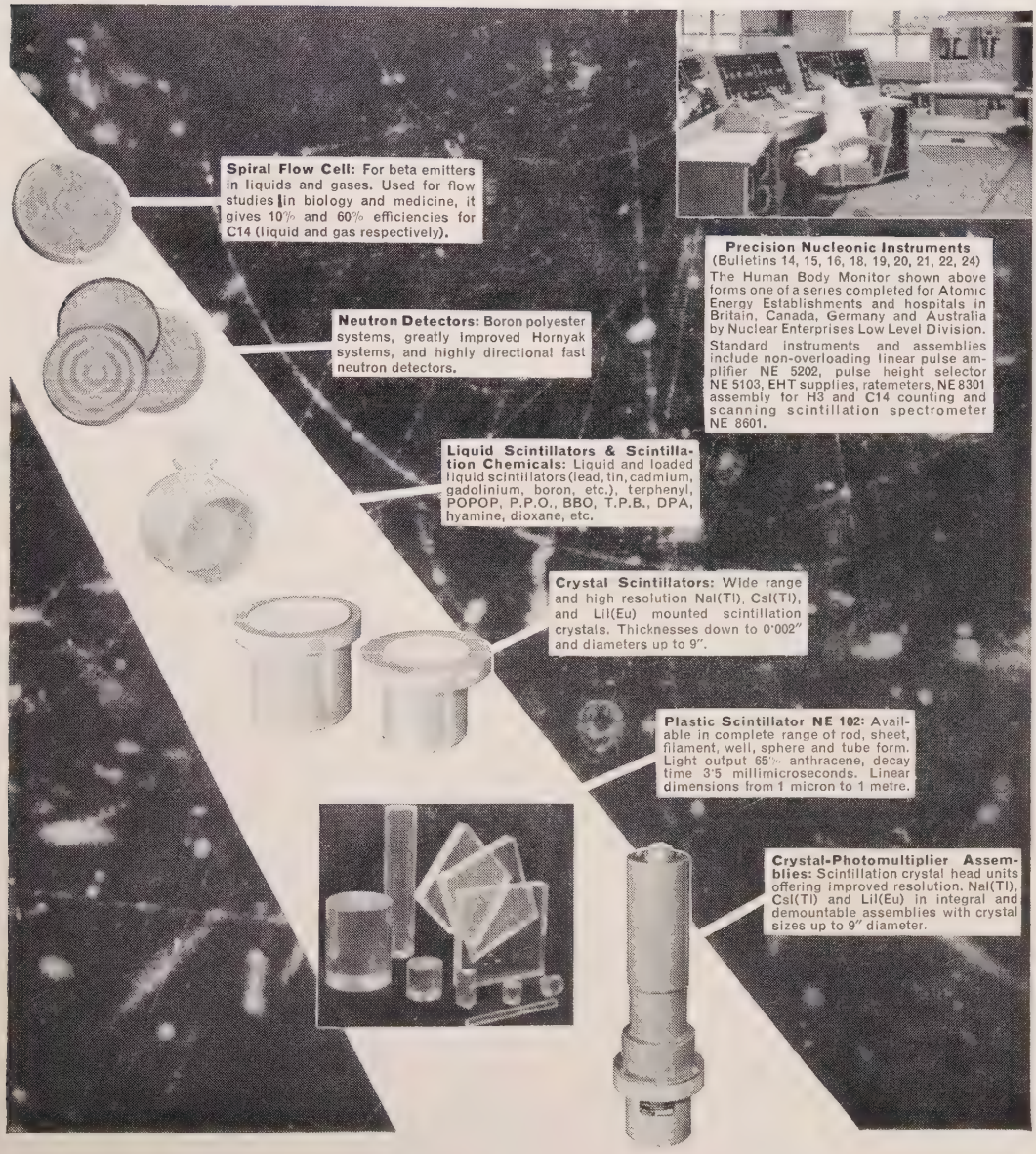

**Spiral Flow Cell:** For beta emitters in liquids and gases. Used for flow studies in biology and medicine, it gives 10% and 60% efficiencies for C14 (liquid and gas respectively).

**Neutron Detectors:** Boron polyester systems, greatly improved Hornyak systems, and highly directional fast neutron detectors.

**Liquid Scintillators & Scintillation Chemicals:** Liquid and loaded liquid scintillators (lead, tin, cadmium, gadolinium, boron, etc.), terphenyl, POPOP, P.P.O., BBO, T.P.B., DPA, hyamine, dioxane, etc.

**Crystal Scintillators:** Wide range and high resolution NaI(Tl), CsI(Tl), and LiI(Eu) mounted scintillation crystals. Thicknesses down to 0·002" and diameters up to 9".

**Plastic Scintillator NE 102:** Available in complete range of rod, sheet, filament, well, sphere and tube form. Light output 65% anthracene, decay time 3·5 millimicroseconds. Linear dimensions from 1 micron to 1 metre.

**Crystal-Photomultiplier Assemblies:** Scintillation crystal head units offering improved resolution. NaI(Tl), CsI(Tl) and LiI(Eu) in integral and demountable assemblies with crystal sizes up to 9" diameter.

**Precision Nucleonic Instruments**
(Bulletins 14, 15, 16, 18, 19, 20, 21, 22, 24)
The Human Body Monitor shown above forms one of a series completed for Atomic Energy Establishments and hospitals in Britain, Canada, Germany and Australia by Nuclear Enterprises Low Level Division. Standard instruments and assemblies include non-overloading linear pulse amplifier NE 5202, pulse height selector NE 5103, EHT supplies, ratemeters, NE 8301 assembly for H3 and C14 counting and scanning scintillation spectrometer NE 8601.

# SCINTILLATORS

The unique scintillation service afforded by Nuclear Enterprises (G.B.) Ltd. includes the highly efficient NE 102 plastic scintillator, liquid scintillators, neutron detectors, scintillation chemicals and an extensive range of crystals & crystal-photomultiplier assemblies.

**NEW** NE 150 plastic phosphor for pulse shape discrimination techniques and NE 160, a special high temperature plastic scintillator.

**Nuclear Enterprises (G.B.) Ltd.**

**Sighthill, Edinburgh, Scotland. — Tel.: Craiglockhart 5262**

**Associate Company: Nuclear Enterprises Ltd.**
**550. Berry Street, Winnipeg 12. Canada.**

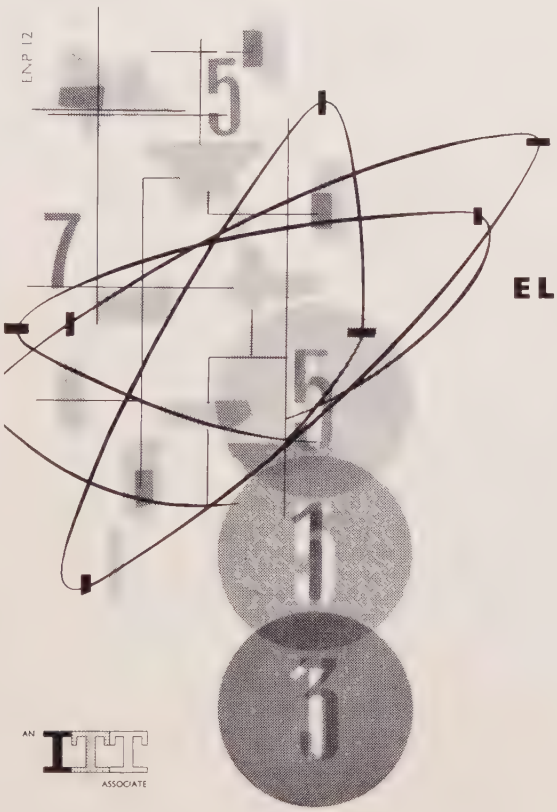


AN ITT ASSOCIATE

**ELECTRONICS FOR NUCLEONICS**

**SCALER CHRONOSCOPE**

Bell Telephone scaler chronoscope gives you top quality reproduction of automatic counting and printing.
It is so constructed that from a small stock of basic modules a wide scope of performances can be covered. This type normally supplied in a metal case is also available for rack mounting

- preset time
- preset count
- result printing facilities
- interchangeable modules
- in line read out
- fully transistorized

*Our staff is always available to answer your inquiries.*

**Bell Telephone Mfg Co**

"Nuclear Energy division"
33, Berkenrodelei
HOBOKEN-Antwerp-BELGIUM

**NANOSECOND PULSES? - MICROSECOND PULSES?**

**MODEL 414**

**CALIBRATION PULSER**

| *Decay Times* | *Ranges* |
|---|---|
| 0.003 microseconds | 0 - 1 millivolts |
| 0.01 microseconds | 0 - 5 millivolts |
| 0.03 microseconds | 0 - 10 millivolts |
| 0.1 microseconds | 0 - 50 millivolts |
| 0.3 microseconds | 0 - 100 millivolts |
| 1. microseconds | 0 - 500 millivolts |
| 3. microseconds | 0 - 5 Volts |
| 10. microseconds | 0 - 10 Volts |
| 100. microseconds | 0 - 50 Volts |
| | 0 - 100 Volts |

Dual purpose- manual or motor driven slider.
Dual 50 ohm output permits coincidence circuit applications.
Internal standard cell calibration.
Polarity switch for positive or negative pulses.
0.1% helical potentiometer.
High pressure hermetically sealed mercury relay.

Write for details.

**$ 785 f.o.b. factory**

**RADIATION INSTRUMENT CO.**

**P.O. BOX 733**

**SILVER SPRING, MARYLAND, U.S.A.**

**NORTH-HOLLAND BOOKS**

*Paul Ehrenfest*

COLLECTED SCIENTIFIC PAPERS

**XII + 632 pages**

**Guilders 45,00 (90s.)**

This volume makes widely scattered publications readily available. All Dutch articles appear here in English; the German publications are in the original language.

**Sole Agency for U.S.A.:**

**Interscience Publishers Inc. — New York**

**NORTH-HOLLAND PUBLISHING COMPANY - AMSTERDAM**

*One of a series of discussions on topics of particular interest to those employing radioisotopes and tracer techniques.*

# LIQUID SCINTILLATION COUNTERS

If you plan to buy a Liquid Scintillation Counting System, the *only* important criteria are:

1. The counting efficiency and background;
2. The number of samples to be counted;
3. The cost of the system and,
4. The reputation and experience of the manufacturer

As you know, the first commercial Liquid Scintillation Counting System was produced at Tracerlab back in 1954, and we believe that our newest system, the LSC-10, is the most economical and practical ever designed.

The Tracerlab system consists of a console for the scaler and associated circuitry, and a freezer containing the sample changer and detectors. The unique detection system is a coincidence type with two photomultiplier tubes mounted at right angles to each other. The freezer, an 11 cubic foot unit, is only 38, wide, and has a capacity of forty-20 ml. samples with an in-freezer storage rack for 40 more. Yet it is compact enough to be practical even for crowded laboratories. Phototubes are fully protected against accidental light exposure by means of a freezer mounted interlock.

Here's another point to consider: In the LSC-10 system, you don't have to open the freezer to transfer samples. External controls are provided—samples remain dark adapted—you get uniform counting conditions. Incidentally, the LSC-10 can be readily converted, *in your laboratory* to fully automatic operation (by means of standard accessories) if an when your volume of work requires it.

Experts agree that both low temperature and coincidence circuitry are an absolute necessity for low background and stable operation when counting tritium or low concentrations of carbon-14. Tritium compounds are among the most difficult to assay, particularly when in aqueous solutions. A look at the final test records made on five typical units, in series shows the following efficiencies and backgrounds for counting aqueous tritium.

And, remember, these units can perform even better when installed in your laboratory with settings optimized for your counting requirements.

| Unit | Efficiency and Background |
|---|---|
| A | 9.0% at 95 cpm |
| B | 6.2% at 70 cpm |
| C | 7.6% at 73 cpm |
| D | 6.2% at 83 cpm |
| E | 5.3% at 64 cpm |

Naturally, much higher efficiencies are obtained when counting non-aqueous tritium or carbon-14 compounds. Greater than 75% efficiency can be expected when counting C-14 samples and greater than 25% efficiency when counting tritium compounds in hydrocarbon solution.

*Further facts about the LSC- 10*

THE COST? The lowest for any fine system.

DELIVERY? Currently less than 30 days.

INSTALLATION. Usually completed in a matter of hours.

SERVICE? It's world-wide, with more than 100 qualified representatives.

INTERESTED? *Write for a quotation and full details.*

Tracerlab KELEKET

Tracerlab *first in radiation measurement*

**TRACERLAB, INC.,** 1610 Trapelo Rd., Waltham 59, Massachusetts • 2030 Wright Ave., Richmond, California

**European Office: TRACERLAB (Holland) N.V. 119 Singel, Amsterdam, Netherlands**

Go International with your Sales Program today-Write

**William F. Baars-Advertising Manager, North-Holland Publishing Company**

**P.O. Box 103, Amsterdam, The Netherlands**

# Transistorized . . . . . Multichannel Analyzers

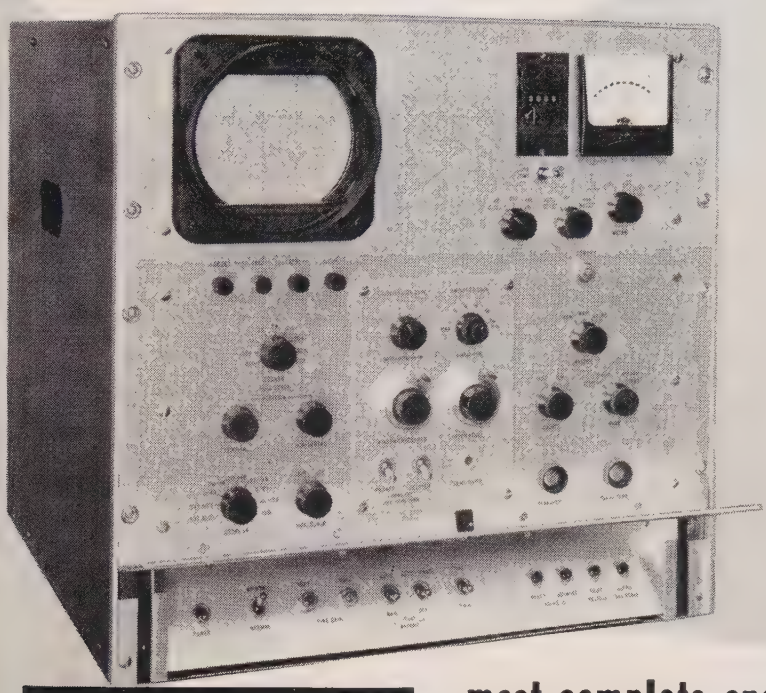

**Model 34-8**

**200-Channel**

**Model 34-12**

**400-Channel**

- automatic programming including
  - Auto-Print
  - Auto-Record
  - Auto-Transfer
- weight less than 80 pounds
- NOT microminiaturized
- ALL coincidence features
- ferrite core memory
- memory subgrouping
- $10^5$ count capacity ($10^6$ OPT.)
- external programming
- LIVE display
- time analyzer mode
- CRYSTAL controlled live timer
- FAILSAFE channel identification
- simultaneous print and record (OPT.)
- 0.5 percent linearity
- dead time meter
- spectrum transfer circuit

## most complete and available line of *TRANSISTORIZED* analyzers

FULLY TRANSISTORIZED . . . Most of the Pulse Height Analyzers produced today are transistorized units, and fully transistorized units have long been in production at RIDL. Full production of complete system RIDL transistorized multi-channel analyzers has allowed RIDL to put many units in the field and to produce additional available 200-channel Model 34-8s and 400-channel Model 34-12s. All models may be operated as **one, two** or **four** independent analyzers, or as multi-channel scalers (time analyzers). All models have **all** the best features of RIDL's best analyzers.

AUTOMATION IN THE LAB . . . RIDL designed the Model 34-8 and Model 34-12 analyzers to save valuable technical man hours through providing such features as **Auto-Print, Auto-Record** and an automatic transfer circuit. A built-in crystal-controlled Live Timer allows automatic **dead time correction.** The addition of automatic **background correction** allows final data readout without laborious manual corrections or replotting of curves.

AUTOMATIC DATA PROCESSING . . . RIDL builds on its maximum development of automatic **data gathering** and **analysis** further possibilities for **automatic data processing.** To normal printing and recording is added readout on **magnetic tape, punched tape,** and parallel or serial entry printers. This allows full control over programming, internal and external data format, and data processing. Whatever your data readout and processing needs may be, our staff is ready at all times to discuss them with you.

**SIXTY DAY DELIVERY ON ANALYZERS IN ANY PART OF THE WORLD**

Light weight makes AIR SHIPMENT economical.
Chicago to Europe — for example — approximately $150.00
RIDL Representatives are located in most areas of the world.
Contact the RIDL home office for prompt service in locating the sales office nearest you.

RIDL INC.

*Radiation Instrument Development Laboratory, Inc.*

61 EAST NORTH AVENUE • NORTHLAKE, ILLINOIS

PHONE: MUrray 1-2323 • Cable Address: RADILAB

# NUCLEAR PARTICL

# ANALYZING MAGNETS

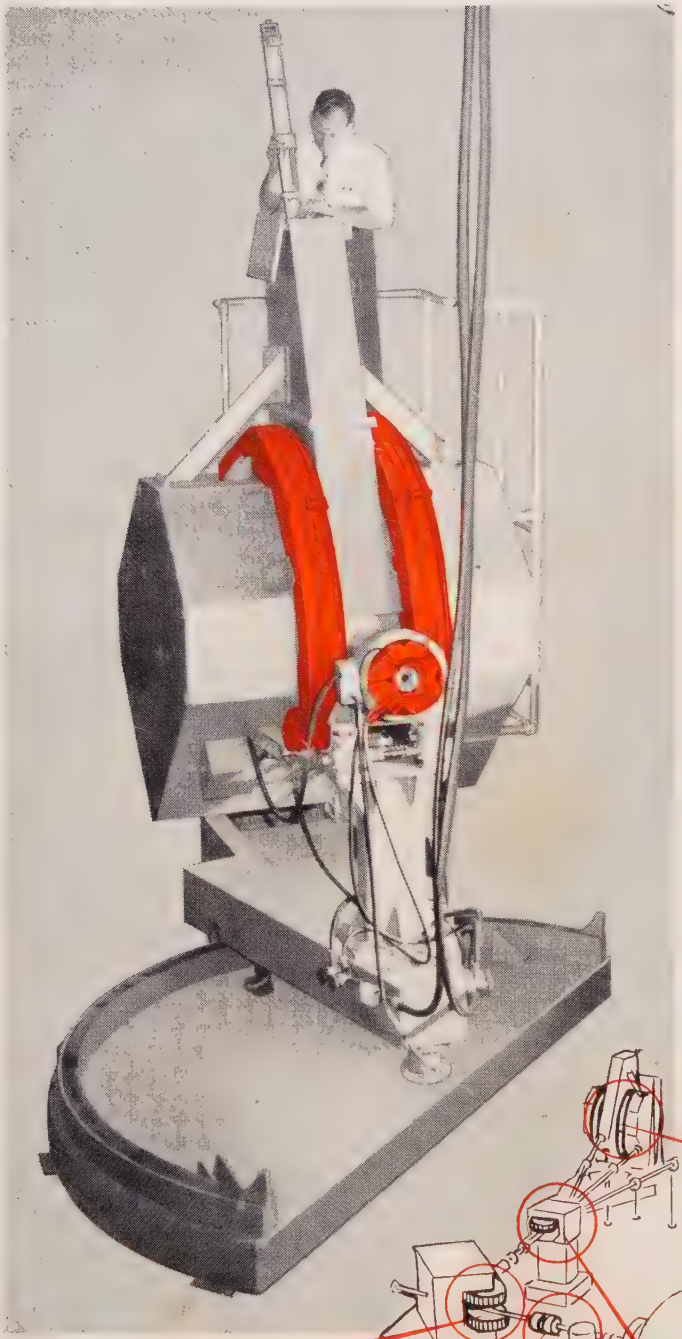

**Combined Magnetic Spectrograph and Spectrometer* designed and built for Chalk River Laboratories, Atomic Energy of Canada, Ltd., for energy analysis of protons, deuterons, and alpha particles.**

- Magnetic rigidity —
  Up to $B\rho$ = 865 kilogauss-cm (12- Mev tritons)
- Resolving power (spectrograph) —
  $E/\Delta E = 10^3$ or better
- Solid angle (spectrograph) —
  $\Omega = 1.4 \times 10^{-3}$ steradians (max)
- Solid angle (spectrometer) —
  $\Omega = 0.9 \times 10^{-2}$ steradians (max)
- Reaction angle —
  $\theta$ = 0 to 135 degrees
- Detector —
  Nuclear track plate and scintillation counter

*For further technical reference, see H.A. Enge, RSI **29**, 885 (1958)

## TYPICAL MAGNET SYSTEM FOR 12-MEV TANDEM *Van de Graaff* ACCELERATOR

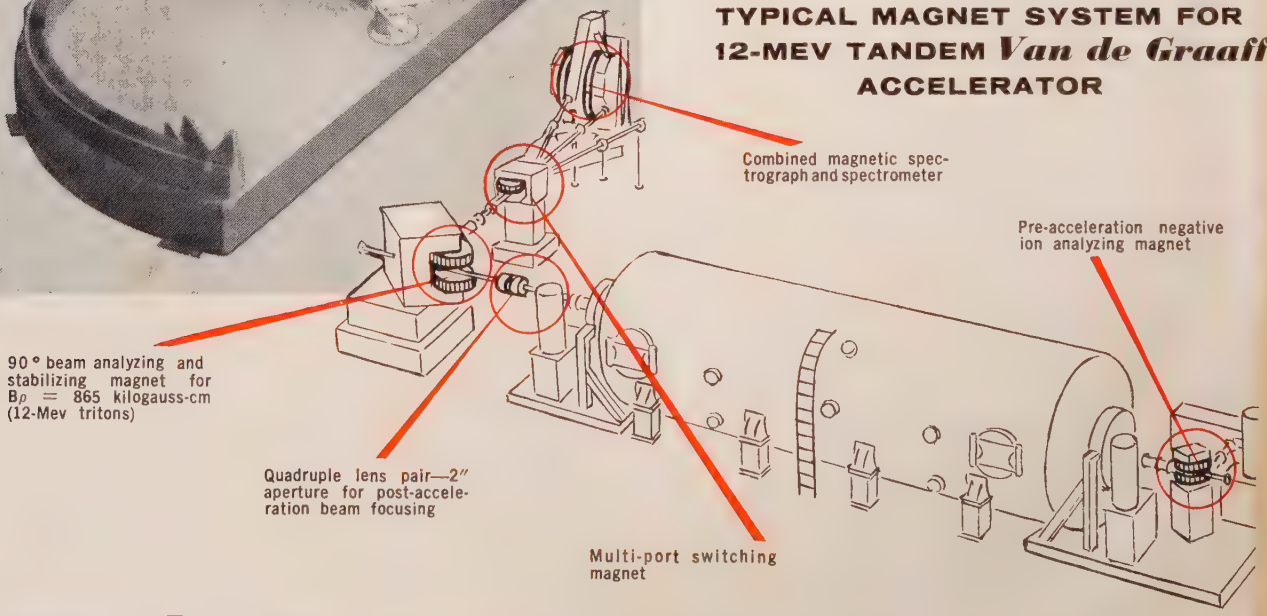
Combined magnetic spectrograph and spectrometer
Pre-acceleration negative ion analyzing magnet
90° beam analyzing and stabilizing magnet for Bρ = 865 kilogauss-cm (12-Mev tritons)
Quadruple lens pair—2″ aperture for post-acceleration beam focusing
Multi-port switching magnet

For detailed information on magnets and accelerators, write to Technical Sales:

# HIGH VOLTAGE ENGINEERING CORPORATION

BURLINGTON, MASSACHUSETTS — U. S. A.

HIGH VOLTAGE ENGINEERING (EUROPA) N.V. AMERSFOORT, THE NETHERLANDS

NUCLEAR INSTRUMENTS AND METHODS **10** (1961) 1–23; NORTH-HOLLAND PUBLISHING CO.

# GAMMA-RAY MEASUREMENTS BY THE MAGNETIC ANALYSIS OF COMPTON AND PHOTO ELECTRONS

MILORAD MLADJENOVIĆ

*Institute of Physics, Faculty of Natural and Mathematical Sciences, Belgrade*

Received 20 July 1960

A review is presented of gamma spectra measurements by external photo conversion and by production of relatively narrow Compton lines. The effects of scattering, energy losses and geometry on the intensities and energies, are discussed. Some spectrometers especially designed for measurements of Compton spectra, are also briefly reviewed.

In the last decade, the most frequently used apparatus for measurement of gamma spectra is the scintillation spectrometer. It has several advantages over the other types of spectrometers, the two most important ones being: (1) high efficiency, so that very weak sources can be measured, (2) it is very convenient for coincidence work. On the other hand, the standard scintillation spectrometer has an inherent limitation: low resolving power, which is of the order of 5%. There are many cases of complex spectra where it cannot be of great help. So, while the scintillation spectrometers are continually improving and increasing their range of applications, there remains the need for an apparatus of higher resolving power.

The crystal diffraction spectrometer of du-

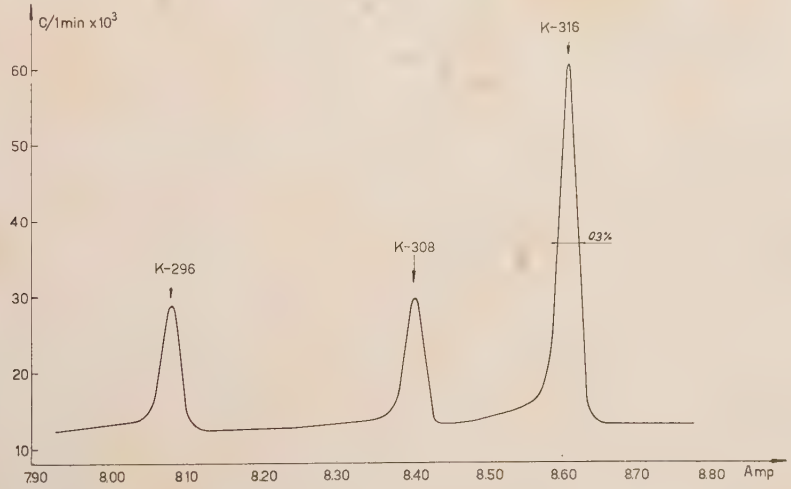


Fig. 1. Part of the external conversion spectrum of $Pt^{192}$, taken with the 50 cm radius iron-free double focusing spectrometer. Uranium convertor had an area 5 × 20 mm² and was 0.5 mg/cm² thick. From Mladjenović *et al.*[1]).

Mond type has very good resolution, but it requires extremely strong sources and the construction is not simple, so that only a few such apparatus have been built up to now.

Good resolutions can be achieved by magnetic analysis of electrons ejected by gamma-rays. A large double focusing beta-ray spectrometer can give external conversion line widths of 0.2–0.5%, (fig. 1) which is an order of magnitude better

than the scintillation spectrometer resolution. Compton lines with a width of 2–3% can be obtained, while any further reduction of line width

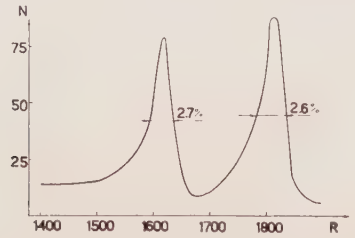


Fig. 2. Compton lines of two $Co^{60}$ gamma rays, measured with the 50 cm radius double-focusing spectrometer. Aluminium radiator had an area $2 \times 2$ cm², and was 5.4 mg/cm² thick. From Mladjenović and Hedgran[2]).

is accompanied by drastic drop of efficiency (line width of 0.3% by reducing the efficiency for a factor of $10^5$ [3])) (fig. 2) An important advantage of the Compton line method is that there is no appreciable background, which is otherwise always present when photo electrons are measured, either magnetically or in scintillation crystal, and is due to Compton electrons†. The price payed for higher resolution is decrease of efficiency, which is especially low in the Compton method.

In the following we shall consider mainly high resolutions, stated above, and we shall pay attention to two most important questions: (1) precision of intensity and energy determinations and, (2) efficiency, which we shall define as the number of photons emitted into $4\pi$, per one electron detected at the peak of the line.

## 1. External Photo Conversion

### 1.1. INTRODUCTION

External conversion measurements are made with conventional beta-ray spectrometers, which in the present discussion we shall divide, according to the beam geometry, into two groups: (1) Central beam and (2) lens types. While precise determination of energies represents no problem, the intensity measurements are quite involved. Angular distribution of photo electrons is energy dependant and is distorted by scattering of electrons in the convertor. Corrections have to be made for the effects of scattering, energy losses and geometry.

The difficulties may be illustrated by considering a typical external conversion arrangement shown in fig. 3a. The gamma-ray source is placed in a copper capsule, sufficiently thick to stop all the beta particles. The capsule is sealed to prevent the escape of radioactive material into the vacuum chamber. The convertor is usually a thin layer of uranium deposited on an aluminium foil.

Fig. 3b shows schematically the geometry of the conversion process. The following factors have to be taken into consideration:

1. The source may have non-negligible dimensions. It should then be divided into sufficiently small volume elements, so that they can be considered as point sources. The emission is isotropic. We consider first a narrow beam of gamma rays emitted from the volume element $d\tau$ within a solid angle element $d\omega$.

2. Some of the gamma-rays in the elementary cone may be absorbed in the source, beta absorber, or the convertor itself. This can be represented by a factor which depends on the energy of gamma rays, atomic numbers and dimensions of source-convertor arrangement.

3. Then the differential cross section for the emission of photo electrons at an angle $\theta$ per unit solid angle has to be used, giving the number of photo electrons ejected into the cone $d\Omega$.

4. Electrons are generated in the whole convertor and those starting from deeper layers are colliding with uranium atoms causing an energy decrease and a direction change. Depending on the energy and convertor thickness, plural scattering, multiple scattering or diffusion my take place. This induces a broadening of cone $d\Omega$, and

† Special methods have to be used to eliminate Compton background, usually based on coincidence techniques. See Motz, Carter and Fisher, Bull. Am. Phys. Soc. II, **4** (1959) 246.

*Note added in proof*: For a more complete description of work done by Motz *et al.*, see report given at Vienna meeting on neutron physics, October 1960. A description of a double-focusing spectrometer is also given.

[1]) M. Mladjenović, T. Novakov and M. Župančić, Bulletin "B. Kidric" **10** (1960) 15.

[2]) M. Mladjenović and A. Hedgran, Arkiv f. Fysik **8** (1954) 49.

[3]) L. Grošev, A. Demidov, V. Lucenko and A. Malov, Report at the Annual Meeting of Nuclear Spectroscopy, Moskov, January 1960.

the new cone has less well defined limits and a different angular distribution.

After the treatment of an elementary cone is finished the following integrations have to be made:

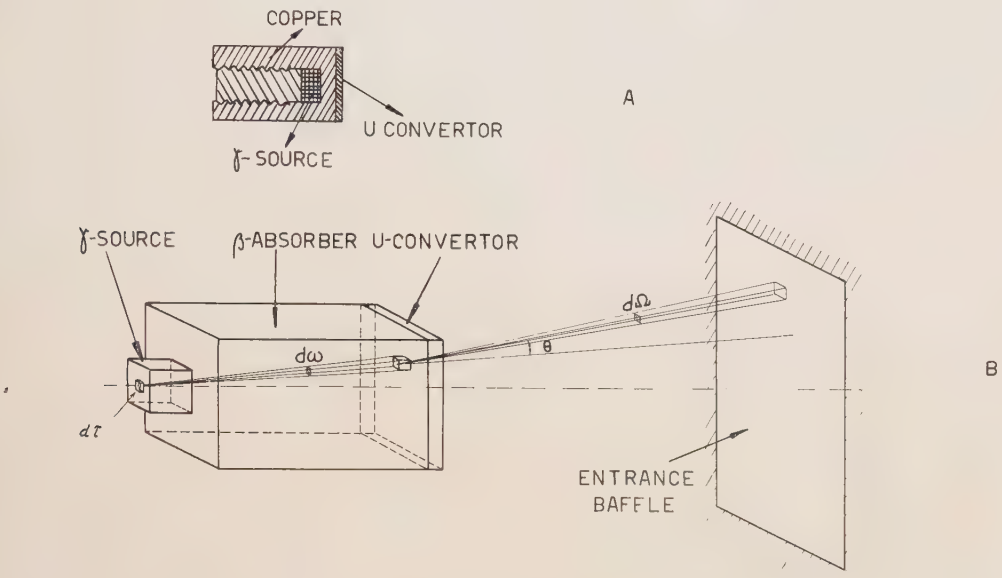


Fig. 3. A. Source-convertor arrangement; B. Schematical illustration of source-convertor-baffle geometry.

1. The integration over the solid angle $\Omega$ subtended by the entrance diaphragm at the convertor.

2. The integration over the solid angle $\omega$, subtended by the convertor at the source volume element.

3. Integration over the source volume.

It is obvious that the general problem is very complex, and several approximations have to be made in order to find a somewhat simpler solution.

Before we pass to a review of some papers on the external conversion measurements, it would be useful to consider first briefly the scattering, energy losses and angular distribution, in order to see what effects can be expected from them, and roughly how they depend on the experimental parameters.

### 1.2. ENERGY LOSSES

Monoenergetic photo electrons are generated at various depths of the convertor, which is usually from 0.3 to 20 mg/cm² thick. Many collisions with convertor atoms can take place, producing an energy loss. An initially monoenergetical line is thereby broadened, and a characteristic low energy tail appears.

Energy loss depends on the energy of photo electrons, so that the line broadening varies with the energy. This effect should be taken into account when intensities are measured by peak heights.

An important factor limiting the convertor thickness, is the line broadening due to energy losses. It is therefore necessary to have a rough idea of the contribution of energy losses broadening to the total line width. We shall characterise this contribution by the full width at half height of the electron energy distribution produced by energy losses in an initially monoenergetic electrom beam.

In the first approximation we can assume that the width caused by energy losses is linearly added to the instrumental width, but we must keep in mind that this might not be true, since the addition of widths depends on the line forms.

The line broadening due to energy losses of charged particles was first treated theoretically by Williams[4]), and later by Landau[5]). They both

[4]) E. J. Williams, Proc. Roy. Soc., London **125** (1929) 420.

[5]) Landau, J. Phys. USSR **8** (1944) 201.

obtain similar distributions. Blunk and Leisegang[6]) have given a correction to Landau distribution by taking into account the losses due to bound electrons, which has the effect of broadening the distributions. There are not enough experimental results to verify the theoretical predictions. It appears[7]) that for thin foils the experimentally found distributions are larger than predicted by Landau and are more in agreement with Blunk and Leisegang.

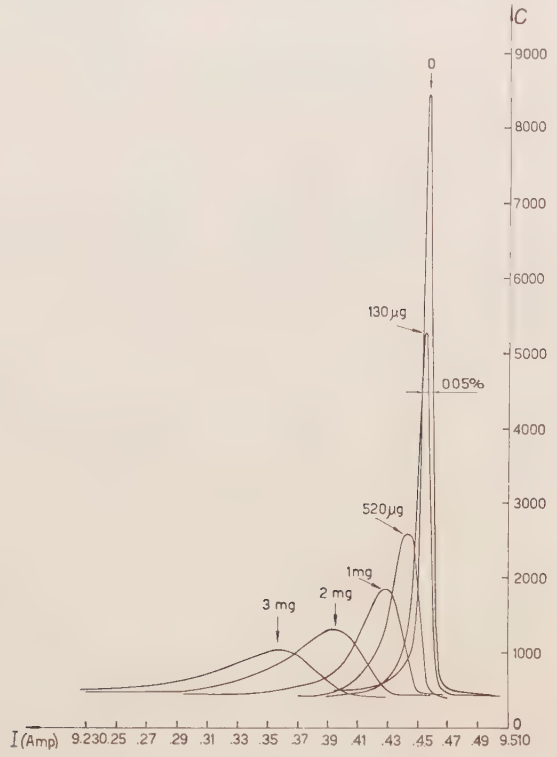


Fig. 4. Line broadening of 238 keV internal conversion line due to energy losses in Al foils.

It should be noted that a precise comparison of experimental results with theoretical predictions requires the use of collimated electron beams, ("narrow beam" geometry), as discussed by Birkhoff[7]). This is not the case with a typical external conversion measurements, where the source is close to absorber ("wide beam" geometry). The gamma ray beam might have an aperture angle of 50–80°, and electrons are also emitted obliquely, having then longer paths. The broadening in wide beam geometry was compared with Landau theoretical predictions by Mladjenović† who measured the line broadening of 238 keV internal conversion line (K line of 316 keV gamma transition in $Pt^{192}$) by thin aluminium foils adjacent to the source. The measurements were made in a 50 cm radius iron-free double-focusing beta spectrometer, which gave a line width of 0.05% without absorbers. The change of line shape due to scattering and energy losses is illustrated in fig. 4. Since the instrumental ("zero thickness") line width is ten times smaller than the line widths with 2 mg/cm² absorber, we shall not make a large error by simply subtracting 0.05% from measured values to obtain the broadening due to absorbers. That broadening is compared in fig. 5 with Landau formula, given below. Experimental line widths are twice as large.

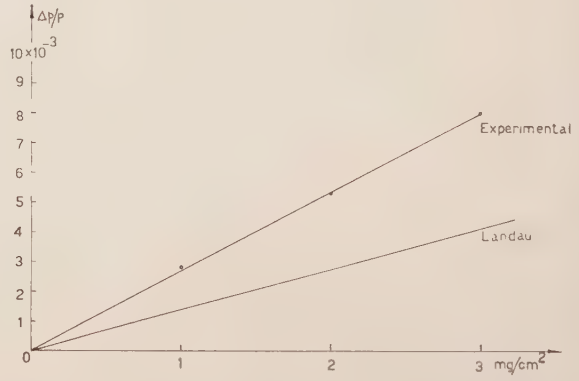


Fig. 5. Comparison of Landau theoretical line widths with experimental values, obtained with wide beam geometry.

In the external conversion measurements electrons are generated at various depths, traversing various thicknesses. It is usually taken that they all traverse half of the convertor thickness. As Landau formula gives about 50% smaller widths, we can get a rough estimate of line broadening by using Landau formula, and by supposing that all electrons are traversing full convertor thickness. It is hardly necessary to stress that this is only meant to be used as a rough guide.

[6]) O. Blunk and S. Leisegang, Zeit. Physik **128** (1950) 500.

[7]) R. D. Birkhoff, Handbuch der Physik **34** (1958).

† Mladjenović, Belgrade Meeting on Nuclear Spectroscopy, September 1959 (unpublished).

The Landau formula for full width at half maximum is given in the case of a uranium absorber, by

$$\Gamma = \frac{236}{\beta^2}\sigma \quad \text{(eV)}$$

where $\sigma$ = uranium convertor thickness in mg/cm².

Fig. 6 shows the relative broadening $\Gamma$ given by this formula. We see that at the energies of a few hundreds keV, the widths are varying rapidly with the energy, so that it is advisable

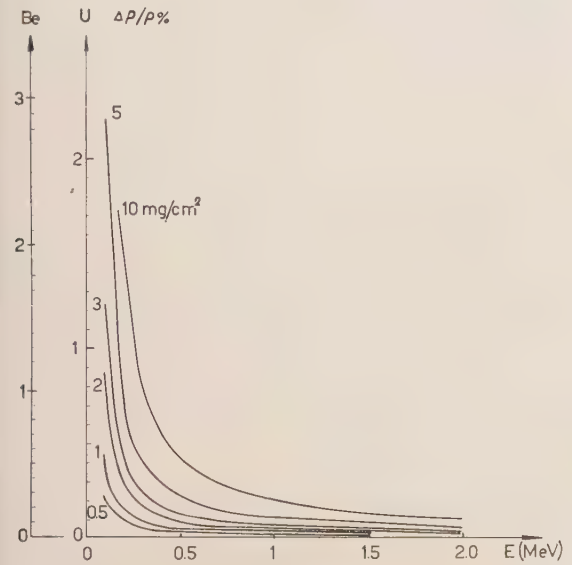


Fig. 6. Landau theoretical predictions of line broadening due to energy losses.

to use several convertor thicknesses to cover a larger energy interval.

When a total line width of about 0.5% is desired, the contribution from energy losses broadening can be about 0.2–0.3%. In that case the convertor thicknesses should be between 0.5 mg/cm² at 100 keV to 10 mg/cm² at 1 MeV.

### 1.3. SCATTERING

When the convertor is very thin, only electrons emitted within angles $\theta_{\min}$ to $\theta_{\max}$ are accepted by spectrometer entrance baffles. In the case of central beam spectrometer, $\theta_{\min} = 0$ and $\theta_{\max} = 60$–$80°$. The scattering which is practically always present with normally used convertor, may introduce angular redistributions. Electrons emitted at angles greater than $\theta_{\max}$ may be scattered within, or those emitted at $\theta < \theta_{\max}$ be scattered outside the spectrometer acceptance angles. The balance between the scattering in and scattering out can be expected in a general case to depend also on the energy.

We can find out what kind of scattering is to be expected in a given arrangement by computing the mean number $n$ of collisions contributing to the scattering and the mean angle of deflection $\bar{\theta}$. The limit between plural and multiple

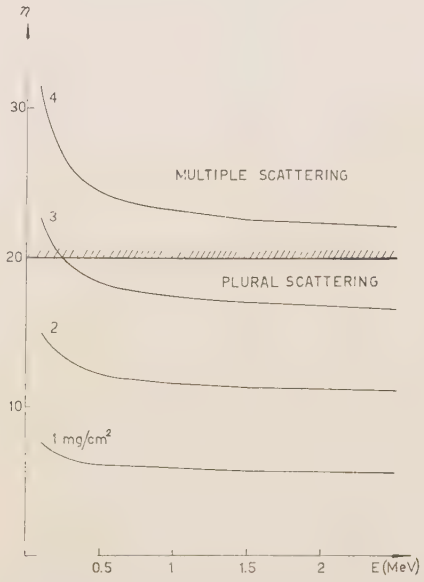


Fig. 7. Mean number of collisions $n$, contributing to the scattering, according to Moliere.

scattering is set at $n \approx 20$, while the multiple scattering develops into diffusion when $\bar{\theta} > 33°$.

According to Moliere[8]), $n$ is given by the following relation

$$\log_{10} n = 8.215 + \log_{10}\left[\frac{\sigma}{A} Z^{-\frac{2}{3}} \frac{\alpha^2}{1.13 + 3.76\,\alpha^2}\right]$$

where $\sigma$ = foil thickness in g/cm²

$$\alpha = Z/137\,\beta\,.$$

Fig. 7 shows $n$ as function of energy for uranium foil. We see from the diagram that for convertor thicknesses smaller than 3 mg/cm², which are of interest in high resolution work, the scattering is plural.

When only a rough estimate of mean angle of deflection is needed, it is sufficient to assume that

[8]) Moliere, Z. Naturforsch. 3a (1948) 78.

the scattering distribution is Gaussian. The mean angle of deflection $\theta$ is then given by a relation derived by Bothe[9]) and recently improved by Kinzinger and Bothe[10]), which in the case of uranium reduces to

$$\bar{\theta} = 1.6 \times 10^2 \frac{1}{V} \frac{V + 511}{V + 1022} \sqrt{l} \text{ radians}$$

$V$ = electron energy in keV
$l$ = foil thickness in mg/cm².

Fig. 8 shows the dependance of mean scattering angle $\bar{\theta}$ on the energy and foil thickness.

The theories of multiple scattering were developed by Williams[11]), Moliere[8]) and others[12–14]). The distributions are given by the expressions which are not convenient for further analytical treatment. On the other hand there is no adequate theory of plural scattering. It is therefore not yet possible to find a precise correction to the scattering in the convertor.

An attempt at an approximate correction may be done using simple Gauss distribution. This was discussed in detail by Dželepov[15]), who

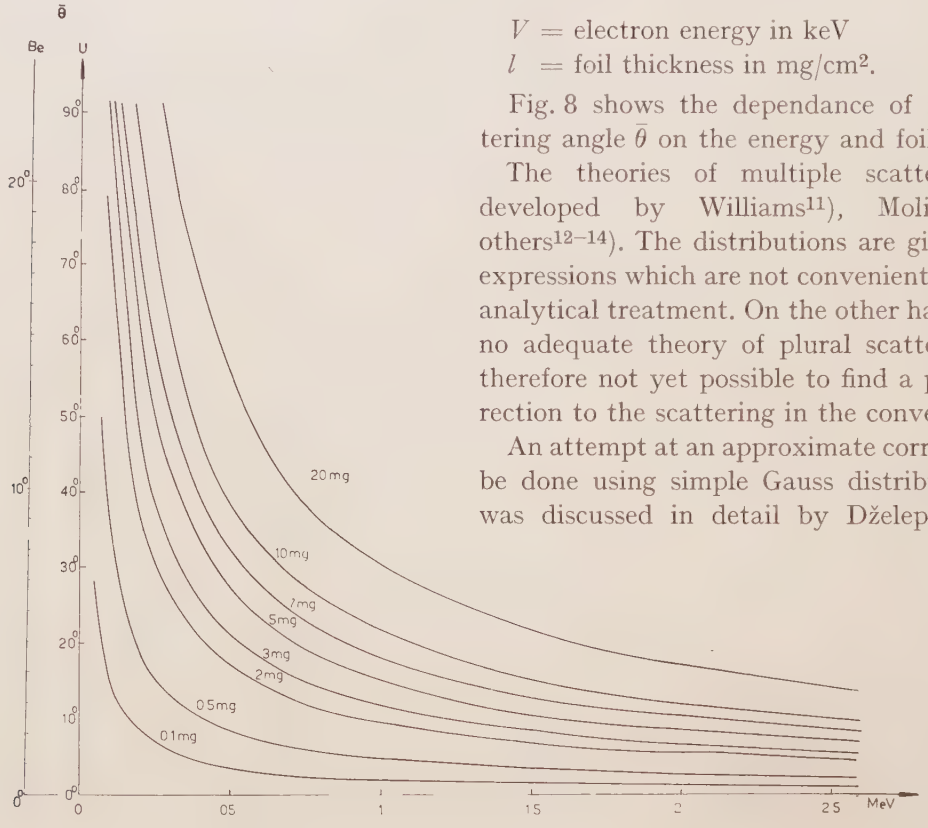


Fig. 8. Mean scattering angle $\bar{\theta}$ given as function of energy and foil thickness.

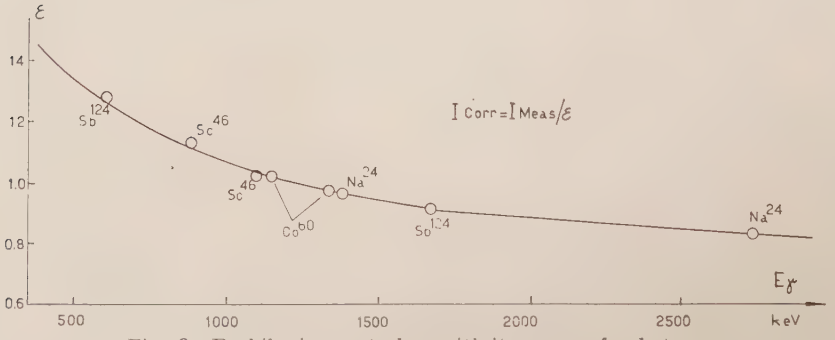


Fig. 9. Bashilov's spectral sensitivity curve for ketron.

[9]) W. Bothe, Handbuch der Physik **22** (1933) 20.
[10]) E. Kinzinger and W. Botte, Z. Naturforschung **7a** (1952) 390.
[11]) E. J. Williams, Proc. Roy. Soc., London A **169** (1939) 531.
[12]) S. Goudsmit and J. L. Saunderson, Phys. Rev. **57**, 24; **58** (1940) 36.
[13]) H. S. Snyder and W. T. Scott, Phys. Rev. **76** (1949) 220.
[14]) W. T. Scott, Phys. Rev. **85** (1952) 245.
[15]) B. S. Dželepov, Izvestia A.N. **18** (1954) 95.

used Williams theory of multiple scattering to correct the angular distributions given by Sauter[16]). Dželepov found the corrections for the ideal case of a parallel beam of gamma rays falling on the convertor. He concludes that it is virtually impossible to derive the corrections for the geometries used in practice and recommends the use of empirical correction curves, which Russian physicists call "spectral sensitivity curve". An example of a spectral sensitivity curve is given on fig. 9. It is used by Bashilov group[17]) for work with ketron. They estimate the precision of that curve as 10%.

### 1.4. ANGULAR DISTRIBUTIONS OF PHOTO-ELECTRONS

One of the most important difficulties in the photoconversion measurements is the lack of both precise theoretical and sufficient experimental data on the angular distributions of photo electrons. Reviews of these problems were given by Morette[18]), Davisson and Evans[19]), and recently by Hultberg[20]) and Bonč-Osmolovskaia[21]).

1.4.1. *Theoretical work* is incomplete, due to known difficulties of treating relativistic electron phenomena in the atomic electron clouds. Several approximate formulae were developed, each valid for a restricted range of parameters.

The formulae are simpler for non-relativistic cases, but in practice the measurements are generally made with relativistic electrons. The differential cross section for angular distribution of relativistic photo electrons ejected from the K shell, was calculated by Sauter[16]), who obtains

$$\frac{\mathrm{d}I}{\mathrm{d}\Omega} = 4r_0^2 Z^5 \alpha^4 \frac{\beta^3(1-\beta^2)^3}{(1-\sqrt{1-\beta^2})^5} \frac{\sin^2\theta}{(1-\beta\cos\theta)^3} \cdot \left\{ \frac{\cos^2\varphi}{1-\cos\theta} - \frac{1}{2}\frac{1-\sqrt{1-\beta^2}}{1-\beta^2}\cos^2\varphi + \frac{1}{4}\frac{(1-\sqrt{1-\beta^2})^2}{(1-\beta^2)^{\frac{3}{2}}} \right\}.$$

Sauter used Born approximation $(Z/137\beta) \ll 1$, which is valid for small $Z$ and $\beta \approx 1$. The convertors used in external conversion measurements have a high $Z$, so that Sauter formula is not valid. This can be seen by comparing the total cross section for K shell ($Z = 84$, $E = 350$ keV), which is $6.02 \times 10^{-23}$ cm$^2$/ at when Sauter formula is integrated, with more exact calculations done by Hulme *et al.*† who get $21 \times 10^{-23}$ cm$^2$/at.

Partial improvements were done recently by Sauter and Wüster[22]) and by Sliv[23])††. Sauter and Wüster recalculated the emission probability at small angles and obtained the ratios of intensities at zero and maximum angle which are in better agreement with recent experimental results.

Sliv[23]) calculated the angular distributions for large angles and for $Z = 20$ and 47. A comparison of Sliv and Sauter values is given in table 1. The differences are larger at greater angles and higher energies. At the angle of 45° they differ by a factor of 0.5–10. We see that $Z$ dependence is quite important. For that reason we can expect large differences between Sauter and more exact theoretical calculations, and until these have been made it is perhaps better to rely on empirical distribution curves.

The situation is not much better with total cross section for photo effect in K shell $\tau_K$. A compilation of $\tau_K$ was prepared by White[24]), who estimates their accuracy at 5–15%†††.

[16]) F. Sauter, Ann. Phys. **11** (1931) 454.

[17]) N. M. Antonieva, A. A. Bashilov and E. K. Kulakovskii, ZETF **37** (1959) 1497.

[18]) C. Morette, J. phys. et radium **7** (1946) 135.

[19]) C. M. Davisson and R. D. Evans, Revs. Mod. Phys. **24** (1952) 79.

[20]) S. Hultberg, Arkiv för Fysik **15** (1959) 307.

[21]) N. Bonč–Osmolovskaia, Atomnii fotoefekt u oblasti $\gamma$-lučei (Akad. Nauk, Moskva, 1959)

[22]) F. Sauter and H. O. Wüster, Zeits. für Physik **141** (1955) 83.

[23]) L. A. Sliv, Disertation, FTI, 1955. Results on angular distribution reproduced in paper[21]) by Bonč- Osmolovskaia.

[24]) G. White Grodstein, X-ray attenuation coefficients from 10 keV to 100 MeV. NBS circular 583 (1957).

† See a comparison table given in Bonč-Osmolovskaya[21]).

†† *Note added in proof*: Calculations are in progress at Stanford University (R. Pratt) and at Stockholm (Olsson, Nagel, Hultberg).

††† *Note added in proof*: Most recent papers on photoeffect are: Nagel, Arkiv för Fysik **18**, 29 (1960);
Pratt, Phys. Rev. **117** (1960) 1017; **119** (1960) 1619;
M. Gavrila, Phys. Rev. **113** (1959) 514; to be published in Phys. Rev.;
Erber (III Inst. of Tech., Chicago, unpublished).

TABLE I

Differential cross section in cm²/at steradian for photoeffect in K shell given by Sliv[23]) and Sauter[16]). Sauters values are in brackets (from[21])).

| $h\nu/m_0c^2$ | $Z$ | 20° | 30° | 45° |
|---|---|---|---|---|
| 2 | 20 | 4.0(4.5) | 2.2(2.5) | 0.75(1.0) $\times 10^{-26}$ |
| | 47 | 3.1(3.3) | 3.8(2.1) | 1.2(0.8) $\times 10^{-24}$ |
| 3 | 20 | 0.86(1.1) | 0.24(0.41) | 0.04(0.1) $\times 10^{-26}$ |
| | 47 | 1.48(0.84) | 0.44(0.3) | 0.07(0.07) $\times 10^{-24}$ |
| 5 | 20 | 0.7(2.6) | 0.12(0.7) | 0.015(0.15) $\times 10^{-24}$ |
| | 47 | 1.1(1.9) | 0.26(0.5) | 0.033(0.11) $\times 10^{-25}$ |

There are few calculations done for L photo electrons†. The ratio $\tau_K/\tau_L$ was recently measured and discussed by Hultberg[20]), and an extensive compilation of experimental data given and discussed by Bonč-Osmolovskaia[21]).

1.4.2. *Experimental work.* A systematic experimental study of photo electron distributions was initiated in Nobel Institute by Hedgran and continued by Hultberg in collaboration with several other physicists[25,20]). The whole work including previous investigations was summarised recently by Hultberg[20]). The measurements were done with the Nobel Institute 50 cm double-focusing spectrometer. In most recently published measurements uranium convertor was 2.19 mg/cm² thick and had a diameter of 1.46 cm. The entrance baffle was subtending an angle of 10° at the convertor. The gamma-ray source was rotated around the convertor at a distance of 3 cm. The angular distribution was measured for the gamma ray energies of 412, 662 and 1322 keV††. The peaks of lines obtained at different angles were plotted to produce the experimental angular distribution. The true distributions were obtained by applying to the experimental curves, the corrections derived theoretically and experimentally. The theoretical corrections were done by establishing a relation between the experimental and theoretical distributions in the form of an integral equation, which is then solved by an iteration method. The corrections were studied experimentally by measuring the ratio of intensity at the angle corresponding to maximum of distribution, to the intensity at zero angle, for different foil thicknesses and for various angles subtended by the radiator at the source. The ratios were then extrapolated to zero thickness and zero angle. The experimental, corrected and Sauter's theoretical distributions of K photo electrons for the energy of 412 keV are shown in fig. 10.

The most important difference between the corrected experimental and Sauter's theoretical distributions exists at large angles where the theoretical intensities are lower. The ratios of intensities at zero and maximum angle for the energy of 1332 keV agree with recent calculations by Sauter and Wüster[22]).

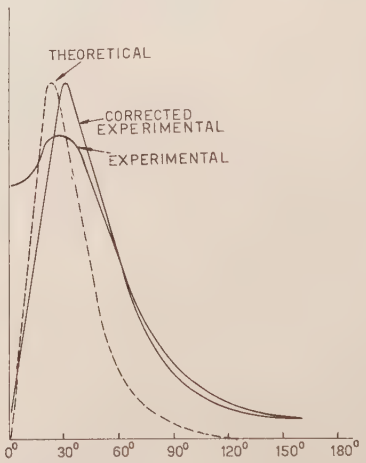


Fig. 10. The experimental corrected and Sauter's theoretical distribution of K photo electrons for the energy of 412 keV. From Hultberg[20]).

A convenient quantity for use in the external conversion work is the ratio of photo electrons emitted within a cone with opening angle $\theta$, to the $4\pi$ emission. It is given in fig. 11 for the energies of 412, 662 and 1332 keV.

† *Note added in proof*: See most recent work of Gavrila and Pratt, cited on the preceding page.

†† Latest list includes the following cases: 103, ($L_I$ + $L_{II}$, $L_{III}$, M); 159 (K, $L_I$ + $L_{II}$, $L_{III}$); 208, 279 (K); 412, 662, 1118, 1332 (K, L, M + N + . . .) (Priv. commun. from S. Hultberg).

[25]) A. Hedgran, Arkiv för Fysik **5** (1952) 13; A. Hedgran and S. Hultberg, Phys. Rev. **94** (1954) 498; S. Hultberg, Arkiv för Fysik **9** (1955) 245; S. Hultberg and T. Novakov, Nucl. Phys. **4** (1957) 120; S. Hultberg and R. Stockendal, Arkiv för Fysik **15** (1959) 33.

1.5. INTENSITY MEASUREMENTS

The preceding discussion shows that the theoretical basis for precise external photoconversion measurements is not quite satisfactory. One of the most important factors is the angular distribution, but we do not even know the error which is introduced when the Sauter formula is used. On the other hand, scattering and energy losses, coupled with geometries, present tedious mathematical problems, and there is no sense in wasting much time to solve them with mathematical computors, before angular distributions are better known.

The corrections used by various authors are all more or less approximate. That can be seen from table 2 where some of the most important papers on the external conversion are briefly summarised. The first work, by Ellis and Aston[26]) is remarkably thorough, considering the state of physics at that time. Their work was further improved by Martin and Richardson[27,28]) who

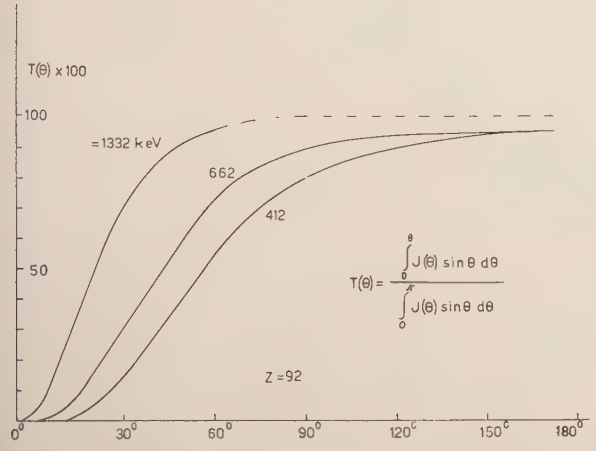


Fig. 11. Ratio of K photo electrons emitted within a cone with opening angle $\theta$, to the $4\pi$ emission. From Hultberg[20]).

recognized however that some discrepances in the intensity measurements might be due to angular distribution variation, caused by energy changes, which were not taken into account. Deutsch *et al.*[29]) preferred a semi-empirical approach, relying on experimental calibration. A detailed theoretical analysis, followed by experimental calibrations was done by Thomas and Lauritsen[30]).

The measurements on photoelectron angular distributions, which were done in Nobel Institute by Hultberg and collaborators stimulated the work on external conversion, and their results were immediately used by other groups in Uppsala, Copenhagen, Amsterdam and Belgrade[31–36]). The initial approach was based on following three points:

1. Use of simple geometries.

2. Use of very thin convertors to reduce the scattering.

3. Use of empirical angular distribution curves. Even uncorrected empirical curves are believed to be better than present theoretical curves.

Hultbergs formula given in table 2 may be then applied. It is derived with the following simplifying assuptions:

1. The source is taken as a point. Radiator is circular.

2. There is no photon absorption in either the source, beta absorber or the convertor.

3. No integration over entrance aperture is made. It is assumed that all electrons are moving to the center of the aperture and a multiplication with solid angle is made.

4. No correction for multiple scattering is applied, since the convertor was very thin.

Starting from this simple formula, more complicated geometries were successively analysed. Hultberg[20]) discusses the case of the extended flat source, by dividing it in smaller parts and concludes, that it is equivalent to a point source with a readjusted opening angle. He also gives formulae for the case of the rectangular convertor,

[26]) C. D. Ellis and G. H. Aston, Proc. Roy. Soc. **129** (1930) 180.

[27]) H. O. W. Richardson, Proc. Phys. Soc. A **63** (1950) 234.

[28]) D. G. E. Martin and H. O. W. Richardson, Proc. Phys. Soc. **63** A (1950) 223.

[29]) M. Deutsch, L. G. Elliot and R. D. Evans, Rev. Sci. Inst. **15** (1944) 178.

[30]) R. G. Thomas and L. Lauritsen, Phys. Rev. **88** (1952) 969).

[31]) S. Hultberg and R. Stockendal, Arkiv för Fysik **14** (1959) 565.

[32]) G. Bäckström and J. Marklund, Arkiv f. Fysik **17** (1960) 393.

[33]) O. Nathan and S. Hultberg, Nucl. Phys. **10** (1959) 118.

[34]) J. Marklund, O. Nathan and O. B. Nielsen, Nucl. Phys. **15** (1960) 199.

[35]) C. de Vries, Dissertation, Amsterdam 1960.

[36]) M. Mladjenović, T. Novakov and M. Župančić, Bulletin "B. Kidrič" **10** (1960) 15.

TABL

| Authors | Type of spectrometer | Correction taken for | | | |
|---|---|---|---|---|---|
| | | Geometry | Energy loss | Angular distribution | Multiple scattering |
| Ellis, Aston[26]) | flat 180° homogenous field, permanent magnet | for cylindrical radiator, factor $C$ is given explicitly in this paper | by factor $\beta^2/(\beta)$ taken from early Bohr theory | no | no |
| Martin, Richardson[28]) | flat, 180° homogenous field | same as above | quantum mechanical $f(\beta)$ | no | no |
| Deutsch, Elliot, Evans[29]) | short lens | by factor $C$ empirically determined | by factors $K/\beta^3$ $K$ is empiricaly determined, $K = 6.4$ | no | no |
| Thomas Lauritsen[30]) | lens | by factor $< \sec\theta >$ | no | by factor $< \sec\theta >$ experimentaly determined | no |
| Hultberg[20]) | double focusing | source geom. by factor $g$ | can be included[20]) | factor $f$ accounts for angular distribution and convertor dimensions; for point source and circular convertor $f = \dfrac{\int_0^{\vartheta_\alpha} J(\vartheta + \Delta)\tan\vartheta\,\mathrm{d}\vartheta}{\int_0^{\pi} J(\theta)\sin\theta\,\mathrm{d}\theta}$ For the rectangular case: see text | no |

which is commonly used in double focusing spectrometers. Angular distribution factor $f$ is then

$$f = \frac{2}{\pi}\frac{\int_0^{\vartheta_2} J(\vartheta+\Delta)\tan\vartheta\,[\arcsin(\tan\vartheta_0/\tan\vartheta) - \arccos(\tan\vartheta_1/\tan\vartheta)]\,\mathrm{d}\vartheta}{\int_0^{\pi} J(\theta)\sin\theta\,\mathrm{d}\theta}$$

where $\vartheta_0$, $\vartheta_1$ and $\vartheta_2$ measure the radial and axial extensions of the convertor and the source. The above formula for point source is illustrated in fig. 12, where $\tau_K f$ values are given for three convertor

| Relation for intensity | Notation | Remarks |
|---|---|---|
| eak height $h_K$<br>$_K = I\tau_K H\rho\beta^2 f(\beta)\cdot C$ | $I$-number photons/sec | Very thick convertor (> 500 mg/cm²)<br>Line shape approx. energy independent |
| $h_K = \dfrac{I\tau_K H\rho\beta^2 C}{nZ\left(\ln\dfrac{Rm^2c^4\beta^4}{J^2Z^2(1-\beta^2)^{\frac{3}{2}}} + 1 + \beta^2\right)}$ | $n$ = number of atoms/cm³<br>$J$ = 13.5 eV<br>$R = \dfrac{\Delta(H\rho)_0}{H\rho}$<br>with $\Delta(H\rho)_0$ = most probable momentum loss | Authors believe that the formula is not very precise, because the angular distribution has not been taken into account |
| $h_K = \dfrac{t_r\tau_K C}{\sqrt{\left(\dfrac{Kt_r}{\beta^3\Delta p}\right)^2 + 1}}$ | $t_r$ = convertor thickness in g/cm²<br>$\Delta p$ = width of transmited momentum | Accuracy = ± 20% |
| area $A$<br>$A = I\dfrac{\Omega}{4\pi}\tau_K n t_r < \sec\theta > \varepsilon\,\Delta p$ | $\varepsilon$ = line shape factor = 1.064 for Gaussian | Main correction factor $< \sec\theta >$ criticaly depends on source-convertor geometry and convertor thickness. |
| absolute intensity<br>$A = I\,\Omega_t\tau_K b t_r f g$<br>relative intensity<br>$I = \text{const} \times \dfrac{A}{\tau_K f g}$ | $Q_t$ = transmission<br>$b = 6.025 \times 10^{-4}$ m<br>$t_r$ = convertor thickness in mg/cm²<br>$J(\theta)$ = probability of photo-electron emission solid angle angle (angular part) | Hultberg estimates errors at<br>$f \approx 1$ 3%<br>$\tau_K \approx 5$% |

dimensions. This formula was integrated by Marklund *et al.*[34]) for the case of rectangular source and results presented in form of a geometry factor $g_{ls}$ given in fig. 13.

Although the use of empirical angular distributions has increased the accuracy of photo electron intensity determinations, the total uncertainly is in most routine measurements over 8%. Hultberg estimates† errors to be

1–3% for $f$ 5 % for $\tau_K$ .

† Private communication.

Even if it were so, there might remain other sources of errors, such as geometry, scattering and statistics of measurements. There is no doubt that in

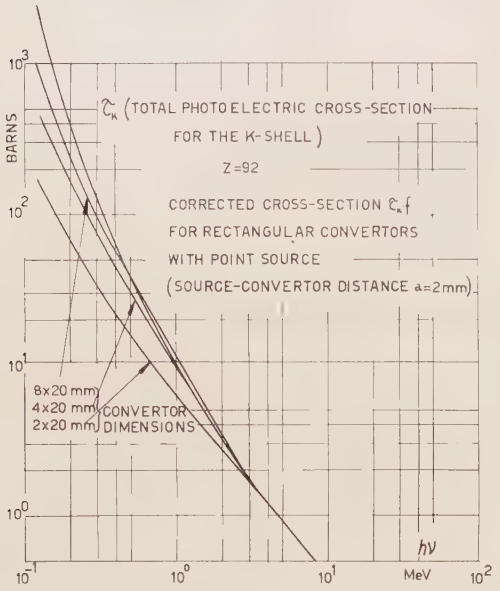


Fig. 12. Values of $\tau_K f$ for three rectangular convertors and point source. From[34]).

future more experimental work would be done to test the importance of various factors. One of the most convenient sources would be $Na^{24}$,

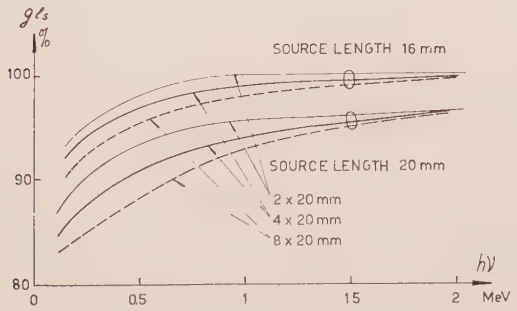


Fig. 13. Relative efficiency $g_{ls}$ of rectangular convertors with line sources. From [34]).

but we have to wait the completion of angular distribution measurement at 2.6 MeV, which is now being done in Nobel Institute by Sujkowski.

### 1.6. ENERGY MEASUREMENTS

High resolution measurements of external conversion spectrum, with line widths of 0.3–0.5%, facilitate rapid and fairly precise energy determinations. This question is discussed by Lind and Hedgran[37]), who show that a precision of 0.05% in energy determination can be achieved.

The case of thicker convertors and the line widths over 1% was discussed by Hornyak, Lauritsen and Rasmussen[38]). They found experimentally that for convertor thicknesses between 7 and 80 mg/cm², for a resolution of 1.5% and energies up to 1.3 MeV, the intersection of the extrapolated front edge with the background is independent of the convertor thickness to within 0.2%. The case of weak lines, when energies have to be determined by peak position was also investigated by them, and it was found that the peak shift is of the order of most probable energy loss.

### 1.7. CONCLUSIONS

The gamma-ray energies can be determined by external photo conversion with a precision of 0.1–0.2% in routine measurements and 0.05% in special high precision experiments.

The intensities are at present measured with an error of about 5–10% or more. In order to improve the precision of intensity measurements, further work is needed on the following subjects:

1. More exact theoretical formulae for the angular distributions of photoelectrons in different shells should be derived.

2. Total photoelectric cross-sections for different shells should be available, computed with higher precision, than the present one, which is estimated at 5–15%.

3. Further experimental determinations of angular distributions for more closely lying energies, over the whole energy range of interest, would be very helpful.

4. When the correct theoretical angular distributions become available, it would be interesting to use the computors to find out the corrections due to geometry and multiple scattering, for typical source-convertor set-ups.

[37]) D. Lind and A. Hedgran, Arkiv f. Fysik **5** (1952) 29.
[38]) W. F. Hornyak, T. Lauritsen and V. K. Rasmussen, Phys. Rev. **76** (1949) 731.

## 2. Compton Line Measurements

When Compton effect is used to measure the gamma-spectra, the main difficulty is that the spectrum is continuous, the energy of electrons depending on the angle of ejection relative to the direction of incident gamma-ray. A relatively narrow line, about 2–5% wide, can be obtained by selecting only a small part of the spectrum

sections for the ejection of the electron at an angle $\theta$, per unit angle, $d\sigma(\theta)/d\theta$ given by the relation.

$$\frac{d\sigma(\theta)}{d\theta} = \frac{8\pi r_0^2(1+\alpha)}{1+(\alpha+\frac{1}{2}\alpha^2)\,\mathrm{vers}\,2\theta}\,\frac{b}{(1+b^2+2\alpha)^2}\left[\frac{b^4+1}{b^2+1}+\frac{2\alpha^2}{(1+b^2+2\alpha)}\right]$$

where

$$\alpha = h\nu/m_0c^2, \quad r_0 = e^2/m_0c^2, \quad b = (1+\alpha)\tan\theta\,.$$

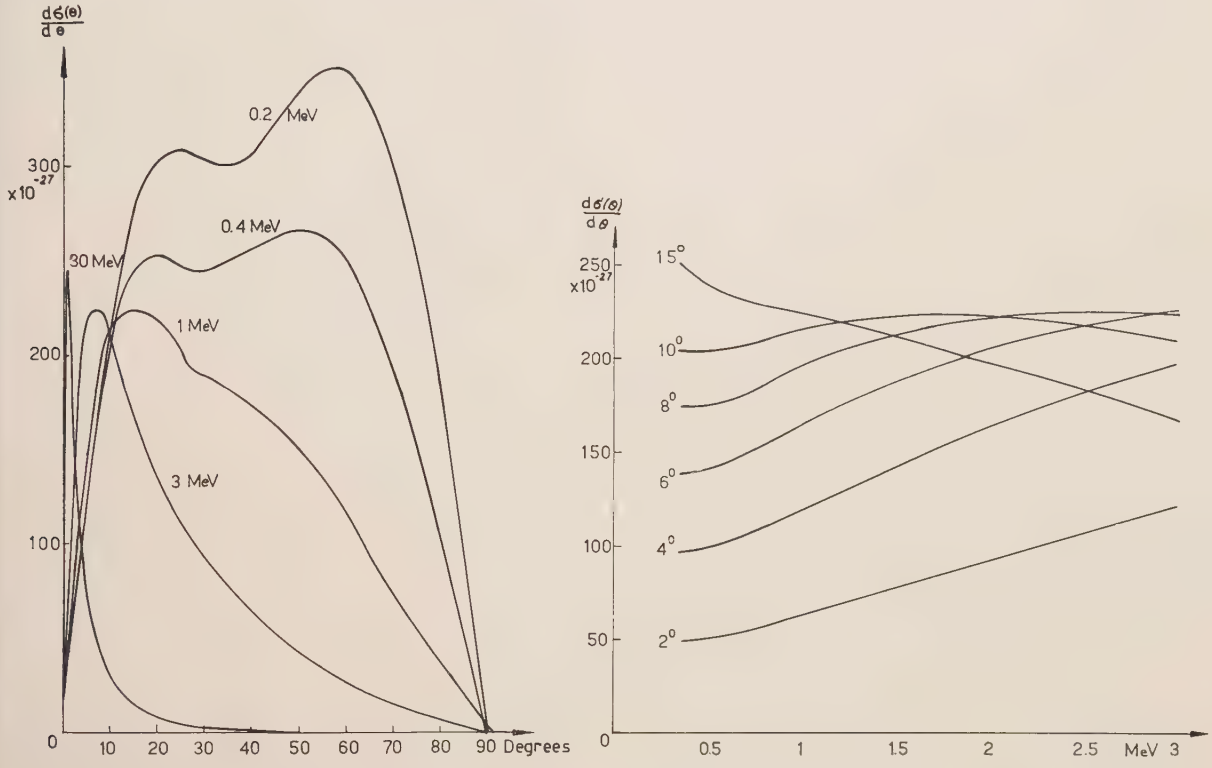


Fig. 14. Differential cross-section $d\sigma(\theta)/d\theta$ in cm² per electron for the number of electrons projected per unit angular interval (radians) at angle $\theta$.

("Compton line" method). The geometry must be such that only the electrons ejected within a small angular interval are accepted by entrance baffles of the spectrometer. This can be done if the gamma-ray beam is quasi-parallel. The solid angle which the radiator subtends at the source is then nearly two orders of magnitude smaller than it is in the case of external photo-conversion and the efficiency is correspondingly reduced.

### 2.1. COMPTON ELECTRON DISTRIBUTIONS AT SMALL ANGLES

The important data necessary for designing of Compton electron spectrometers are the cross-

This equation was computed for energies from 10 keV to 30 MeV and results given in tables, by Johns *et al.*[39]). We reproduce the angular distributions for certain energies and angles in fig. 14. It can be seen that Compton electron distributions tend to approach the forward direction as the energy increases, so that although the total cross section decreases with the energy, the number of electrons emitted within a small cone in the forward direction increases. For energies up to 3 MeV, the cross section per angle increases with the energy up to the angles of 10°. For higher

[39]) H. E. Johns, D. V. Cormack, S. A. Denesuk and G. F. Whitemore, Canadian J. Phys. **30** (1952) 556.

energies (10–30 MeV) most of the ejected electrons are concentrated in the forward cone with the angles $\theta$ of 10°–5°. For these reasons central beam spectrometers are more convenient for the measurements of Compton lines.

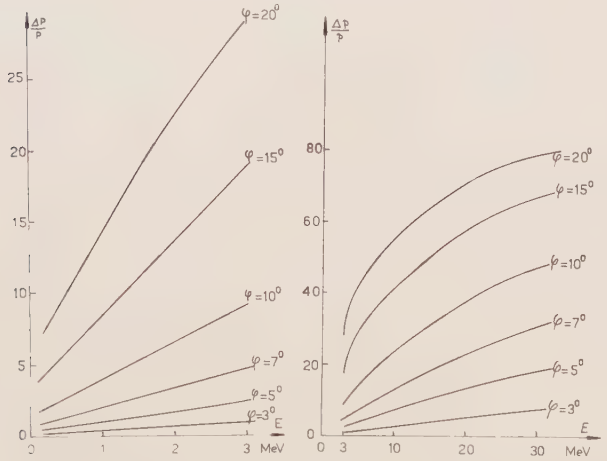


Fig. 15. Relative momentum width of Compton electrons.

Another quantity of interest is the relative momentum width of the electron beam accepted by the entrance baffles. In the central beam apparatus, with an aperture $\theta_0$, the relative momentum width $\Delta p/p$ is given by

$$\frac{\Delta p}{p} = \left[1 - \frac{(2\alpha + 1)\cos^2\theta_0}{(1-\alpha)^2 - \alpha^2\cos^2\theta_0}\right]\left(\frac{1+\alpha}{2+\alpha}\right).$$

This relation is shown in fig. 15, for several small angles. The relative width increases with the energy. It is about 1% at 1 MeV for an aperture of 5°.

## 2.2. SPECTROMETERS

Among the conventional types of spectrometers, the double focusing instruments are most convenient for Compton line measurements, because they have a central beam, a relatively large radiator can be used, the detector may be well shielded from strong sources and resolution-transmission characteristics are good. The only inconvenience is that the source with heavy shielding has to be mounted in the spectrometer[2]). A sector double-focusing with a source outside would be better for this purpose.

The geometry for Compton line measurement is shown in fig. 16, which is taken from Mladjenović and Hedgran[2]). The importance of entrance baffles and radiator thickness is illustrated in fig. 16(b), where the line widths are given as functions of these parameters.

Various other conventional types of spectrometers have been used for Compton lines measurements, such as lenses[40]) and the homogenous field flat spectrometer[41,42]).

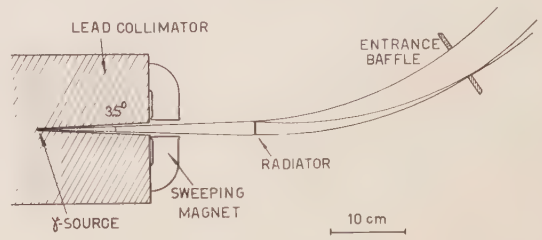


Fig. 16a. Geometry for Compton line measurements in double-focusing spectrometer.

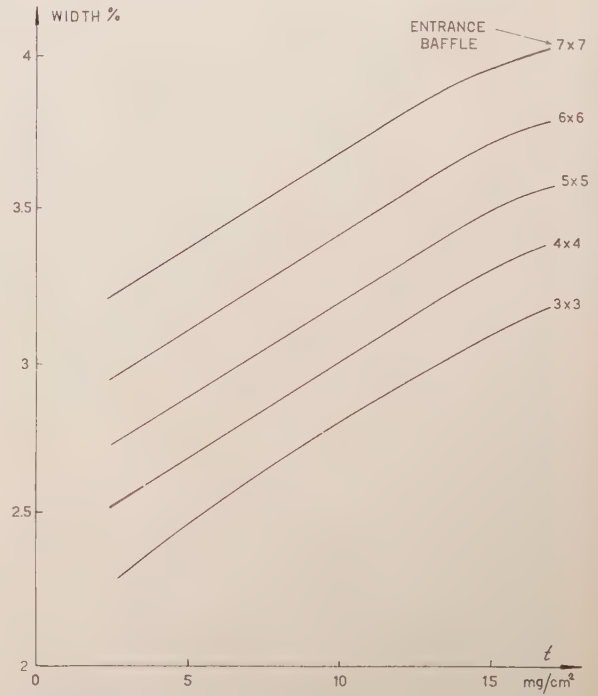


Fig. 16b. Dependance of line width on radiator thickness and the aperture, for gamma ray energy of 1.3 MeV. From[2]).

[40]) W. K. Rasmussen, W. F. Hornyak, C. C. Lauritsen and T. Lauritsen, Phys. Rev. **77** (1949) 617.

[41]) D. G. Martin and G. Parry, Physica **18** (1952) 1157.

[42]) G. D. Latyshev, A. F. Kompaneetz, N. P. Borisov and I. M. Gusak, J. Phys (USSR) **3** (1940) 251.

Several new types of spectrometers were especially designed for Compton electron measurements. We shall briefly discuss three of them:

1. Motz *et al.*[43]) described an homogenous field flat type of spectrometer, with the gamma-ray source and detector outside the field. The angle of beam deflection is 55°. (Fig. 17.) Beryllium radiator was 1.3 cm long and 0.37–0.8 cm wide. Its thickness was from 1 to 10 mils. The aperture angle was about 3°. The typical performance of this spectrometer is as follows

TABLE 3

| Foil size in path of photon beam | Number of photons required per cm² at position of foil to produce one count at the detector | Resolution (%) |
|---|---|---|
| 1 mil thick<br>3.7 mm wide<br>1.3 cm long | $1.6 \times 10^5$ | 2.8 |
| 3.7 mils thick<br>4 mm wide<br>1.3 cm long | $9.2 \times 10^4$ | 4.9 |
| 5.5 mils thick<br>4 mm wide<br>1.3 cm long | $7.5 \times 10^4$ | 8.7 |
| 10.3 mils thick<br>4 mm wide<br>1.3 cm long | $6.5 \times 10^4$ | 17.0 |

2. The gamma-hodoscope was proposed by Dželepov[44]) and constructed by Tschubinskii[45]). The design principle is illustrated on fig. 18. A collimated beam of gamma rays is falling on a radiator situated between flat pole-pieces which produce an homogenous magnetic field. Compton electrons ejected in a plane parallel to the pole-pieces, or at a small angle to it, follow circular paths and pass through three rows of Geiger counters. Triple coincidences are recorded on a display, on which each counter is represented by a glow tube. There are $10^3$ possible combinations of triple coincidences. Knowing the three points of electron trajectory, it is possible to calculate the energy by neglecting the axial component and by assuming that all trajectories are in the median plane.

The spectrometer chamber is filled with 26 cm of helium and 4 cm of methan, because there are no windows on the Geiger counters. The scattering is important at low energies, so that is preferable to measure the energies above 1.5 MeV. The line form depends on several factors. Besides the scattering in the gas which increases the line widths, there is also scattering from Geiger counters, which produces tails on both sides of the line. The full width at half maximum vary from 10–12% at 1 MeV, to 6% at 4 MeV (fig. 19).

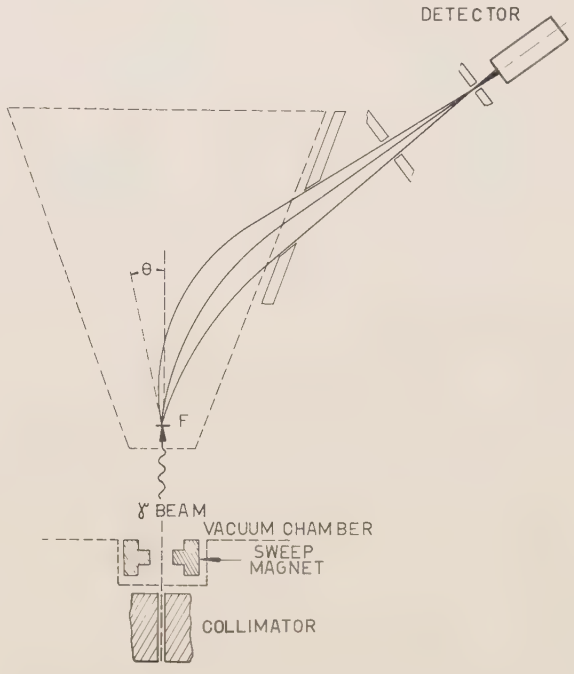


Fig. 17
Sketch of Compton spectrometer designed by Motz *et al.*[43]).

A part of the spectrum is measured simultaneously. For instance, at 600 gauss, the energy interval from 1.2 to 2.4 MeV is covered. The same energy may be measured at different field strengths, but the height of the line would vary, being maximum when the electrons ejected in the center of the radiator follow the central ray. For that reason spectral sensitivity curves are field dependent. Tschubinskii has computed spectral sensitivity curves under simplifying

[43]) J. W. Motz, W. Miller, N. O. Wyckoff, H. F. Gibson and F. S. Kiru, Rev. Sci. Instr. **24** (1953) 929.
[44]) B. S. Dželepov, Izvestia AN **21** (1958) 1580.
[45]) O. V. Tschubinskii, Izvestia AN **21** (1958) 1583.

assumptions that all electrons are moving in the median plane and neglecting the scattering and energy losses (fig. 20). The intensities are measured with an error of 10–30%. The error in energy determinations is 1–3%.

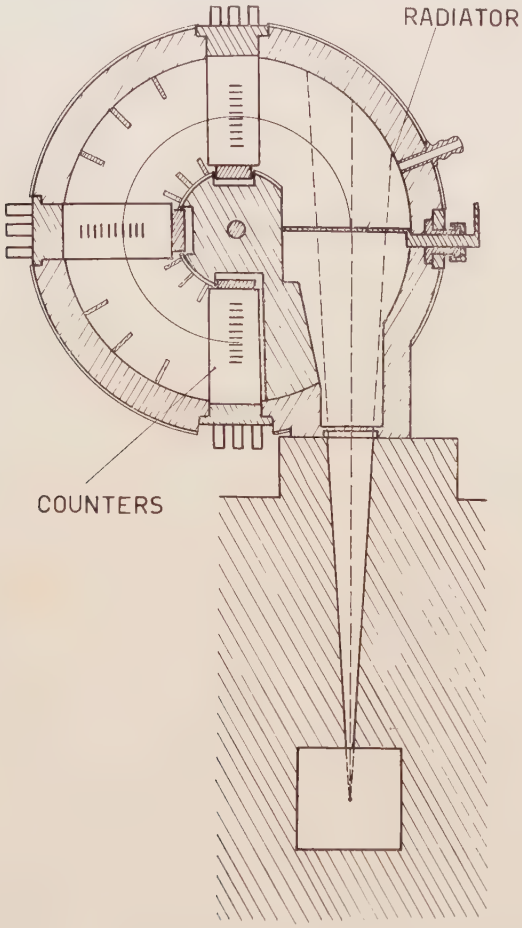


Fig. 18. Gamma-hodoscope.

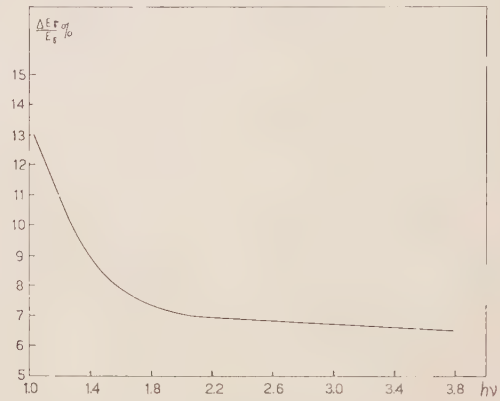


Fig. 19. Line widths in gamma-hodoscope.

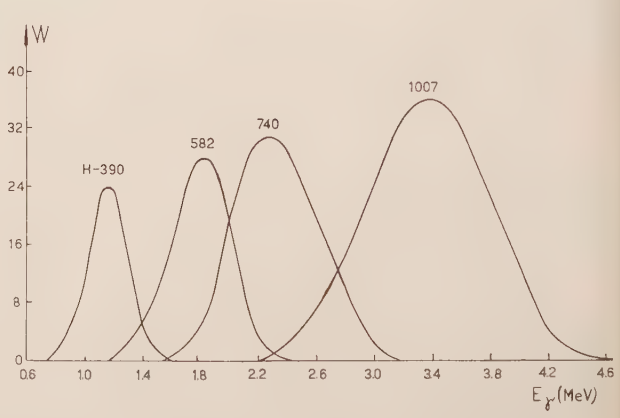


Fig. 20. Spectral sensitivity curves for gamma-hodoscope.

According to Tschubinskii, the main advantages of this spectrometer are the following:

(a). Spectrometer is designed to measure very weak gamma transitions. The natural background is reduced by triple coincidences to 1 count per 6 hours. It is possible to measure gamma rays in the energy range from 2 to 4 MeV with the intensity of $10^{-5}$–$10^{-6}$ quanta per disintegration, for a source 1c strong.

(b). A part of the spectrum is measured simultaneously, which is convenient for short lived sources or work with accelerators.

It should also be mentioned that the same type of spectrometer may be adapted for the measurement of weak, high energy beta transitions†. The beta ray source is then placed at radiator position.

3. Another Compton electron spectrometer, proposed and developed by Dželepov and his collaborators in Leningrad[46–50]), was first called ritron and an improved version was named

† Private communication by B. S. Dželepov and Tschubinskii.

[46]) B. S. Dželepov and M. L. Orbeli, Dokladi AN **62** (1948) 615.

[47]) B. S. Dželepov, Dokladi AN **77** (1951) 389.

[48]) B. S. Dželepov, N. Žukovskii, Y. Holnov, Izvestia AN **18** (1954) 599.

[49]) B. S. Dželepov, N. Žukovskii, A. Karamian and S. Šestopalova, Izvestia AN **17** (1953) 518.

[50]) B. S. Dželepov, S. A. Šestopalova, Izvestia AN **20** (1956) 328.

elotron. Others were later built in several laboratories in USSR[51]).

This type of apparatus consists essentially of two flat spectrometers, the focus of the first one coinciding with the source of the second one

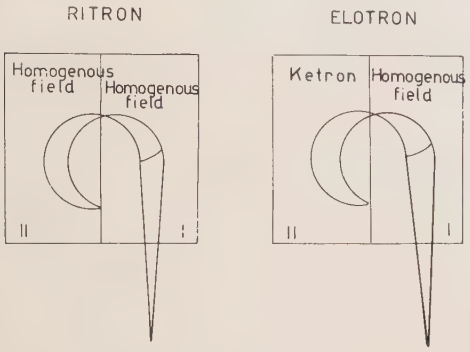


Fig. 21. Schematical drawings of ritron and elotron geometry.

(fig. 21). The contribution of the source width to the resolution is then not determined directly by the radiator dimensions, but by the extension of the first focus. In the first paper on this spectrometer[46]) Dželepov and Orbeli show that it should give an order of magnitude better intensity than an ordinary homogenous field flat spectrometer[42]) used under similar conditions.

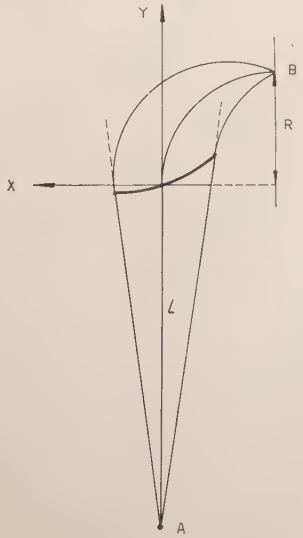


Fig. 22. Radiator shape in electron.

Dželepov[47]) has calculated the shape of the radiator, so that the electrons ejected in the direction of slightly diverging gamma-rays, after deflection of 90° in an homogenous magnetic field fall into a line focus (fig. 22). The shape of the radiator is given by equation:

$$(x+1)^2 + (1-y)^2 = z\,\frac{x+y+L(x+1)}{\sqrt{x^2+(L+y)^2+z^2}}$$

where $L$ is source-radiator distance (see fig. 22). It may be approximated with a cylinder, the axis of which is parallel to magnetic field.

In ritron the second spectrometer is an homogenous field flat type with the 180° focusing. It is described in detail by Dželepov, Zukovskii and Holnov[48]).

An improved version called elotron was first reported by Dželepov *et al.*[49]) and later described in detail by Dželepov and Šestopalova[50]). In elotron, homogenous field spectrometer was replaced by ketron.

Before we continue with elotron, we should summarise briefly the characteristics of ketron. They are described in references[52–56]). Ketron is a combination of homogenous field and the field decreasing in one direction. The source and detector are in the homogenous field and the

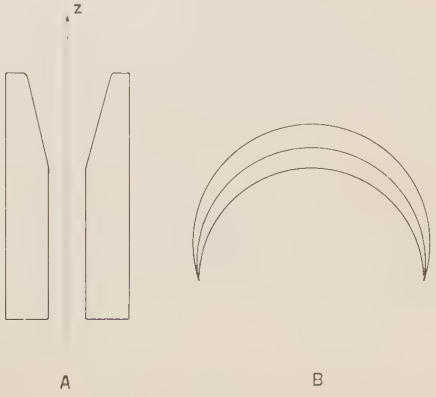


Fig. 23. Ketron. A. Shows the form of pole-pieces producing field falling off in $z$-direction; B. Trajectories pass partially through inhomogenous part of the field.

[51]) L. V. Grošev, B. P. Adijasevich and A. M. Demidov, Proceed, Geneva Conference 1955, vol. 2, p. 39. (Ketron replaced by radially decreasing field.)

[52]) M. Korsunskii, V. Kelman and B. Petrov, JETP (1944) 394.

[53]) B. S. Dželepov, and A. A. Bašilov, Izvestia AN **14** (1950) 263.

[54]) P. P. Pavinskii Izvestia AN **18** (1954) 175.

trajectories pass partially through the inhomogenous field. The shortest trajectory passes tangentially at the limit between the two fields. The pole shapes and the trajectories are shown in fig. 23. This spectrometer has radial and axial focusing. Axial focusing does not appear to be so

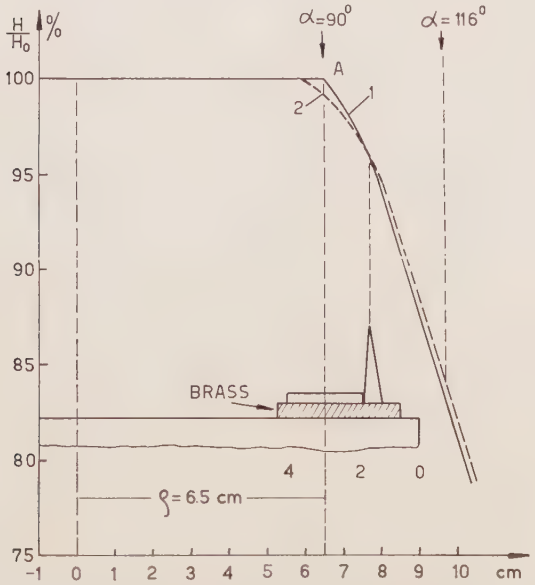


Fig. 24. Schimming for ketron field.
1. Theoretical field shape. 2. Experimental.

good as in the Siegbahn–Swartholm double focusing spectrometers so that axial openings are small, while radial can be relatively large.

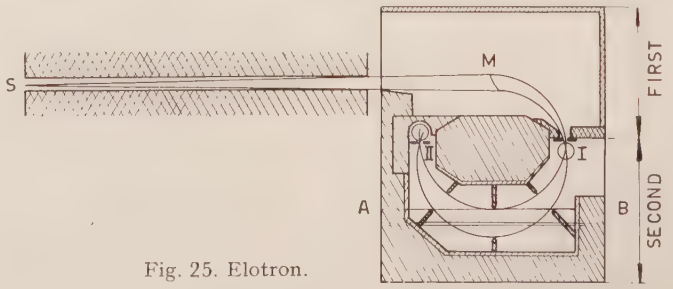


Fig. 25. Elotron.

According to Bashilov and Bernotas[55]) the resolution of this spectrometer is theoretically the same as in the flat homogenous field type.

Theoretical field shape has a discontinuity at the limit between the homogenous and inhomogenous field which is difficult to produce experimentally. Dželepov and Šestopalova use the empirically found shimming, shown in fig. 24 and get a field shape which deviates less than 1% from the theoretical.

We can now return to elotron (fig. 25). It has two counters, one in the intermediate focus and one in the final focus. In the early type of elotron, the counters had no windows and the whole chamber was filled with the gas at pressures from 120 to 380 mm Hg, and later on the resolution was improved by introducing counter windows and having the usual vacuum in the chamber.

Although larger elotrons have been built recently, no detailed description of their performances has yet been published, so that we shall give the early data of Dželepov and Šestopalova:

| | |
|---|---|
| source-radiator distance | 41 cm |
| radiator/celophane/: area | 2.1 × 1.2 cm² |
| thickness | 4 mg/cm² |
| radius of shortest trajectory | 6.5 cm |
| Full width at half maximum | from 5% at 500 keV to 2% at 2 MeV. |

Two new elotrons were reported at the 1960 Annual Meeting of Nuclear Spectroscopy in Moskow†. The full description was not yet published at the time this paper was completed. The Dželepov group[60]) reported an elotron with a radius of 26 cm. A line width of 1% at 1 MeV is

[55]) Bašilov and V. I. Bernotas, Izvestia AN **18** (1954) 192.
[56]) G. D. Latišev, A. G. Sergeyev, Y. M. Krisyuk. L. A. Ostrecov, Y. S. Yegorov and N. M. Širšov, Izvestia AN **20** (1956) 354.

† *Note added in proof*: Spectrometer reported by Grose[3]) was described in the meantime at the Vienna meeting on neutron physics, Sept. 1960 and in Izvestia AN **24** (1960) 791. It appears to be an excellent instrument made from two double-focusing sectors.

achieved, with an efficiency of $5 \times 10^{-10}$. Grosev's group[3]) reported a Compton spectrometer for (n–$\gamma$) measurements. The distance between the source and radiator is 5 meters. A line width of 0.3% can be produced, at energies over 2 MeVs, with an efficiency of $1.4 \times 10^{12}$.

It is quite probable that the elotron type of Compton spectrometers can be further improved. The most important problem in the design of Compton spectrometers is the efficiency, which requires high transmission. The homogenous and ketron fields used in elotron have both low transmission. Overall performances would probably improve with the use of double focusing fields, either the well known Siegbahn-Swartholm type with $n = \frac{1}{2}$ or still unexplored types with $n \neq \frac{1}{2}$ [57]).

Whenever the radiator is in the field, it has to have a special shape, which is not very convenient. With sector type of spectrometers, a flat radiator may be placed in the field-free region. This possibility shall be discussed in greater detail, in a forthcoming paper by Mladjenović.

### 2.3. ENERGY LOSS AND SCATTERING

Radiators are made of light materials such as aluminium, celophane or beryllium. These materials have $Z/A$ approximately equal to 0.5, so that the full width at half maximum of the energy loss distributions becomes

$$\Gamma = \frac{305}{\beta^2} \sigma \quad \text{(eV)} .$$

It is about 30% larger than the corresponding width in uranium foils of the same surface density. The widths as functions of energy and foil thickness are shown in fig. 6.

Compton spectra are usually measured with a line width of 3–5%, and the energies are greater than 0.5 MeV. We see then that radiator thicknesses of about 10–20 mg/cm² would make a contribution to the width smaller than 1%.

Multiple scattering is smaller in light material. According to the Bothe formula, the mean angle of deflection is proportional to

$$\left(\frac{z^2 + z}{A}\right)^{\frac{1}{2}} .$$

The values of this expression are given for some materials in the following table

| | Be | C | Al | U |
|---|---|---|---|---|
| $\left(\frac{z^2 + z}{A}\right)^{\frac{1}{2}}$ | 1.47 | 1.87 | 2.27 | 6 |

It follows that the scattering is appreciably diminished by using the material with lowest possible $Z$, and beryllium is therefore the best choice.

The mean angles of deflection are given in fig. 8.

### 2.4. INTENSITY MEASUREMENTS

The corrections for geometry and scattering are somewhat simpler for Compton electron lines because:

1. All the cross sections including the one for the angular distribution are precisely known.

2. The source is far away from the radiator, so that usually it can be considered as a point source, and the gamma-ray beam has a small opening angle which can be precisely determined.

Latyshev *et al.*[42]) computed the corrections by solving the electron diffusion equation, earlier given by Bethe, Rose and Smith[59]).

Holnov[58]) obtained the spectral sensitivity curve for ritron, by dividing the radiator into small elements, and computed the multiple scattering effects according to a previous analysis by Dželepov[15]). Russian physicists working with elotrons in general prefer to use the spectral sensitivity curves, obtained experimentally by measuring the spectra with well known intensity ratios.

The case of Compton electron measurements with lens spectrometer was discussed in detail by Pasadena group. Thomas and Lauritsen[30]) first derived an exact expression for the number of

[57]) M. Mladjenović, Nucl. Instr. and Meth. **7** (1960) 11.

[58]) Y. Holnov, Disertation, Radium Institute, Leningrad, 1952.

[59]) H. A. Bethe, M. E. Rose and L. P. Smith, Proc. Am. Phil. Soc. **78** (1938) 573.

[60]) V. Vitınan, B. Dželepov and A. Karan, Annual Meeting of Nuclear Spectroscopy, Moscow 1960.

Compton electrons ejected into the effective spectrometer solid angle $\Omega$, from an infinitely thin radiator. The effect of scattering and energy losses is then taken into account by introducing a factor $\mu_e$, by which the differential electron path length (in the direction of the spectrometer acceptance solid angle) is to be multiplied in order to obtain the energy loss in the convertor. The number of electrons (emerging from the radiator into the spectrometer effective solid angle $\Omega$) in the energy range

$$x \quad \frac{E_\gamma}{E_\gamma} \quad \frac{E_e}{} \quad \text{to} \quad x \; + \; dx$$

is given by

$$CYF(x)\ \Omega \frac{\mu_e}{1}\, dx$$

where

$$C = \tfrac{1}{4} Z N r_0 m_0 c^2$$

is constant for given radiator material

$Y$ = yield for a particular radiation from the source

$F$ = an integrated form of the energy dependent part of Klein-Nishina formula. It is given explicitly in [31]).

The factor $CYF$ can be precisely computed. Effective solid angle $\Omega$ has to be determined for a given spectrometer geometry, but $\mu_e$ is more complicated to derive. The authors show how to compute approximately $\mu_e$.

Comparison with the observed spectrum can be done after folding the above distribution with the spectrometer window curve. They find that the intensities can be determined in this manner with an error within 10%.

A detailed discussion of corrections for central beam spectrometers was given by Motz *et al.*[43]). They give the following relation for the peak counting rate $R(k)$.

$$R(k) = P(k) n\ T(t,k)\ A \int_0^{\frac{1}{2}\pi} f(\theta) \frac{d\sigma(k)}{d\theta}\, d\theta$$

where

$P(k)$ = photon flux in photons/cm²/sec
$n$ = number of electrons/cm² in foil
$T(t,k)$ = scattering correction
$A$ = area of the foil in the beam, in cm²
$\frac{d\sigma(k)}{d\theta}$ = Klein Nishina differential cross section in cm²/electron
$f(\theta)$ = fraction of the electron leaving foil at angle which can be focused at the detector.

The quantity $T(t,k)$ contains two factors, which are $T_{el}$ accounting for scattering and $T_d$, representing the energy loss. Authors assume that scattering out is more important than scattering into entrance baffles. The reduction in peak counting rate $T_{el}$ is obtained in series form, after integrating over the foil thickness an appropriate Gauss curve, representing the broadening. On the other hand, authors do not give an analytical relation for energy loss factor $T_{el}$. They calculate the energy loss from the stopping power formula, and by broadening the line over that energy interval (in momentum units), obtain the corresponding peak reduction.

In the case of circular entrance baffle, $f(\theta)$ would be a simple rectangular function, equal to unity for angles from zero to aperture angle $\psi$, and equal to zero for angles greater than $\psi$. The baffles have usually a rectangular form and the focusing also contributes to angles accepted into spectrometer, so that $f(\theta)$ has to be calculated for each given geometry. The authors give $f(\theta)$ for their spectrometer.

The authors tested their intensity analysis procedure by measuring the gamma-rays from $Na^{24}$, and found an agreement within 3%.

### 2.5. DETERMINATION OF ENERGIES

The measurement of energy of Compton electrons is simpler in the central beam spectrometer. When the lines are resolved, the extrapolated edge gives the momentum of electrons with maximum energy. The precision is greater with thin foils, and for usual thicknesses it is about 1%. If the lines are not resolved, peak values have to be used and a correction for peak shift due to energy loss has to be made. Motz *et al.*[43]) assume that the peak is located at the energy

$$E_{max} - \tfrac{1}{2} \Delta E$$

where $\Delta E$ is the most probable energy loss when all electrons traverse the given radiator thickness, which can be calculated from Landau's formula. They find that this procedure gives precision of about 2%.

### 3. Comparison of Photo and Compton Methods

Finally it might be of interest to compare typical performances of photo and Compton methods. Since many different arrangements are being used, the choice of "typical" parameters is by no means unique, and does not demonstrate necessarily all the possibilities of a given method. Still, such a comparison can show some of the main characteristics and can serve as a rough guide.

We shall take the following parameters:

a. EXTERNAL CONVERSION

convertor = uranium foil 1 cm², thickness $d = 1$ mg/cm² effective solid angle of the spectrometer = 0.25%, half aperture of the cone from source to circular radiator, $\vartheta_0 = 70°$.

b. COMPTON SPECTRUM

radiator = beryllium foil 1 cm², thickness $d = 1$ mg/cm² solid angle subtend by source at radiator = $1.2 \times 10^{-3}$ of $4\pi$, electrons emitted between 0 and 5° accepted into spectrometer.

The number of photons of a given energy which should be emitted isotropically from the source, to produce one electron in the spectrometer counter is given as function of energy in fig. 26. The following conclusions could be made.

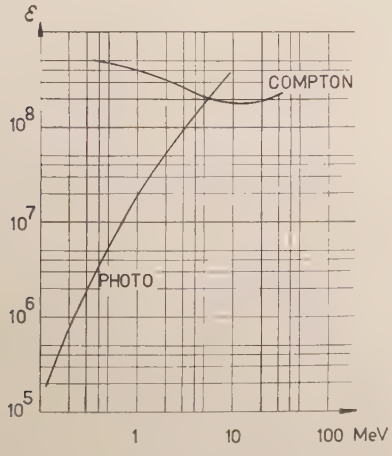


Fig. 26 Efficiency of photo and Compton measurements.

1. Weaker sources may be measured with photo conversion, especially at lower energies. If there is no high continuous Compton background or another unresolved photo line in neighbourhood, external conversion lines could be obtained with gamma-ray intensities of about 10$\mu$c at 100 keV to 10mc at 2 MeV.

2. The parameters were chosen to give the line width of 0.5% for photo and 3% at 1 MeV for Compton spectra. The line width decreases with energy increase for photo spectra, while Compton lines are broader at higher energies, because larger energy intervals are accepted by spectrometer entrance baffles. The line width of photo lines can be reduced to 0.1–0.2%, which is practically impossible with Compton lines.

The most important disadvantage of photo conversion is the presence of continuous Compton background. In some cases this background may become so high that it is impossible to measure the weakest transitions in the spectrum. Then above stated advantages of external conversion are useless and the Compton method might be more appropriate, even at lower energies.

4. The Compton method becomes comparable to external conversion at energies, higher than few MeV. Its main problem is low efficiency. Further development of the elotron type spectrometers would be very useful.

### 4. Compton Spectrometer with Two-Directional Focusing Proposed by Lee-Whitting

Just before sending this manuscript to the editor, author received June 1960 the number of Canadian Journal of Physics, containing a paper with a very detailed discussion of an improved type of Compton spectrometer, written by Lee-Whitting. It is a new version of the elotron type improved by the use of two-directional focusing fields with $n \neq 0.5$. In the following we shall sketch briefly the main characteristics of the new spectrometer. The spectrometer is designed primarily for the measurements of gamma-rays from (n,$\gamma$) reactions. The source is then far away from the radiator, and the gamma ray beam may be considered in first approximation as parallel. The radial focusing in the median plane is shown in fig. 27. The magnetic field is cylindrically symmetric about an axis passing perpendicularly

through O, and can be represented in the median plane by the series

$$H_z(r_1 0) = H_0 \sum_{n=0}^{\infty} a_n \left( \frac{r - r_0}{r_0} \right)^n$$

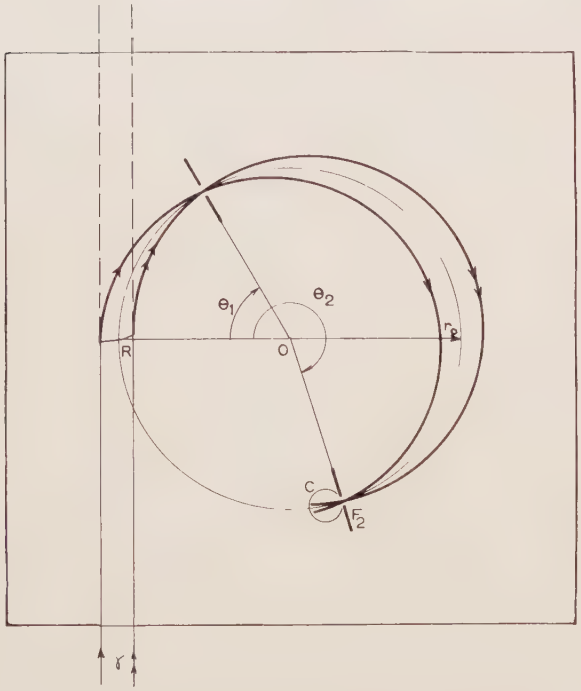


Fig. 27. Sketch of two-directional focusing Compton spectrometer proposed by Lee-Whiting. R = radiator, $F_1$ and $F_2$ are the first and second focus respectively.

The focalisation is determined by angles $\theta_1$, and $\theta_2$, and by first few coefficients $a_n$. (In the Siegbahn-Swartholm type $a_1 = -\frac{1}{2}$ and $a_3 = \frac{3}{8}$, $\frac{1}{8}$ or $\frac{2}{8}$.)

Lee-Whiting first calculates the shape of radiator which he assumes to have cylindrical shape for practical reasons. It turns out that it can be very roughly approximated by a flat foil inclined at a definite angle to the beam. The radiator shape for a point source is more complicated.

The electron beam is focalised twice radially, at $F_1$ and $F_2$, while axial focalisation is only achieved at $F_2$. The final choice of parameters is dictated by the need to minimize second order abberations, to achieve the optimum luminosity and to find a convenient geometry, removing the detector from the gamma-ray beam. Lee-Whiting considers in detail each of these factors, with the view to achieve the half widths of about 0.2%. He finally choses the following parameters

$a_1 = -0.14$
$a_2 = -0.505$
$\theta_1 = 46°42'$
$\theta_2 = 240°5'$

First slit width $= 2.2 \times 10^{-3} r_0$

Second slit width $= 3.2 \times 10^{-3} r_0$.

Angle between the radiator and the gamma-ray beam $= 45°52'$.

Radiator area $A$, efficiency $\varepsilon$ and radiator thickness $\xi$ depend on the energy. For 2 MeV, the optimum values are

$A = 5.8 \times r_0^2$
$\varepsilon = 3.2 \times 10^8$ photons/electron entering the slits.
$\xi = 0.37$ mg/cm² (radiator with $Z = 7$, $A = 14$).

These characteristics compare very favourably with those of spectrometers described on preceding pages.

At high resolutions considered by Lee-Whiting, the inherent Compton electron line width, due to the bound electron motion in the

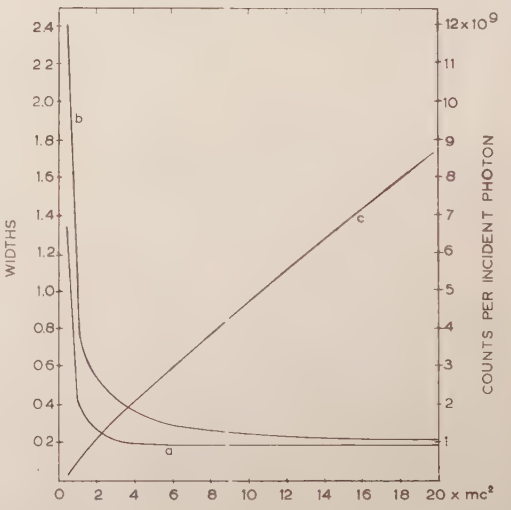


Fig. 28. Instrumental width (a), instrumental plus inherent widths (b), and the efficiency (c) of the Lee-Whiting Compton spectrometer, as function of gamma-ray energies in $mc^2$ units.

radiator atoms, become important, especially at low energies. This question was also treated by Lee-Whiting. The results applied to the spectro-

meter with above given characteristics, is shown in fig. 28. Curve (a) represents the instrumental line width as function of energy in $mc^2$ units. When inherent widths are added, curve (b) is obtained. One should also note important increase of the efficiency with energy, shown by curve (c).

At the end of his paper, Lee-Whiting calculates the shape of the iron pole pieces which should produce the desired field.

The spectrometer proposed by Lee-Whiting represents an important advance in this field and the completion of the apparatus itself shall be eagerly awaited by the physicists interested in this type of measurements.

**Acknowledgements**

Thanks are due to Director of "B. Kidrich" Institute of Nuclear Sciences for the permission to use Institutes facilities while preparing this paper. The author is grateful to Dr. S. Hultberg for remarks, suggestions and information on some most recent works.

## COMPUTER SERVICE FOR CALCULATION OF THE PHOTOELECTRIC *f* FACTOR

*Sample of form,* issued to be filled out and sent to the "BESK *Service", Nobel Institute of Physics, Stockholm 50, Sweden,* for a calculation on the Swedish electronic computer BESK of the photoelectric *f*-factor. For the definition and use of *f*, see S. Hultberg and R. Stockendal, Arkiv för fysik **14** (1959) 565; S. Hultberg, Arkiv för fysik **15** (1959) 307, section H; S. Hultberg and Z. Sujkowski, Phys. Rev. Letters **3** (1959) 227. The calculations take the finite dimensions of the source into full account. This means that the source can be allowed to be *larger* (along one or both dimensions) than the converter. Rectangular shape is assumed for both source and converter. The calculations are based on experimentally measured photoelectric angular distributions $J(\theta)$ for uranium, but they can equally well be performed on any other $J(\theta)$, if specified numerically. The gamma-ray attenuation in the material that is usually put in between source and converter to absorb beta-rays and internal conversion electrons is taken into account correctly if the parameters $g$ and $Z_{abs}$ are specified below.

Each calculation results in two *f* factors: $f_p$ and $f$. Here $f_p$ is the point-source value (i.e. with $c_Q = h_Q = 0$) and $f$ is the desired result for the actual source size. A comparison of $f_p$ and $f$ clearly shows the effect of source size ($f < f_p$). From the $J(\theta)$ functions now available for BESK calculations, $f$ can be found as a function of energy with an overall accuracy of approximately 1 %.

Calculated *f* factors are, at present, strictly valid only for uranium as converter material. There is, however, evidence that the $Z$ dependence of the *f* factor is rather weak. Also, the calculations are exact only for an infinitely thin source. However, the source thickness can easily be taken into account by averaging over calculations with different source-to-converter distances. So far the calculations apply only to the flat type spectrometer.

At present, the following $J(\theta)$ functions are available for *f*-factor calculations at BESK:

159 K, $L_I + L_{II}$, L; 208 K; 412 K, L, M′;

662 K, L, M′; 1118 K, L, M′; 1332 K, L, M′;

Here we use $L = L_I + L_{II} + L_{III}$ and $M' = M + N + \ldots$ Energies are in keV. It should be observed that the calculated *f* factors permit obtaining ratios of photoline intensities of different shells, at the same energy. Results will be returned to the applicant usually within three weeks after receiving the application. As far as free machine time can be granted by the Swedish Board for Computing Machinery this service will be free of charge.

August 1960 S. HULTBERG

**Sample of form, to be filled out** .....

| Experiment 1 | | Experiment 2 | |
|---|---|---|---|
| Parameters† | $J(\theta)$†† | Parameters† | $J(\theta)$†† |
| $c$ | | $c$ | |
| $h$ | | $h$ | |
| $c_Q$ | | $c_Q$ | |
| $h_Q$ | | $h_Q$ | |
| $a$ | | $a$ | |
| $m$ | | $m$ | |
| $g$ | | $g$ | |
| $Z_{abs}$ | | $Z_{abs}$ | |

† All lengths should be given in centimeters

†† $J(\theta)$ should be specified by showing energy and shell as in text above: 662 K, etc.

††† Cf. Arkiv för fysik **15** (1959) 307, Fig. 12.

*Definitions:*†††

| | |
|---|---|
| $c$ | converter half width |
| $h$ | converter half height |
| $c_Q$ | source half width |
| $h_Q$ | source half height |
| $a$ | source-to-converter distance |
| $m$ | converter-to-aperture distance |
| $g$ | absorber thickness |
| $Z_{abs}$ | $Z$ value of absorber |

Date: .....

Name: .....

Address: .....

Remarks: .....

NUCLEAR INSTRUMENTS AND METHODS **10** (1961) 25–30; NORTH-HOLLAND PUBLISHING CO.

# FAST TRANSISTORIZED PULSE HEIGHT ANALYZER

ALESSANDRO ALBERIGI QUARANTA and BRUNO RIGHINI

*Instituto di Fisica dell'Università, Centro Elettronica, Bologna, Istituto Nazionale di Fisica Nucleare, Sezione di Bologna*

Received 5 August 1960

A completely transistorized single channel pulse-height analyzer with a dead time of 0.13 $\mu$sec is described. The channel width is determined by the passive characteristic of a delay line and is a constant percentage of the discriminator setting. Circuit diagrams and calibration curves at various frequencies are given.

## 1. Introduction

In a previous work a logarithmic, constant percentage error pulse height analyzer was described[1]). The operation of it and of the one described in this paper was suggested some years ago[2]).

The operation is such that the amplitude pulse $V_0$ to be analyzed and the one delayed by a time $\tau$ with respect to $V_0$ and attenuated by $e^{-\gamma L}$ are both fed to a threshold discriminator which gives either one or two, or else no output pulses according to one of the three following cases:

| Input pulse amplitude | Number of output pulses from the threshold discriminator |
|---|---|
| 1) $V_0 e^{-\gamma L} < V_t < V_0$ | 1 |
| 2) $V_t < V_0 e^{-\gamma L} < V_0$ | 2 |
| 3) $V_0 < V_t$ | 0 |

where $V_t$ is the discriminator threshold and $\gamma$ the cable characteristic attenuation per meter and $L$ the cable length. The discriminator output therefore gives numerical information about the input pulse amplitude.

The analyzer described in this paper performs this operation and also includes circuitry able to convert the numerical information received from the discriminator so as to give an output pulse only in case 1.

Fast transistors being now available[3,4]), we could make a completely transistorized single channel pulse height analyzer which offers good threshold precision and stability, short dead time (also at high input repetition rates) and an input-output delay only slightly affected by input pulse amplitude. This is in addition to the well-known advantages of any transistorized circuits (such as lower power consumption, smaller size, compactness, presumed greater reliability, etc.).

## 2. The Circuit

The block diagram is shown in fig. 1 and the complete circuit in fig. 2.

The circuit operation may be described as follows: the input pulse to be analyzed is fed to the bases of the two emitter followers T-1, T-2 and from their emitters to the bases of T-3 and T-4. The pulse coming from T-1 and delayed by $\tau(L_1)$, and the one to be analyzed coming from T-2 are mixed at the common emitters of T-3 and T-4; in our case $\tau$ was 80 ns.

The potentiometer P-1 reduces further and continuously the pulse amplitude already attenuated by $L_1$ and varies the amplitude interval limits for which an output pulse is available.

[1]) A. Alberigi-Quaranta, C. Bernardini, I. F. Quercia, Nucl. Instr. and Meth. **3** (1958) 201–203.

[2]) A. Alberigi-Quaranta, C. Bernardini, C. Infante, I. F. Quercia, Nucl. Instr. and Meth. **5** (1959) 120–123.

[3]) Val L. Fitch, Transistors in High Energy Research (Princeton University).

[4]) A. Barna, J. Howard Marshall, M. Sands, Nucl. Instr. and Meth. **7** (1960) 124–134.

Transistors T-5, T-7, T-8 form the threshold discriminator $U_1$ [5]).

Threshold voltage of the discriminator is determined by the emitter voltage of T-5 (normally cut-off) which is obtained by the emitter follower T-6 characterized by a very low internal resistance.

This device also stabilizes the T-5 emitter voltage for high repetition rates and fast input pulses.

by $\tau(L_3)$; $U_2$ threshold is always less than $V_t$.

It can be easily shown (fig. 3)[1,2]), that, when an output pulse is given by the anticoincidence circuit, it is delayed either by $\tau$ or by $2\tau$, dependent on the discriminator having given either one or two pulses separated by $\tau$.

The coincidence, therefore, gives an output pulse in case (1) only (see Introduction).

Only coincidence pulses trigger the transistor T-18 which is the analyzer output stage and at

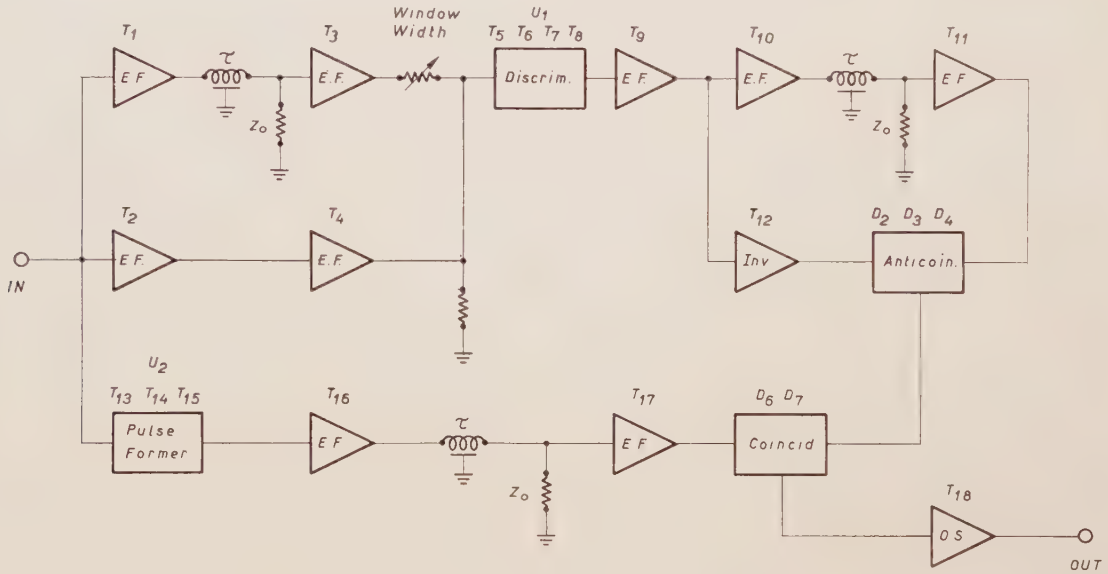


Fig. 1.

Output pulses coming from $U_1$ are 40 ns wide and their rise time is about 20 ns; they are delayed by $\tau(L_2)$ and fed via the emitter followers T-9, T-10, T-11 to the anticoincidence diodes D-2, D-3. D-4, not essential for correct anticoincidence operation, reduces the circuit dead time.

Anticoincidence veto pulses are the same pulses from the discriminator $U_1$, inverted by T-12.

In the coincidence D-6, D-7, whose resolving power is 10 ns, the output pulses coming from the anticoincidence circuit are selected in time by the pulses coming from the univibrator $U_2$ (T-13, T-14, T-15), which are afterwards delayed

[5]) R. Gabriel, E. L. Garwin, C. M. York, Nucl. Instr. and Meth. 5 (1959) 247–253.

the same time it selects the coincidence pulses and removes the non-coincident ones.

The output pulse is positive and more than 3 volts; its width is 40 ns and the rise-time is 18 ns.

A prototype of the analyzer has been made (fig. 4) on a modular chassis ($7 \times 26.5 \times 23.7$ cm).

The whole has been wired on a single silvered copper plate, 0.2 cm thick, on which the grounded circuit terminals have been soldered directly.

The delay lines used were pieces of the delay cable Dätwyler HFK 5614.

Transistors T-3, T-4, T-7, T-8, T-14, T-15, indicated in fig. 2 as 2 N 501[illegible]1, have been selected in order to have the $\beta$ between 40 and 60; the remaining transistors needed no selection.

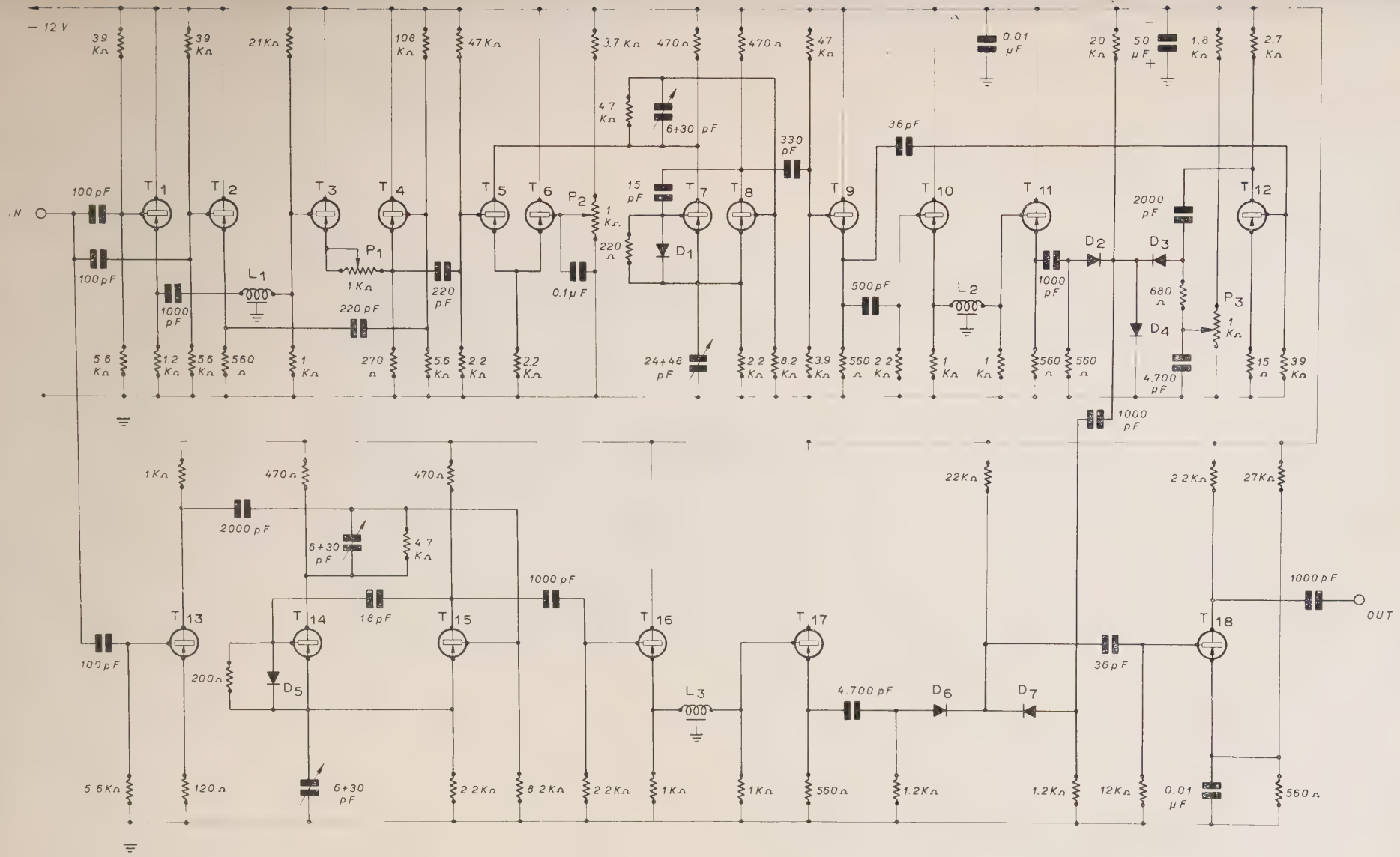


Transistors: all PHILCO 2N501 $T_3$ $T_4$ $T_7$ $T_8$ $T_{14}$ $T_{15}$: 2N501-1

$D_1$ $D_2$ $D_3$ $D_4$: Qutronic Q·6/100 $D_5$ $D_6$ $D_7$: Transitron S·570G

$L_1$ $L_2$ $L_3$: Dätwyler HFK 5614

Resistors: 1/2 W 10 %

Fig. 2

The leads shown by heavy lines in fig. 2 are cut to 0.5 cm and wired as directly as possible to reduce to a minimum their capacitance and inductance.

formances for high repetition rates: in fig. 5 and fig. 6 analyzer calibration curves are drawn for input pulses 20 ns wide and for repetition rates

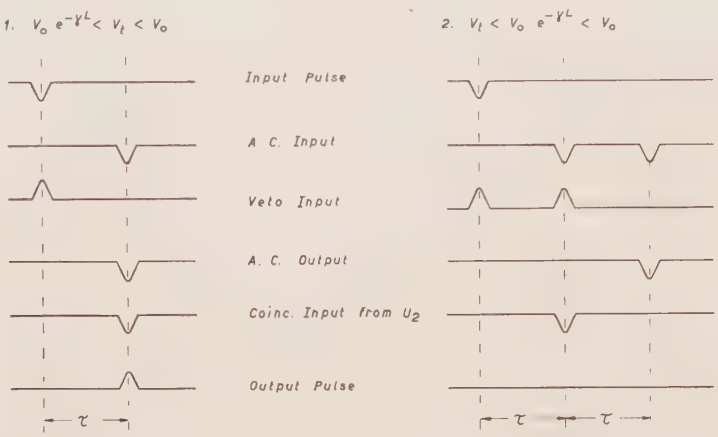


Fig. 3

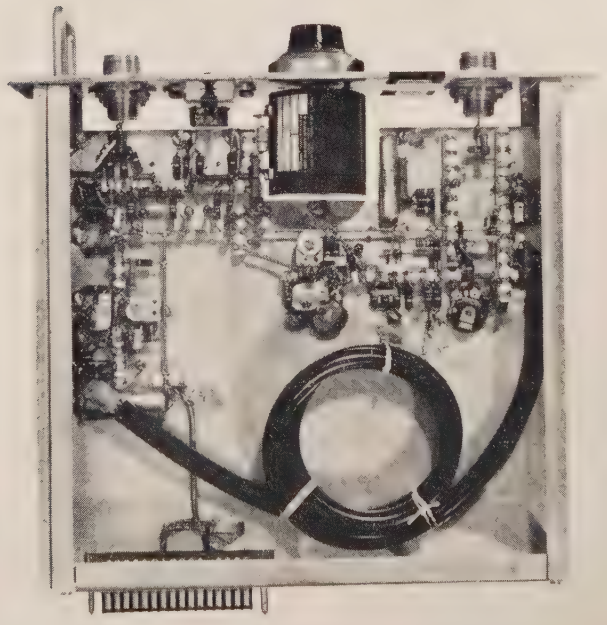

Fig. 4

The supply voltage was –12 volts, and the current was about 25 mA.

### 3. Performance

The following measurements were carried out on this analyzer to verify particularly its per-

of 25 kc/s and 2 Mc/s respectively.

From these curves it is evident that, for frequencies less than or equal to 2 Mc/s there is no appreciable drift of the amplitude interval limits when the frequency of the input pulses is changed.

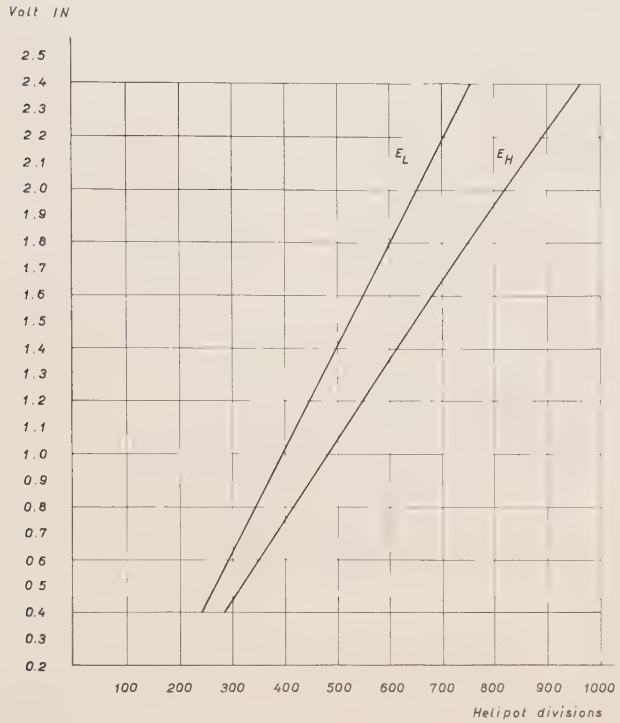


Fig. 5.

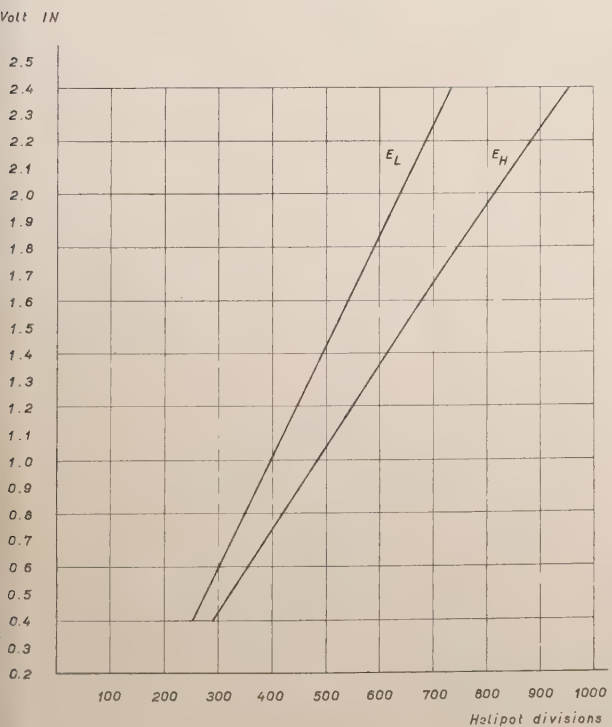


Fig. 6.

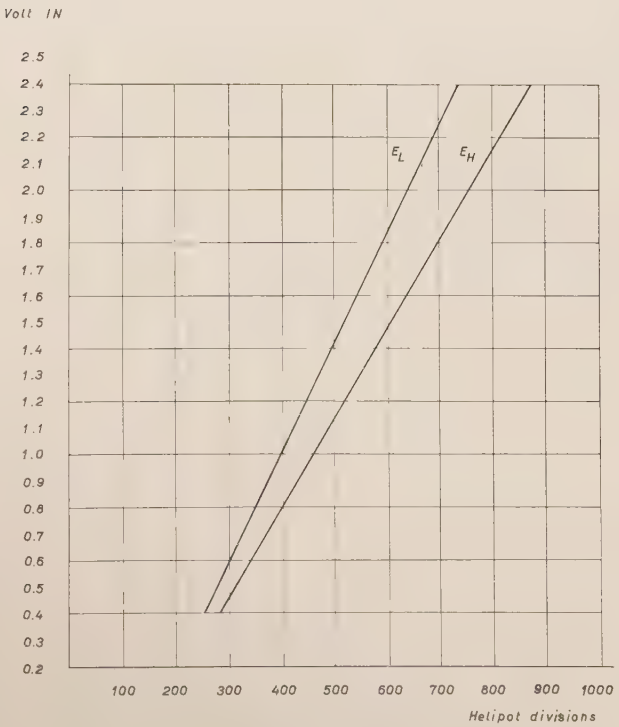


Fig. 7.

A calibration curve for input pulses at 4 Mc/s repetition rate is shown in fig. 7; at this frequency there is a little change of the indicated limits.

In fig. 5, 6, 7 $E_H$ and $E_L$ indicate the upper and lower limits of the amplitude interval for which the analyzer gives an output pulse.

The lowest value of $E_L$ (0.4 V) depends on the attenuation of the emitter followers T-1, T-2, T-3, T-4 and on the minimum pulse amplitude required to trigger $V_1$.

The highest value of $E_H$ is limited by the maximum base inverse voltage of T-6 ($BV_{EB\,max} = -2$V for the 2N 501).

Input pulses of a width ranging between 20 and 55 ns were used without appreciable change of the calibration curves.

The narrowest separation between two input pulses correctly analysed, depends also on $\tau$: in our case $\tau$ was 80 ns and the dead time was 130 ns.

The delay between input and output, with $\tau = 80$ ns, was 120 ns when $V_0$ (input pulse amplitude) was equal to $E_L$ and it was 115 ns when $V_0$ was equal to $E_H$.

Threshold drift during a period of 24 hours was less than 4 mV; temperature changes, ranging about $\pm$ 10°C from room-temperature (20°C), did not alter the threshold value more than 4 mV.

We wish to thank Professor I. F. Quercia, Director of the National Laboratories at Frascati, for having allowed us to carry out some of our work in the Laboratories and Dr. C. Infante for some helpful discussions.

NUCLEAR INSTRUMENTS AND METHODS **10** (1961) 31–36; NORTH-HOLLAND PUBLISHING CO.

# USE OF (p, γ) REACTIONS IN THE EFFICIENCY CALIBRATION OF A NaI CRYSTAL

K. J. VAN OOSTRUM† and A. C. MEIJER

*Laboratorium voor Technische Natuurkunde der Technische Hogeschool, Delft*

Received 30 September 1960

The determination is described of the efficiency of a NaI crystal counter for detecting gamma rays with energies up till 6 MeV. The usual two-lines method[1]) was applied to low energy gamma rays by using radio-active samples and to gamma rays with energies above 3 MeV by using (p, γ) reactions. Cascades of gamma rays and annihilating positons are then used in an extension of this method.

Various necessary corrections are discussed. The purely experimental results are compared with those of the semi-empirical approach[2]) usually applied for these high gamma ray energies.

## 1. Introduction

Gamma ray intensities can be derived from a measured spectrum, if the efficiency of the detection equipment is known. We define this efficiency $\varepsilon$ as the number of pulses counted in the full-absorption peak in the gamma ray spectrum divided by the number of quanta emitted by the source, since this part of the spectrum is usually taken as a convenient measure of the intensity.

The efficiency, thus defined, can be determined with a semi-empirical method[2]) using calculated values of the intrinsic efficiency $\varepsilon_i$ for total absorption. The purely experimental way based on the two-lines method[1]) has been limited to gamma ray energies below 2.76 MeV up till now. However, the use of some suitable (p,γ) resonances will be shown to extend the experimental determination of $\varepsilon$ to higher gamma ray energies.

This paper reports the experimental determination of $\varepsilon$ for the scintillation counter equipment (fig. 1) used in the investigation of (p,γ) reactions with the Delft 2.5 MeV van de Graaff generator[3]). The scintillation counter consists of a 3″ × 3″ NaI (Tl) crystal mounted on an EMI photomultiplier. The gamma ray source is a target mounted in a target holder shown in fig. 1 and bombarded by protons from the generator

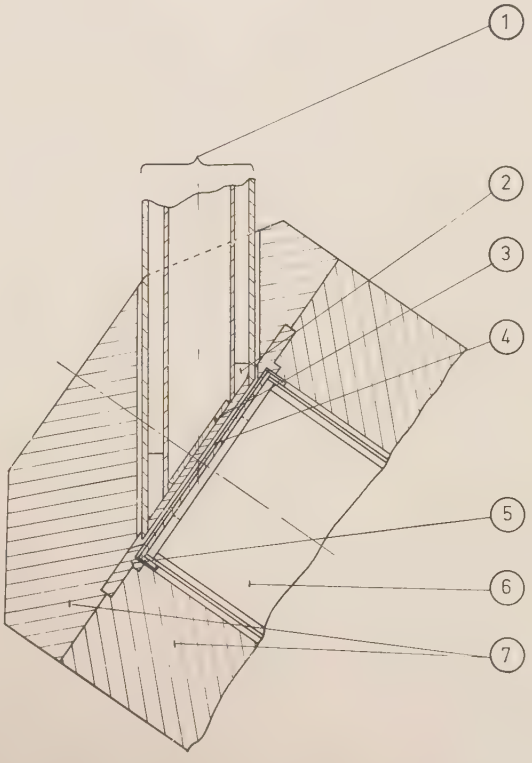


Fig. 1. Gamma ray detection equipment: 1. target holder; 2. cooling oil passage; 3. target; 4. aluminium foil; 5. ring supporting the aluminium foil inserting the NaI crystal; 6. NaI crystal; 7. lead shielding.

† Present address: Instituut voor Kernphysisch Onderzoek, Amsterdam, Netherlands.

[1]) B. Aström, A. H. Wapstra, S. Thülin and I. Bergström, Ark. Fys. **7** (1954) 247.

[2]) W. E. Mott and R. B. Sutton, Encyclopedia of Physics **45** (1958) 86.

[3]) K. J. van Oostrum, thesis, Delft, 1960.

mentioned above. The crystal axis makes an angle of 55° with respect to the bombarding proton beam in order to ensure, that the measured intensities are averaged for possible angular distributions (at least for dipole radiations). The close distance between target and crystal enables the observation of very weak gamma ray intensities. If a larger distance is used, $\varepsilon$ must be remeasured, because it strongly depends on the geometry of the arrangement.

## 2. Two-Lines Method

The two-lines method mentioned above was used to obtain values of $\varepsilon$ for gamma ray energies up till 2.76 MeV. These determinations were carried out with radio-active samples, data of which are given in table 1. All these samples were mounted on tantalum target backings in the target holder in order to obtain efficiency values, which could be applied to the (p,$\gamma$) experiments. Spectra from $^{22}$Na, $^{88}$Y and $^{24}$Na were measured in this way. The ratio of efficiencies for the two energies of gamma rays emitted by each source was calculated from the measured line ratio in the spectrum and the well-known intensity ratio in the source given in table 1. Care was taken, that all positons emitted by the $^{22}$Na sample annihilated near the source so as to apply the intensity ratio given for $^{22}$Na. A curve giving $\varepsilon$ as a function of gamma ray energy was obtained from these three efficiency ratios by assuming this curve to be smooth. The absolute efficiencies were obtained by measuring the spectra produced by $^{198}$Au and $^{137}$Cs standard sources of well-known strength.

TABLE 1
Gamma ray sources used in the efficiency determination

| Source | Gamma ray energy (MeV) | Intensity ratio | Ref. |
|---|---|---|---|
| $^{198}$Au | 0.412 | | [4] |
| $^{137}$Cs | 0.662 | | |
| $^{22}$Na | 0.511 | 1.78 | [4] |
| | 1.277 | to 1 | |
| $^{88}$Y | 0.908 | 1 | [4] |
| | 1.853 | to 1 | |
| $^{24}$Na | 1.369 | 1 | [4] |
| | 2.756 | to 1 | |
| $^{29}$Si(p,$\gamma$)$^{30}$P | 0.684 | 1.09 | [5] |
| at $E_p$ = 0.414 MeV | 5.28 | to 1 | |
| $^{29}$Si(p,$\gamma$)$^{30}$P($\beta^+$)$^{30}$Si | | $\beta^+$ 1 to | [5] |
| at $E_p$ = 0.326 MeV | 5.88 | $\gamma$ 0.86 | |
| $^{28}$Si(p,$\gamma$)$^{29}$P($\beta^+$)$^{29}$Si | | $\beta^+$ 1 to | [3] |
| at $E_p$ = 1.64 MeV | 4.35 | $\gamma$ 0.88 | |

The two-lines method could be applied too by using suitable (p,$\gamma$) reactions producing higher energy gamma radiation. Resonance levels deexciting to the ground state only via a cascade of one high energy and one low energy gamma ray are rather seldom; mostly, too many modes of decay are possible[6,7]) giving rise to a too complicated spectrum for the purpose of calibration. Only the 414 keV resonance in the reaction $^{29}$Si(p,$\gamma$)$^{30}$P was found to show approximately the required features[5]). Figure 2d shows its decay scheme. There is a small intensity difference between the 5.28 MeV and the 0.68 MeV lines due to other modes of decay of the resonance level, which must be taken into account when the ratio of the efficiencies for both lines is calculated. Furthermore, the weak ground state transition produces a background in the gamma ray spectrum, which must be subtracted; yet, this resonance gives rather an accurate determination of $\varepsilon$ for a gamma ray energy of 5.28 MeV.

## 3. Application of Annihilation Radiation

No more suitable cascades for the determination of efficiencies in the way described above could be found in litterature[6,7]). However, some more measurements were desired to determine the efficiency curve well enough for higher

[4]) A. H. Wapstra, G. J. Nijgh and R. van Lieshout, Nuclear spectroscopic Tables (North-Holland Publ. Co., Amsterdam, 1959).

[5]) C. van der Leun and P. M. Endt, Phys. Rev. **110** (1958) 96.

[6]) P. M. Endt and C. M. Braams, Revs. mod. Phys. **29** (1957) 683.

[7]) F. Ajzenberg and T. Lauritsen, Revs. mod. Phys. **27** (1955) 77.

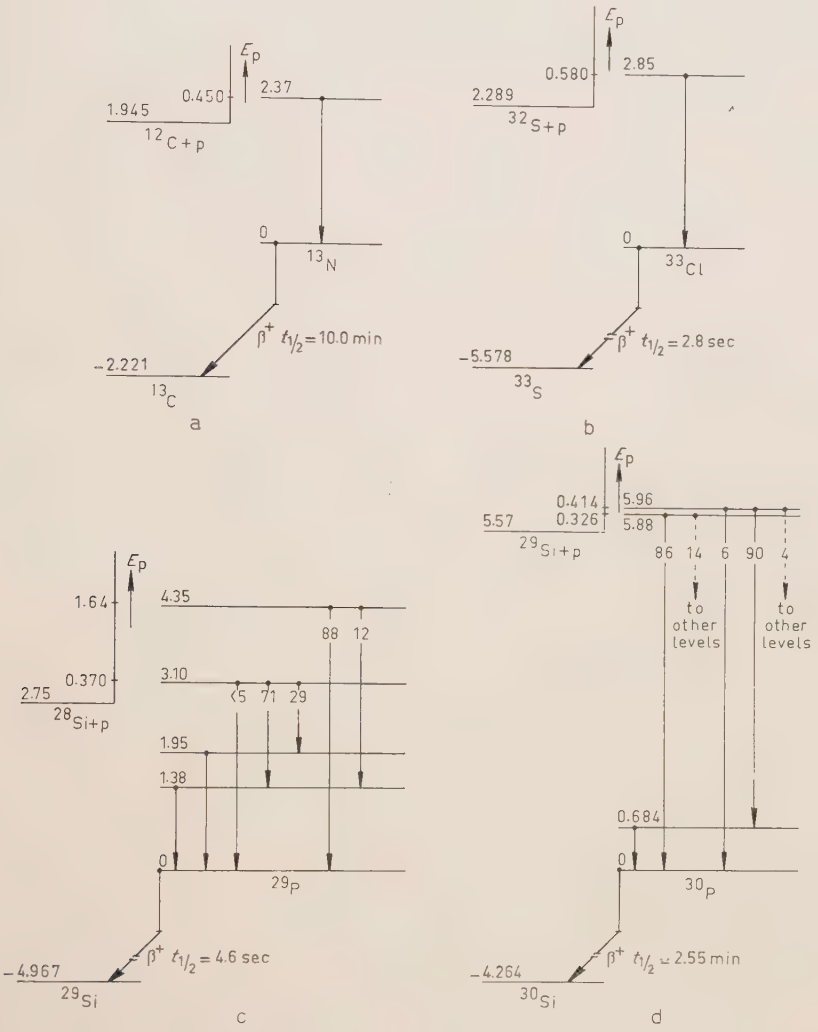


Fig. 2. Decay schemes used in the efficiency determinations. Energies are given in MeV

a. $^{12}C(p,\gamma)\ ^{13}N(\beta^+)\ ^{13}C$ data given in ref.[7])

b. $^{32}S(p,\gamma)\ ^{33}Cl(\beta^+)\ ^{33}S$ data given in ref.[8])

c. $^{28}Si(p,\gamma)\ ^{29}P(\beta^+)\ ^{29}Si$ data given in ref.[3])

d. $^{29}Si(p,\gamma)\ ^{30}P(\beta^+)\ ^{30}Si$ data given in ref.[5])

TABLE 2

Determinations of the factor $g$

| Reaction | Proton energy | Gamma ray energy (MeV) | $g$ | Ref. |
|---|---|---|---|---|
| $^{32}S(p,\gamma)^{33}Cl(\beta^+)^{33}S$ | 0.580 | 2.85 | 1.43 ± 0.10 | [8]) |
| $^{12}C(p,\gamma)^{13}N(\beta^+)^{13}C$ | 0.450 | 2.37 | 1.37 ± 0.10 | [7]) |
| $^{28}Si(p,\gamma)^{29}P(\beta^+)^{29}Si$ | 0.370 | 1.14 | 1.45 ± 0.10 | [3]) |
| | | 1.38 | | |
| | | 1.72 | | |
| | | 1.95 | | |

energies. We obtained them in the following way:

Resonances were selected, in which a strong ground state transition is followed by short-lived positon emission. The positons annihilate in the target backing or in the surrounding material of the target holder and produce two annihilation quanta of 0.511 MeV each. Thus, a well determined intensity ratio of high and low energy gamma rays is obtained permitting use of the principle of the two-lines method.

If all emitted positons annihilate within a close distance from the target, the gamma ray source emits two times as much 0.511 MeV quanta as high energy gamma quanta from the ground state transition (the effect of electron capture can be neglected for the low $Z$ nuclei and large positon energies used in these experiments). Of course, all nuclei produced in this reaction must emit their positons during the measurement of the spectrum. Therefore, this measurement must be continued after the proton bombardment for a time equal to several half-lives for positon emission of the decaying nucleus.

Not all emitted positons annihilate near the target. Half of them enter the backing material and annihilate there or in the brass part of the target holder behind it. The other half goes the opposite direction and annihilates in the brass wall facing the target (fig. 1) or enters the vacuum tube and annihilates far away from the target. Thus, a geometrical factor $g$ between 1 and 2 enters the measured intensity of the annihilation radiation. This factor $g$ is very nearly the same for different reactions, if the same target holder is used; it can be determined with a reaction involving a gamma transition with an energy, for which the efficiency is known already, and which is followed by positon emission.

The value of $g$ for the arrangement shown in fig. 1 was determined with three different reactions, data of which are given in table 2 and fig. 2. From these three reactions an averaged value of $g$ was derived: $g = 1.42 \pm 0.07$.

Apart from the corrections for other modes of decay and for $g$, another effect must be taken into account in applying this method. High energy gamma radiation will cause pair production in the surrounding material, especially in the lead around the crystal. The created positons produce annihilation radiation giving a contribution to the 0.511 MeV peak in the gamma ray spectrum. In order to correct for this effect we define a symbol $f$:

$$f = \frac{N_{\text{ann}}}{N_\gamma} \tag{1}$$

where:

$N_{\text{ann}}$ is the number of counts in the full-absorption peak of the annihilation radiation from the surrounding material

$N_\gamma$ is the number of counts in the full-absorption peak of the gamma ray causing this annihilation radiation.

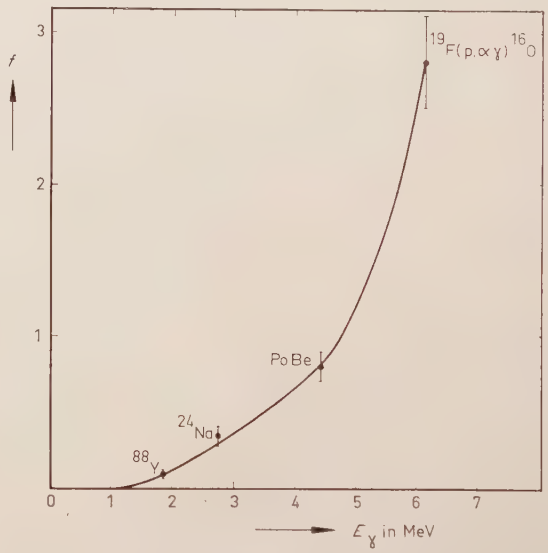


Fig. 3. The factor $f$ defined by eq. (1) as a function of the gamma ray energy.

Values of $f$ for several gamma ray energies were determined from spectra taken from some gamma rays not accompanied by any other annihilation radiation. Of course, these $f$ values are only valid for the arrangement, that is used for the whole efficiency calibration. Fig. 3 shows the results of these measurements.

In a gamma ray spectrum measured at a resonance with the features mentioned above the

[8]) C. van der Leun and P. M. Endt, Physica **24** (1958) 1095.

following equation holds for the number of counts in the 0.511 MeV peak:

$$N_{0.511} = b_\gamma \, g \, \frac{\varepsilon_{0.511}}{\varepsilon_\gamma} N_\gamma + f N_\gamma \qquad (2)$$

in which $b_\gamma$ is the number of (p,γ) resonance levels divided by the number of gamma quanta from the transition under consideration.

Values of $\varepsilon$ were determined for two high ventional semi-empirical method. We use the following equation for this purpose:

$$\varepsilon = \varepsilon_i \, (1 - a) \, \Omega R \; . \qquad (3)$$

$\varepsilon_i$, the intrinsic total efficiency of the NaI crystal, is defined as the number of gamma quanta detected in the whole spectrum divided by the number of quanta entering the front face of the crystal.

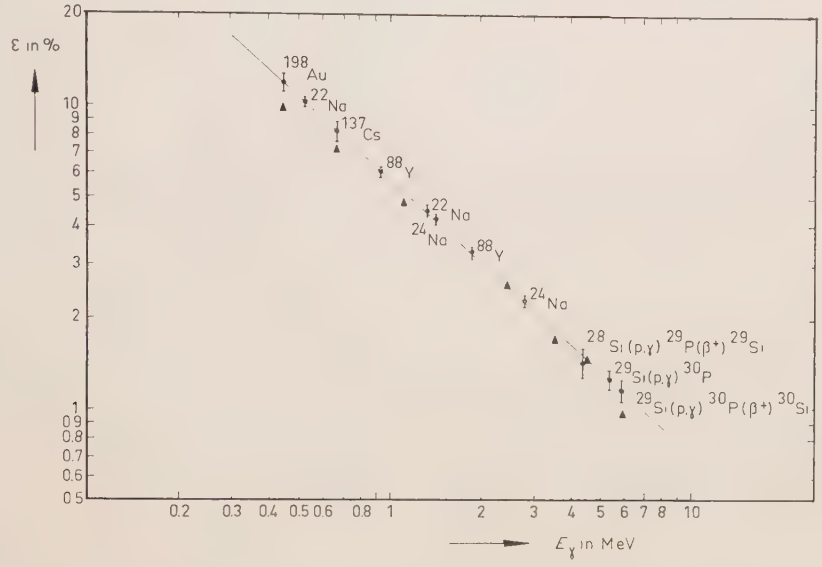


Fig. 4. The efficiency $\varepsilon$ as a function of gamma ray energy for the detection equipment shown in fig. 1. Values obtained by the semi-empirical method are indicated as triangles.

gamma ray energies with this method use being made of the 326 keV resonance in $^{29}Si(p,\gamma)^{30}P$ and the 1.64 MeV resonance in $^{28}Si(p,\gamma)^{29}P$, data of which are given in table 1 and fig. 2.

Values of $\varepsilon$ for a sufficient number of gamma ray energies are available now to draw the efficiency curve, shown in fig. 4 in a double logarithmic scale. This curve is only valid for the arrangement shown in fig. 1. However, a measurement of the dependence of $N_\gamma$ of some gamma ray on the distance between source and crystal yields similar efficiency curves for various distances.

## 4. Semi-empirical Method

As a check on the applicability of the method described above values of $\varepsilon$ were determined for some gamma ray energies also with the con-

$a$ is the fraction of gamma rays absorbed in the material between source and crystal (crystal casing, light shield, target backing and such).

$\Omega$ is the solid angle of the crystal front face with respect to the source.

$R$ is the ratio of the number of counts in the full-absorption peak to that in the whole spectrum.

Graphs of calculated values of $\varepsilon_i$ as a function of the gamma ray energy are given by Mott and Sutton[2]) for various distances between source and crystal and for various crystal sizes.

Values of $R$ given in table 3 were determined from gamma ray spectra taken from monoenergetic sources in the arrangement of fig. 1, while it was assumed, that the compton distribution of each gamma ray was approximately

constant down to zero energy. Such an assumption had to be made, since some gamma radiation of lower energy always accompanies a high energy gamma ray. The values of $\varepsilon$ obtained in this way are shown as triangular points in fig. 4.

TABLE 3
Determinations of the ratios $R$ of full-absorption peak to total spectrum.

| Gamma ray energy (MeV) | Gamma ray source | $R$ |
|---|---|---|
| 0.412 | $^{198}$Au | 0.60 |
| 0.662 | $^{137}$Cs | 0.44 |
| 1.11 | $^{65}$Zn | 0.33 |
| 2.37 | $^{12}$C(p,$\gamma$)$^{13}$N at $E_p$ = 0.450 MeV | 0.20 |
| 3.51 | $^{12}$C(p,$\gamma$)$^{13}$N at $E_p$ = 1.70 MeV | 0.13 |
| 4.43 | PoBe | 0.12 |
| 5.88 | $^{29}$Si(p,$\gamma$)$^{30}$P at $E_p$ = 0.326 MeV | 0.073 |

Comparison of both methods gives approximately the same result. However the semi-empirical points lie on the average somewhat below the experimental curve. This difference may be explained by a systematical error in the experimental curve made in the absolute intensity determination of the $^{198}$Au and $^{137}$Cs sources. On the other hand, gamma rays scattered into the crystal by the lead shielding may increase the value of $\varepsilon_i$ above that given by Mott and Sutton for an unshielded crystal. A correction for this effect would diminish the difference between both results.

**Acknowledgements**

The authors are very much indepted to Prof. Dr. A. H. Wapstra for many fruitful discussions of these experiments.

Our thanks are also due to Prof. Dr. Ir. F. A. Heyn for his permission to use the van de Graaff generator and to Ir. J. H. Makkink and his collaborators for their assistance in the operation of the generator.

NUCLEAR INSTRUMENTS AND METHODS **10** (1961) 37–44; NORTH-HOLLAND PUBLISHING CO.

# THEORY OF "ION-BUNCHING" IN RELATION TO THE DEVELOPMENT OF AN ELECTROSTATIC TIME-OF-FLIGHT MASS SPECTROMETER

P. K. DUTT

*Saha Institute of Nuclear Physics, Calcutta, India*

Received 5 August 1960

In Part I a theoretical expression has been worked out up to a first order of approximation for the shape of electrostatic pulse necessary for acceleration of ions of any particular mass from the ion-source to get them bunched at an instant during their flight in field-free space afterwards. Prior to the "pulsed" acceleration the ions from the source are supposed to undergo steady (D.C.) acceleration.

In Part II an expression for the Resolving Power of an instrument utilizing the time-of-flight principle has been put forward. The factors affecting the resolution have been discussed.

The effect of space charge on bunching has not been taken into account.

## PART I

Physically the process of ion-bunching in an electrostatic time-of-flight mass spectrometer can be pictured as follows:

Let ions of any particular "mass" from a plane source extending in two dimensions, say $y$–$z$

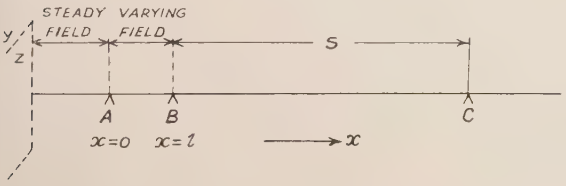


Fig. 1. Outline of the physical processes involved.

plane, arrive at A (fig. 1) moving in the $x$-direction under the action of a steady (D.C.) field between the source and an electrode placed at A. They are then subjected to an electric pulse which produces varying electric field between A ($x = 0$) and another electrode placed at B ($x = l$) called the "buncher" grid. After this, they move through the field-free space with uniform velocity and bunch at C where the ion-collector is placed for detection of ions of that particular "mass". Other "masses" will bunch at different distances along the field-free region (ref. Part II); they are selected out by electronic devices[1,2]).

The object of the present investigation is to find out the nature or shape of the varying field (i.e. for a particular mass the nature of acceleration relating to time) which will produce perfect bunching of ions of that "mass" at C. The distance from B to C we call the bunching distance $s$. An ion suffers different accelerations at different instants while it travels through the varying field region.

Let an ion-particle arrive at A at an instant $T$ with velocity $v_0$ and go through the varying field thereby suffering acceleration. Then $x$, the distance traversed by the particle can be taken as a function of time $t$, and $T$ (taken as a parameter).

Thus, $x =$ function of $t$ and $T$.

The function, being single-valued, can be written in terms of inverse function as

$$t = f(x, T) . \tag{1a}$$

As per fig. 1, at $x = l$, we can write the function as

$$t_1 = f(l, T) \tag{1b}$$

and at $x = 0$, as

$$T = f(0, T) . \tag{1c}$$

[1]) R. R. Wilson, "The Isotron", Document No. AECD-3373, (1952) United States Atomic Energy Commission.

[2]) W. E. Glenn, Jr., Document No. AECD-3337 (1952) United States Atomic Energy Commission.

Then
$$\frac{1}{v} = \frac{\partial f(x, T)}{\partial x} \tag{2a}$$
$$\frac{1}{v_1} = \frac{\partial f(l, T)}{\partial x} \tag{2b}$$
$$\frac{1}{v_0} = \frac{\partial f(0, T)}{\partial x} \tag{2c}$$

$v$ representing velocity.

From the condition of the problem of bunching, as the particles arriving at B at time $t_1$ move with velocity $v_1$, throughout the bunching distance $s$ (from B to C) we put,

$$t_1 + \frac{s}{v_1} = f(l, T) + s\frac{\partial f(l, T)}{\partial x} = \lambda_l \text{ (const.)} . \tag{3}$$

The function $f(x,T)$ can be written as the sum of two other functions, as

$$f(x, T) = \psi(x, T) + \chi(x) \tag{4}$$

then,

$$t_1 + \frac{s}{v_1} = \psi(l, T) + \chi(l) + s\frac{\partial \psi(l, T)}{\partial x} + s\chi'(l) .$$
$$= \lambda_l \tag{5}$$

where
$$\chi'(l) \text{ means } \frac{\partial \chi(l)}{\partial x},$$

whence
$$\psi(l, T) + s\frac{\partial \psi(l, T)}{\partial x} = 0 \tag{6a}$$
$$\chi(l) + s\chi'(l) = \lambda_l . \tag{6b}$$

If $\psi(x,T)$ is expanded in a Taylor's series near $T = 0$,

$$\psi(x, T) = \phi_0(x) + \phi_1(x)T + \phi_2(x)T^2 + \cdots + \phi_n(x)T^n + \cdots$$
$$= \sum_0^\infty \phi_n(x)T^n \tag{6c}$$

where $\phi_0$, $\phi_1$, $\phi_2$ $\cdots\cdots$ indicate terms containing the zero, 1st, 2nd order partial differential coefficients.

Then,

$$\psi(l, T) + s\frac{\partial \psi(l, T)}{\partial x} = \sum_0^\infty \{ \phi_n(l) + s\phi'_n(l) \} T^n = 0 , \tag{7}$$

for every $T$.

Therefore,
$$\phi_n(l) + s\phi'_n(l) = 0 .$$

Hence $\phi_n(x)$ can be expressed as,
$$\phi_n(x) = \psi_n(x) - s\psi'_n(l) - \psi_n(l) \tag{8}$$

$\psi_n$ being an arbitrary function.

Therefore
$$f(x, T) = \sum_1^\infty \{ \psi_n(x) - s\psi'_n(l) - \psi_n(l) \} T^n + \chi(x) \tag{9}$$

from relation (4).

Here, both $\psi_n$ and $\chi$ are arbitrary functions. So that,

$$\begin{aligned} f(0, T) = T, \text{ from (1c)} \\ - \{ \psi_1(0) - s\psi'_1(l) - \psi_1(l) \} T \\ - \{ \psi_2(0) - s\psi'_2(l) - \psi_2(l) \} T^2 \\ - \cdots\cdots \quad \cdots\cdots \quad \cdots\cdots\cdots \\ - \{ \psi_n(0) - s\psi'_n(l) - \psi_n(l) \} T^n \\ + \chi(0) \quad \cdots\cdots \quad \cdots\cdots\cdots \end{aligned} \tag{10}$$

from which we get,

$$\begin{aligned} \psi_1(0) - s\psi'_1(l) - \psi_1(l) &= 1 \\ \chi(0) &= 0 \\ \psi_n(0) - s\psi'_n(l) - \psi_n(l) &= 0 , \quad \text{for } n > 1 . \end{aligned} \tag{11}$$

From relation (2c),

$$\frac{1}{v_0} = \frac{\partial f(0, T)}{\partial x} = \psi'(0, T) + \chi'(0) .$$

Therefore,
$$\psi'(0, T) = 0$$

and,
$$\chi'(0) = \frac{1}{v_0} . \tag{12}$$

Hence, the general form of $f(x,T)$ with 1st order of approximation, can be written as

$$t = f(x, T) = \{ \psi(x) - s\psi'(l) - \psi(l) \} \frac{T}{\psi(0) - s\psi'(l) - \psi(l)} + \chi(x) \tag{13a}$$

where $\psi$ and $\chi$ are arbitrary functions satisfying the relation,

$$\psi'(0,T) = 0 , \qquad \chi(0) = 0 , \qquad \chi'(0) = \frac{1}{v_0} . \tag{13b}$$

Differentiating eq. (13a) twice with respect to $x$, we get,

$$\frac{d^2t}{dx^2} = \frac{\psi''(x)T}{\psi(0) - s\psi'(l) - \psi(l)} + \chi''(x) .$$

Therefore,

$$\frac{d^2x}{dt^2} = -\frac{\frac{d^2t}{dx^2}}{\left(\frac{dt}{dx}\right)^3}$$

$$= -\frac{\frac{\psi''(x)\cdot T}{\psi(0) - s\psi'(l) - \psi(l)} + \chi''(x)}{\left(\frac{\psi'(x)\cdot T}{\psi(0) - s\psi'(l) - \psi(l)} + \chi'(x)\right)^3} . \quad (14)$$

We assume a simple solution,

$$\psi(x) = \cos\frac{x}{\beta}$$

and

$$\chi(x) = \frac{\beta}{v_0}\sin\frac{x}{\beta}$$

satisfying the condition (13b).

We have,

$$t = f(x, T) = \frac{\cos\frac{x}{\beta} + \frac{s}{\beta}\sin\frac{l}{\beta} - \cos\frac{l}{\beta}}{1 + \frac{s}{\beta}\sin\frac{l}{\beta} - \cos\frac{l}{\beta}} T + \frac{\beta}{v_0}\sin\frac{x}{\beta}$$

$$= K_1\cos\frac{x}{\beta}T + K_2\sin\frac{x}{\beta} + K_3 T , \quad (15a)$$

where

$$K_1 = \frac{1}{1 + \frac{s}{\beta}\sin\frac{l}{\beta} - \cos\frac{l}{\beta}}$$

$$K_2 = \frac{\beta}{v_0}$$

$$K_3 = \frac{\frac{s}{\beta}\sin\frac{l}{\beta} - \cos\frac{l}{\beta}}{1 + \frac{s}{\beta}\sin\frac{l}{\beta} - \cos\frac{l}{\beta}}$$

$$= 1 - k_1 . \quad (15b)$$

Therefore

$$\frac{1}{\beta}\ddot{x} = \frac{t - K_3T}{\{T^2(K_1^2 - K_3^2) + 2K_3tT + K_2^2 - t^2\}^{\frac{3}{2}}}$$

$$= \Psi \text{ (say)} . \quad (23)$$

(vide Appendix IA)

From the foregoing analysis as $T$ comes in the expression for $\Psi$, it appears that different ion particles arriving in the varying field region with different $T$ 's will require different accelerations according to eqn. (23) for bunching, which is not attainable in practice.

So, for minimum variation of $\Psi$ with $T$, for a particular value of $t$ we get a condition

$$-\frac{1}{3}\frac{K_2^2}{t^2} = \frac{(K_3 - 1)^2}{K_3} , \quad (26)$$

(vide Appendix IB)

*The significance of the condition (26), viz.*

$$-\frac{1}{3}\frac{K_2^2}{t^2} = \frac{(K_3 - 1)^2}{K_3} .$$

The above expression contains the constants $K_2 (= \beta/v_0)$ and

$$K_3 \left( = \frac{\frac{s}{\beta}\sin\frac{l}{\beta} - \cos\frac{l}{\beta}}{1 + \frac{s}{\beta}\sin\frac{l}{\beta} - \cos\frac{l}{\beta}} \right),$$

and the variable parameter "$t$".

Using this condition we are to find out the value of the acceleration $\ddot{x}$ by the expression (23) at different $t$ 's, required for bunching of ions of a particular mass.

For an experimental set up, $l$ is a constant, $s$ is also a constant being the distance between the bunching grid B and the collector (fig. 1) and $v_0$ is also fixed by the D.C. potential creating the steady electrostatic field; the only arbitrariness remains in choosing the value of the constant $\beta$.

For any particular value of $t$ we can choose one value of $\beta$ which satisfies the condition (26) thereby making the variation of $\Psi$ with $T$ 's minimum. So, if we plot a curve for acceleration $\ddot{x}$ required for bunching against time $t$, retaining that particular value of $\beta$ the variation of $\ddot{x}$ with $T$ 's will be minimum near one value of $t$ only.

For an experimental condition, we have chosen the values of $l = 2$ cm, $s = 100$ cm, $v_0 = 10^7$ cm/sec and $\beta = 100$, and have obtained (fig. 2), the acceleration vs. time plots for a particular mass. As the curve depicts, the

different values of $\ddot{x}$ for a particular value of $t$ are coming in due to different $T$ values. Actually, the curve (A, fig. 2) has been shown as voltage (across the buncher grid B and A) vs. time plot

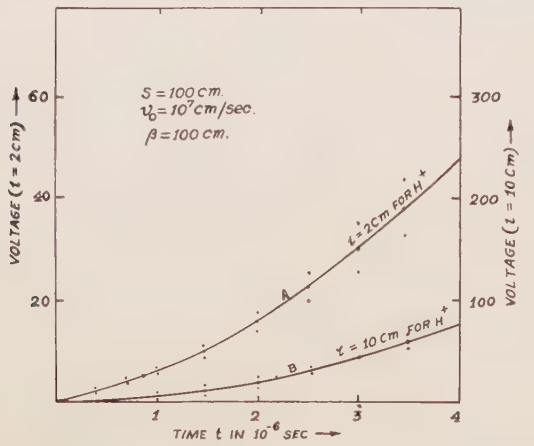


Fig. 2. Figure shows theoretically obtained voltage pulse shapes in case of protons for two values of $l$ ($l$ = 2 cm and $l$ = 10 cm) and for $s$ = 100 cm, $\beta$ = 100 cm, $v_0 = 10^7$ cm/sec.

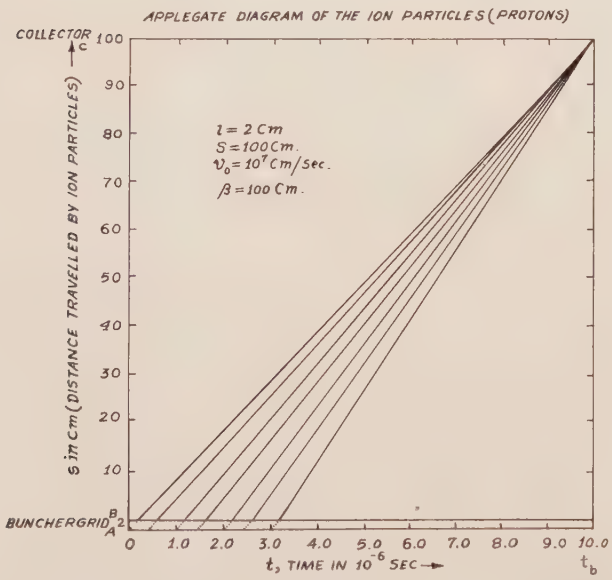


Fig. 3. Figure shows an Applegate diagram (distance versus time plot) of the ions (protons) for $l$ = 2 cm $s$ = 100 cm, $\beta$ = 100 cm and $v_0 = 10^7$ cm/sec.

for atomic hydrogen ions (protons), and is a mean curve for different values of $T$ 's.

For comparison, another curve (B) has been shown on the same graph, using all the constants same, excepting $l$ = 10 cm in this case.

In choosing the value of $\beta$, it is to be remembered also that the voltage calculated thereby for a value of $t$ should be within a practical limit.

We can take over the idea of the so called Applegate diagram (distance travelled by ions plotted as a function of time) in the study of klystrons and apply it to the ions. The curves of fig. 3 represent the Applegate diagram. These curves have been obtained, for $l$ = 2 cm, $s$ = 100 cm, $v_0 = 10^7$ cm/sec and $\beta$ = 100 cm by a two-fold integration of the acceleration vs. time curve (A) of fig. 2 done graphically; thereby the positions of the individual ion-particles arriving at different instants in the varying field region between the buncher grid B and A are shown. After the ions cross the second buncher grid B they move with uniform velocity towards the collector, so in fig. 3 (distance vs. time plot) their positions are represented by drawing straight lines tangential to the curves obtained for individual particles in traversing the varying field region.

## Appendix 1A

The expression in (15a) can be written as

$$t = \tau + K_3 T \tag{16}$$

where

$$\tau = K_1 \cos\frac{x}{\beta}\cdot T + K_2 \sin\frac{x}{\beta}.$$

Therefore,

$$\tau = t - K_3 T. \tag{17}$$

From (15a) we get, on differentiation,

$$\frac{1}{v} = \frac{\mathrm{d}t}{\mathrm{d}x}$$

$$= \frac{1}{\beta}\left(K_2 \cos\frac{x}{\beta} - K_1 T \sin\frac{x}{\beta}\right)$$

$$= \frac{1}{\beta}\cdot \Phi, \tag{18}$$

writing

$$\Phi = K_2 \cos\frac{x}{\beta} - K_1 T \sin\frac{x}{\beta}.$$

From (17) and (18) we have

$$\Phi^2 + \tau^2 = K_1^2 T^2 + K_2^2 \tag{19}$$

whence

$$\Phi^2 = K_1^2T^2 + K_2^2 - \tau^2$$

$$= T^2(K_1^2 - K_3^2) + 2K_3tT + K_2^2 - t^2 . \quad (20)$$

Now,

$$\tau = t - K_3T$$

$$= K_2 \sin\frac{x}{\beta} + K_1T\cos\frac{x}{\beta} \text{ substituting the value of } \tau$$

$$= -\beta\,\Phi' \quad (21)$$

where

$$\Phi' = \frac{\partial\Phi}{\partial x} .$$

Thus, from the relations (18) and (21) we get,

$$\frac{d^2t}{dx^2} = -\frac{\Phi'}{\beta} = -\frac{\tau}{\beta^2} .$$

Therefore,

$$\frac{d^2x}{dt^2} = -\frac{\dfrac{d^2t}{dx^2}}{\left(\dfrac{dt}{dx}\right)^3}$$

$$= \frac{\tau\beta}{\Phi^3}$$

$$= \frac{\beta(t - K_3T)}{\{\, T^2(K_1^2 - K_3^2) + 2K_3tT + K_2^2 - t^2 \,\}^{\frac{3}{2}}} \quad (22)$$

writing down the values of $\tau$ and $\Phi$.

**Appendix 1B**

$$\frac{d\Psi}{dt} = \{\, T^2(K_1^2 - K_3^2) + 2K_3tT + K_2^2 - t^2 \,\}^{-\frac{5}{2}}$$

$$[K_3\{\, T^2(K_1^2 - K_3^2) + 2K_3tT + K_2^2 - t^2 + \tfrac{3}{2}\,(t - K_3T)$$

$$\{\, 2T(K_1^2 - K_3^2) + 2K_3\,t \,\}\,] = 0 . \quad (24)$$

Making an approximation as $t = T$ at a particular value of $t$, $(t > T > t - l/v_0)$, we can still find a minimum variation of $\Psi$ with respect to $T$.

From eq. (24)

$$K_3\left\{\frac{K_2^2}{t^2} + K_1^2 - K_3^2 + 2K_3 - 1\right\}$$

$$= 3(K_3 - 1)\,(K_1^2 - K_3^2 + K_3) .$$

In the above expressions the factor $\{\, t^2(K_1^2 - K_3^2) + 2K_3t^2 + K_2^2 - t^2 \,\}^{-\frac{5}{2}}$ arising from eq. (24) has been discarded, as putting this equal to zero makes $K_2 = 0$, which is not possible.

Simplifying we get,

$$\frac{K_3K_2^2}{t^2} = 2K_3K_1^2 + 4K_3^2 - 3K_1^2 - 2K_3 - 2K_3^3$$

$$= -3(K_3 - 1)^2 , \quad (25)$$

since

$$K_1 = 1 - K_3$$

or

$$-\frac{1}{3}\frac{K_2^2}{t^2} = \frac{(K_3 - 1)^2}{K_3} .$$

This gives a condition for minimum variation of $\Psi$ with $T$.

## PART II

In Part I of this article the shape of the pulse producing the varying electric field necessary for bunching of ions upto a first order of approximation has been worked out. Now, an expression for the Resolving Power of an electrostatic time-of-flight mass-spectrometer will be arrived at on the basis of some simplifying assumptions.

Let us assume that the pulse (the Modulating Voltage $V'$) be repeated continuously[1]) as shown in fig. 4 having a period $\tau_p$ which is much less than the bunching time $t_b$ ($\tau_b \ll t_b$). Or, in other words, the duration through which the ion-particles pass through the varying field region to form a bunch in the field-free region is much less than the time required for them to move in the field-free space with uniform velocities.

Then for exact bunching

$$t_b = \frac{v_0\tau_p}{v_{\tau p} - v_0} \quad (27)$$

where $v_{\tau_p}$ = velocity acquired by an ion-particle coming through the buncher grid at the end of the period $\tau_p$.

and $v_0$ velocity acquired by the particle at the beginning of the period (due to the D.C. voltage).

It can be seen that the successive bunches of the same mass are separated by a bunch distance, $\Delta s = v_0\tau_p$. The value of $v_{\tau_p}$ can be written as

$$v_{\tau p} = \frac{\beta}{K_2\cos\dfrac{l}{\beta} - K_1\tau_p\sin\dfrac{l}{\beta}} \quad (28)$$

which is obtained from eq. (18) by writing down the value of $v$ at $x = l$; and $T = \tau_p$ (as $T$ in the

expression for $v_{\tau p}$ will have its value within $\tau_p > T > \tau_p - l/v_0$, and the transit-effect is neglected).

Then eq. (27) can be written after substitution

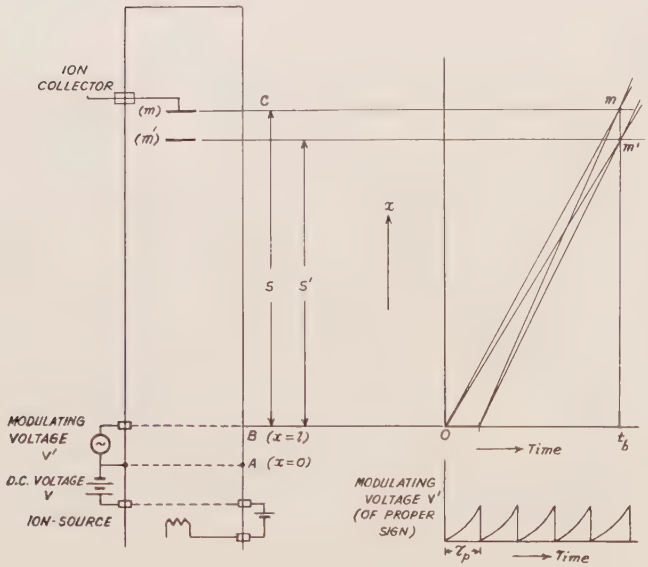


Fig. 4. An explanatory diagram for the physical processes involved for a particular experimental setup.

of the values of $K_1$ and $K_2$ as

$$t_b = \frac{v_0 \tau_p}{\beta \left( \frac{\beta}{v_0} \cos \frac{l}{\beta} - \left( \frac{\tau_p \sin \frac{l}{\beta}}{1 + \frac{s}{\beta} \sin \frac{l}{\beta} - \cos \frac{l}{\beta}} \right) \right) - v_0} \qquad (29)$$

For a set of experiments, for assumed fixed values of $\beta$, $l$, $s$, $v_0$ if $\tau_p$ is very small, the term within bracket of the above expression can be neglected.

Thus,
$$t_b = \frac{\tau_p}{\frac{1}{\cos \frac{l}{\beta}} - 1} = \text{constant} \qquad (30)$$

fixed by the experimental parameters.

As the bunching time is same for ions of two different masses $m$ and $m'$, $m'$ differing from $m$ by a very small amount $\Delta m$, we can get a formula for Resolving Power.

Let for a particular experimental arrangement the ions of mass $m$ bunch at a distance $s$, and the ions of mass $m'$ bunch at a distance $s'$ differing from $s$ by an amount $\Delta s'$.

Then the bunching time, $t_b$ (say) according to eq. (3) is given by,

$$t_b = t_1 + \frac{s}{v_1}, \text{ for mass } m$$

$$= t_2 + \frac{s'}{v_2} \text{ for mass } m' . \qquad (31)$$

Now,

$$t_1 = K_1 \cos \frac{l}{\beta} \cdot T + K_2 \sin \frac{l}{\beta} + K_3 T$$

and

$$v_1 = \frac{\beta}{K_2 \cos \frac{l}{\beta} - K_1 T \sin \frac{l}{\beta}}$$

from eq. (15a) and eq. (18), putting $x = l$. the values of $K_1$, $K_2$, $K_3$ being given by (15b).

Similarly for mass $m'$,

$$t_1 = K'_1 \cos \frac{l}{\beta} \cdot T + K'_2 \sin \frac{l}{\beta} + K'_3 T .$$

and

$$v_2 = \frac{\beta}{K'_2 \cos \frac{l}{\beta} - K'_1 T \sin \frac{l}{\beta}}$$

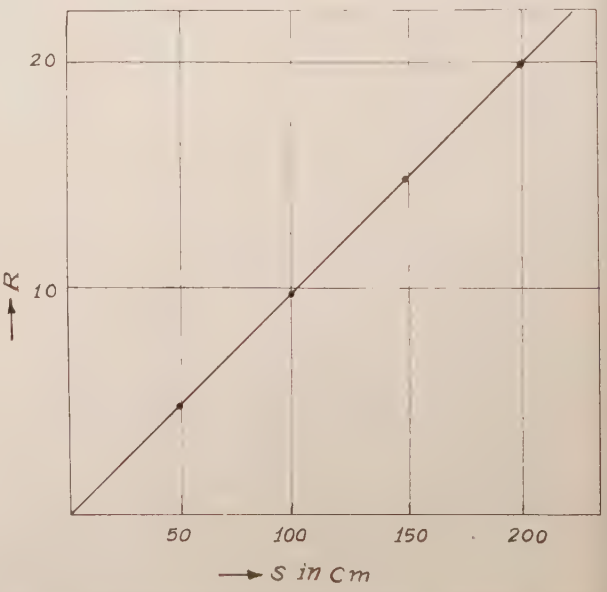


Fig. 5. Figure shows the variation of the Resolving Power $R$ with $s$.

$K'_1$, $K'_2$, $K'_3$ being the corresponding values for mass $m'$.

Writing out the expressions for $K_1$, $K_2$, $K_3$ and $K'_1$, $K'_2$, $K'_3$, we get from eq. (31)

$$\frac{\left(\cos\frac{l}{\beta}-1\right)T}{1+\frac{s}{\beta}\sin\frac{l}{\beta}-\cos\frac{l}{\beta}}+\frac{\beta}{v_0}\sin\frac{l}{\beta}+T+$$

$$+\frac{s}{\beta}\left(\frac{\beta}{v_0}\cos\frac{l}{\beta}-\frac{T\sin\frac{l}{\beta}}{1+\frac{s}{\beta}\sin\frac{l}{\beta}-\cos\frac{l}{\beta}}\right)$$

$$-\frac{\left(\cos\frac{l}{\beta}-1\right)T}{1+\frac{s'}{\beta}\sin\frac{l}{\beta}-\cos\frac{l}{\beta}}+\frac{\beta}{v_0'}\sin\frac{l}{\beta}+T+$$

$$+\frac{s'}{\beta}\left(\frac{\beta}{v'_0}\cos\frac{l}{\beta}-\frac{T\sin\frac{l}{\beta}}{1+\frac{s'}{\beta}\sin\frac{l}{\beta}-\cos\frac{l}{\beta}}\right) \qquad (32)$$

$v'_0$ being the velocity acquired by the mass $m'$ due to the D.C. voltage, $V$ (say), then

$$v'_0=\sqrt{\frac{2eV}{m'}}$$

$$=v_0\sqrt{\frac{m}{m'}}.$$

Putting the value of $v'_0$ in the expression (32) and simplifying we get,

$$\frac{\left(\frac{\beta}{v_0}\sin\frac{l}{\beta}+\frac{s}{v_0}\cos\frac{l}{\beta}\right)^2}{\left(\frac{\beta}{v_0}\sin\frac{l}{\beta}+\frac{s'}{v_0}\cos\frac{l}{\beta}\right)^2}=\frac{m'}{m} \qquad (33)$$

or

$$\frac{m'-m}{m'+m}=$$

$$=\frac{\left(\frac{\beta}{v_0}\sin\frac{l}{\beta}+\frac{s}{v_0}\cos\frac{l}{\beta}\right)^2-\left(\frac{\beta}{v_0}\sin\frac{l}{\beta}+\frac{s'}{v_0}\cos\frac{l}{\beta}\right)^2}{\left(\frac{\beta}{v_0}\sin\frac{l}{\beta}+\frac{s}{v_0}\cos\frac{l}{\beta}\right)^2+\left(\frac{\beta}{v_0}\sin\frac{l}{\beta}+\frac{s'}{v_0}\cos\frac{l}{\beta}\right)^2}. \qquad (34)$$

Writing $m'-m=\Delta m$ and $\frac{1}{2}(m'+m)=\mu$, the mean mass, we get from the above equation an expression for Resolving Power,

$$R=\frac{\mu}{\Delta m}=$$

$$=\frac{1}{2}\frac{2\beta^2\sin^2\frac{l}{\beta}+(s^2+s'^2)\cos^2\frac{l}{\beta}+2\beta(s+s')\sin\frac{l}{\beta}\cos\frac{l}{\beta}}{(s^2-s'^2)\cos^2\frac{l}{\beta}+2\beta(s-s')\sin\frac{l}{\beta}\cos\frac{l}{\beta}}. \qquad (35)$$

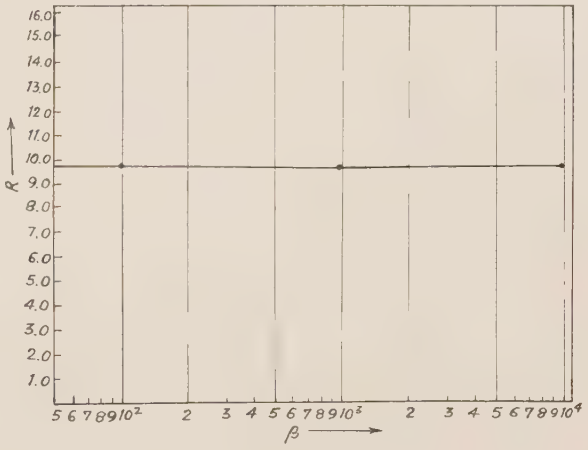


Fig. 6. Variation of the Resolving Power $R$ with $\beta$.

For the ions of a mass $m$ to form a bunch halfway between the bunches of mass $m'$, it is required that $\Delta s'=\frac{1}{2}\Delta s$.

Substituting this value of $\Delta s'$ in the expression (35) we get,

$$R=\frac{\mu}{\Delta m}=\frac{1}{2}\frac{2\beta^2\sin^2\frac{l}{\beta}+\left(\frac{v_0^2\tau_p^2}{4}-v_0\tau_p s+2s^2\right)\cos^2\frac{l}{\beta}+4\beta\left(s-\frac{v_0\tau_p}{4}\right)\sin\frac{l}{\beta}\cos\frac{l}{\beta}}{\left(v_0\tau_p s-\frac{v_0^2\tau_p^2}{4}\right)\cos^2\frac{l}{\beta}+\beta v_0\tau_p\sin\frac{l}{\beta}\cos\frac{l}{\beta}}. \qquad (36)$$

For a set of experiment, putting typical values in the expression (36), say, $\tau_p = 2 \times 10^{-6}$ sec, $v_0 = 10^7$ cm/sec, $l = 2$ cm, $\beta = 100$ cm the values of $R$ obtained for different values of $s$ are shown in fig. 5. These values of Resolving Power are for a relative separation of bunches $\Delta s' (= \frac{1}{2} v_0 \tau_p)$ between ions of two different masses $m$ and $m + \Delta m$ equal to 10 cm.

The effect of $\beta$ on the Resolving Power $R$ for the above experimental arrangement with $s =$ 100 cm is shown in fig. 6.

It is not very difficult in practice to detect by electronic means a relative separation $\Delta s'$ to within a fraction of a centimeter, so actually Resolving Power higher by several factors can be attained. Fig. 7 shows the relation between the Resolving Power $R$ with $\Delta s'$ for the above-mentioned values of $\tau_p$, $v_0$, $l$, $\beta$ and $s$.

The author acknowledges his indebtedness to Dr. U. C. Guha of Pure Mathematics Department, Calcutta University for invaluable help in the mathematical treatment of the subject. The author wishes to thank Prof. B. D. Nag and Prof. D. N. Kundu for helpful discussions and encouragement.

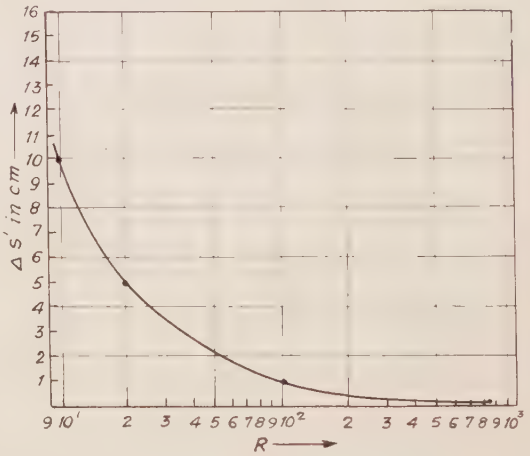


Fig. 7. Variation of the Resolving Power $R$ with $\Delta s'$ (the relative separation between bunches of different masses).

NUCLEAR INSTRUMENTS AND METHODS **10** (1961) 45–47; NORTH-HOLLAND PUBLISHING CO.

# SOME EXPERIMENTS ON MOISTURE DETERMINATION WITH BETA-RAY TRANSMISSION†

T. WESTERMARK and B. SJÖSTRAND

*Division of Physical Chemistry, The Royal Institute of Technology, Stockholm 70, Sweden*

and

H. G. FORSBERG

*The Isotope Techniques Laboratory, Stockholm Ö, Sweden*

By using a transmission geometry of beta rays from $Pm^{147}$ it is shown that recording of moisture changes in hydrophilic materials—kinetics as well as equilibria—is readily achieved. Some data from experiments on filter paper are described and further applications are discussed.

## 1. Introduction

It is well known[1]) that the transmission of a pencil of beta particles through a layer of matter is a measure of mass per unit area of the latter, provided the geometry is not changed[2]). There are effects on the energy loss properties of the beta particles which are dependent on chemical valence states[3]) but they are of small magnitude ($\sim 0.1\%$ in stopping power) and are largely counteracted by the use of an ionization chamber detector which is short in comparison with the beta range. An increased energy loss will namely be observed as an increased ionization since the specific ionization increases with decreasing energy. Thus the expected *intensity* decrease does not take place. We therefore have good arguments for assuming that the transmission properties are very insensitive to chemical changes when ionization chambers (or other energy loss responding devices) are used.

The general case of the application of beta ray transmission was discussed by one of the authors[1]) and some examples were given of the recording of electrolytic concentrations and the sorption of organic vapours in materials such as charcoal. Later the equally promising possibility of recording water sorption in hydrophilic materials was realized[4]). Hansson[6]) used this procedure to measure the water content of a paper-machine felt.

The present paper will deal with the possibilities of following sorption kinetics and equilibria in the laboratory and perhaps in industry for materials which are difficult to measure with noncontacting devices. This group comprises cellulose materials such as paper and pulp as well as textiles. Many other hydrophilic materials are open for study. As will be shown, the point is that an electrical signal can be easily recorded to study the process without contact. On the other hand a balance can in principle afford the same result and the range of application is therefore of course restricted to the case of moving materials and cases where the labour is reduced.

## 2. Experimental

Many sheets of material have thicknesses of the order of 5 mg/cm², viz paper of many sorts. The

† Given as a lecture before the Instruments and Measurements Conference, Stockholm, September 15–17, 1960.

[1]) T. Westermark, Some applications of beta-radiation. Transactions, Instruments and Measurements Conference, Stockholm, 1949 p. 308–14.

[2]) T. Westermark, Sv. Papperstidn. **55** (1952) 178 (in Swedish, references in Sv. Papperstidn. **56** (1953) 597.

[3]) T. Westermark, Some measurements of energy loss of 2.8 MeV electrons in light elements and chemical compounds, Arkiv Kemi (in press).

[4]) T. Westermark, Note on the sorption rate of water vapour in nearly dry ion exchangers (Acta Chemica Scandinavica, in press).

optimum choice of a beta radioactive source is one having a half-thickness of about the same order. $Pm^{147}$ was accordingly selected. It has a 2.6 years' half-life and 223 keV beta energy. A source of about 500 $\mu$c strength was used.

The transmission curve found for filter paper justified the assumptions and showed the half-thickness in paper to be about 5.2 mg/cm$^2$.

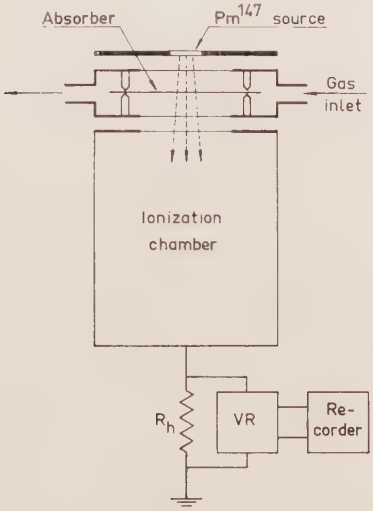


Fig. 1. Apparatus for recording of sorption processes, e.g. drying, by beta-ray transmission. Symbols: VR = vibrating-reed-electrometer, $R_h = 5 \times 10^{10} \Omega$ resistor.

In order to follow sorption processes a device shown in fig. 1 was constructed. The sorbing material under study is placed between two layers of pliofilm (this is "rubber-hydrochloride" or roughly $C_5H_8 \cdot HCl$), each 0.6 mg/cm$^2$. A perspex box contains devices for gas flushing and for keeping the absorber in a fixed position. The detector is an air ionization chamber provided with a thin window (0.9 mg/cm$^2$ Al coated mylar). The output of the chamber is fed to a high-ohm resistor ($5 \times 10^{10}$ $\Omega$ of Victoreen's well-known design). The voltage across the resistor is measured by a vibrating-reed-electrometer, model 33C from Electronic Instruments Ltd, Richmond, England. The output of the latter is fed to a conventional Speedomax potentiometer recorder (10 mV deflection on most sensitive range). The output of the recorder measures, as is seen the transmitted intensity, $I$, of the beam. By taking out the absorber the intensity without it, $I_0$, is obtained for these conditions.

## 3. Results

Many experiments showed successfully that moisture changes can be easily detected. We shall restrict the presentation here to just one case, namely the drying, by admitting dry tank nitrogen through the absorber chamber, of a filter paper with different moisture contents. In fig. 2 the kinetics, expressed as fractional attainment of equilibrium, are plotted versus time. These data were obtained from records of the

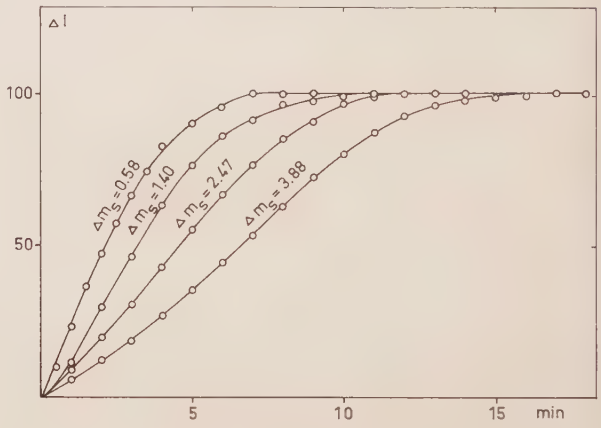


Fig. 2. Recording of drying of filter papers by $Pm^{147}$ beta rays. $\Delta m_s$ is total change of water content expressed as mg/cm$^2$. (Dry paper is $\sim$ 7 mg/cm$^2$.) Each drying step has been normalized to 100 for output signal corresponding to dry state.

desorption process by using the corresponding transmission increase as traced on the recorder. The equilibrium position corresponds to the apparently dry paper.

From the curves in fig. 2 it is seen that equilibrium is obtained faster the smaller the original water content. These data enabled the calculation of the desorption rate from the instrument output per unit time. This property turned out to be relatively insensitive to the original water content.

Further calibrations established that the intensity expressed as $\Delta I/I_0$ versus extra absorber thickness (or moisture) as mg/cm$^2$ was linear near the zero point but that certain deviations occur which have to be known for exact results.

If true exponential absorption takes place we expect as is known[1]):

$$-\frac{\Delta I}{I} \backsimeq \mu_m \cdot \Delta m_s \qquad (1)$$

where $\mu_m$ is the mass absorption coefficient (in

he case of $Pm^{147} \sim 115$ cm$^2$/g). The exponential elation is seldom fulfilled and so a calibration nas to be made.

## 4. Conclusions and Suggested Applications

It is concluded that sorption or desorption phenomena taking place in thin sheets of material can be recorded by beta ray transmission using an optimum selection of transmission data in relation to absorber thickness. In the case reported, the drying, from the ordinary air equilibrium state, of filter paper (about 6% moisture) is easily followed down to about 0.7% in this case. The statistical fluctuations, which set a limit for $\Delta I/I$, are in accordance with[5])

$$E = \frac{1}{\sqrt{2I \cdot t}} \qquad (2)$$

where $I$ is again the transmitted intensity, $t$ the time constant and $E$ the percentage statistical fluctuation. The factor 2 was unfortunately not included in an earlier paper[1]).

Thus the increase of source strength, which is quite possible, can contribute a good deal to the achieving of a considerably better sensitivity than for the case presented. Thus very small moisture changes can be recorded.

Several improvements have been introduced in the apparatus since 1949[1]). The use of the modern vibrating-reed-electrometers instead of electrometer tubes and D.C.-amplifiers is of considerable importance. The use of the hard $P^{32}$ beta rays in 1949[1]) required thick absorbers to get optimum results. The use of $Pm^{147}$ as in the present case is close to the optimum. This is illustrated by the absolute amount of water ($\sim$ 0.6 mg) detected in the experiments reported in fig. 2.

It seems justified to suggest that the apparatus is very handy for use in the laboratory to produce records of sorption or desorption processes of interest. It will act as an automatic balance and save the same amount of labour as such a unit. As no contact with the matter under study is required, the set-up is easy to establish. Other laboratory applications, in addition to paper and pulp, are other hydrophilic materials such as wood, textiles, certain plastics, biological tissue including botanical material (leaves, seed, flour), clay etc. Of course quite similar techniques can be applied to the sorption of organic vapours or substances like iodine by sorbents[7]).

A modification of the method is to heat the absorber, e.g. by infra-red lamps or high-frequency devices, and to arrange two radiation transmission paths for the material (supposed to be in motion). The difference in the outputs, a property readily measured electrically, will give the desorption rate if the heating device is placed between the two measuring units. Provided the power and time are sufficient, the moisture (or content of other volatile substance) is directly given. This procedure might be readily carried out under laboratory or somewhat larger conditions. In industrial plants it seems that the speed of the moving material is so large that drying is impossible. For instance, two detectors may be placed 20 m apart in a paper machine but not much more. The time of drying is only one second or so and as the drying rate might be diffusion-controlled the system will hardly work. For slower machines (perhaps for plastics) the solvent content might be followed by this method. In all these cases only a narrow strip should be heated because the process involves an amount of energy supplied that cannot be neglected. If the passage time of the material is of the same order or shorter than the electrical time constant, the longitudinal thickness variations will not enter and the differential output will give the loss of matter between the two points. The system for instance can give the amount of water evaporated in a certain section of the drying cylinders in a paper mill. This possibility has already been realized[8]).

## Acknowledgements

The authors are indebted to Mr. K. Ljunggren, The Isotope Techniques Laboratory, for valuable discussions and to Mr. E. Somer for providing the $Pm^{147}$ sources used.

[5]) L. I. Schiff and R. D. Evans, Rev. Sci. Instr. **7** (1936) 456.

[6]) K. E. Hansson, Sv. Papperstidn. **56** (1953) 625.

[7]) T. Westermark, Sorption of organic vapours in organic ion exchanging substances (Acta Chem. Scand., in press.).

[8]) Frieseke & Hoepfner, G.m.b.H., Germany, Company pamphlets.

NUCLEAR INSTRUMENTS AND METHODS **10** (1961) 48–52; NORTH-HOLLAND PUBLISHING CO.

# BETA-RAY SPECTROMETER WITH CURVED EXIT SLIT†

H. DANIEL†† and L. JACKSON LASLETT

*Institute for Atomic Research and Department of Physics, Iowa State University. Ames, Iowa*

Received 10 October 1960

Computer calculations have been performed for a high-resolution beta-ray spectrometer with curved exit slit. Models with focusing angles of 324.50°, 484.66°, 655.21°, and 829.74° have been explicitly treated. Results are given for the shape of the exit slit and for the resolution and transmission.

## 1. Introduction and General Considerations

There are essentially two types of double focusing beta-ray spectrometers: (1) almost perfect focusing in the radial emission angle $\zeta_r$, with an aperture aberration proportional to $\zeta_z^2$, and (2) almost perfect focusing in the axial emission angle $\zeta_z$, with an aperture aberration proportional to $\zeta_r^2$. It has been shown[1,2], however, that one can attain a much better resolution for a given transmission when abandoning first order double focusing. In this case the exit slit is curved and the resolving width depends, in its lowest power, only on fourth-order terms in $\zeta_r$ and $\zeta_z$. Electrons starting with different angles $\zeta_z$ at the source pass the exit slit at different

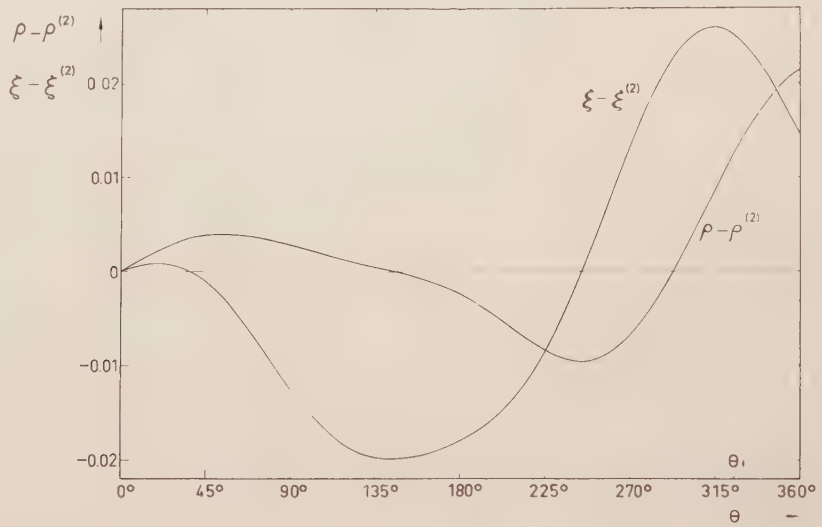


Fig. 1. Difference between the orbit $(\rho,\xi)$ determined with the computer and the orbit $(\rho^{(2)}, \xi^{(2)})$ calculated by second-order perturbation theory, for the case $m = 2$. Eqs. (3) an (4) of reference 1 were used for determination of $\rho^{(2)}$ and $\xi^{(2)}$, respectively, except that $\zeta_r$ and $\zeta_z$ were replaced by tan $\zeta_r$ and tan $\zeta_z$. The initial conditions were $\rho_0 = \xi_0 = 0$, tan $\zeta_r = 0.1414$, and tan $\zeta_z = 0.3145$.

† Contribution No. 912. This work was performed in the Ames Laboratory of the U.S. Atomic Energy Commission.

†† Present address: Max Planck Institute for Nuclear Physics, Heidelberg, Germany. The major portion of the present work was performed while this author was on leave from the Max Planck Institute.

[1]) H. Daniel, Bull. Am. Phys. Soc. Ser. II, **4** (1959) 326; Rev. Sci. Instr. **31** (1960) 249.

[2]) The special case of 324.50° focusing has independently been treated by Trier [J. O. Trier, Physikal. Verhandlungen **10** (1959) 73 (abstract)].

heights but electrons starting with the same angle $\zeta_z$ pass the exit slit at the same height, independent of the source height in first order.

The analytic treatment[1]) has been done with second-order perturbation theory. Hence the exact shape of the exit slit as well as the magnitude of the remaining aberrations were undetermined and a more extended investigation accordingly was required. Numerical calculations have been performed to determine both the shape of the exit slit and the resolving power for the cases $m = 2$, 3, 4, and 5, $n = 1$ of ref.[1]). All the calculations are for a source located at the radius of the stationary orbit, $\rho_0 = 0$. It is the main purpose of the present paper to present the results of this numerical work. Results for the special case in which $m = 1$ and $n = 1$ are treated in an Appendix.

With proper choice of the magnetic field and of the exit slit no aperture terms (terms in $\zeta_r$ and $\zeta_z$ only) contribute to the resolution width when $\zeta_r = 0$ or $\zeta_z = 0$. The entrance diaphragm may appropriately have the shape of a diamond, therefore, to provide a large radial aperture angle $\zeta_r$ and a large axial aperture angle $\zeta_z$ but only small cross products $\zeta_r \cdot \zeta_z$. The optimum shape of the entrance diaphragm depends on the actual size of the remaining terms in $\zeta_r$ and $\zeta_z$. For symmetry reasons only aperture terms with even powers of $\zeta_z$ can contribute. The only remaining fourth-order term is then the term with $\zeta_r^2 \cdot \zeta_z^2$. It turns out, however, that even this term is small. The resulting actual resolving width is chiefly due to a variety of higher-order terms, and no attempt has been made to separate the components.

## 2. Computer Calculations and Discussion

The general procedure for the computations has been described in a previous paper[3]). Table 1 lists the field coefficients employed. Table 2 contains the coordinates for several points of the exit slit as determined directly by the computer calculations. Table 3 gives the coefficients of proposed interpolation formulas for the exit slit,

[3]) H. Daniel and L. Jackson Laslett, submitted to Rev. Sci. Instr. **31** (1960) 1225.

TABLE 1
Field coefficients employed in the computational work[a])

| $m$ | $-\alpha$ | $\beta$ | $-\gamma$ | $\delta$ |
|---|---|---|---|---|
| 2 | 0.69230770 | 0.46153846 | 0.31656 | 0.22965 |
| 3 | 0.86206897 | 0.75862069 | 0.68192 | 0.62285 |
| 4 | 0.92452830 | 0.86792453 | 0.82361 | 0.78722 |
| 5 | 0.95294118 | 0.91764706 | 0.88934 | 0.86551 |

[a]) The fifth and higher-order coefficients were taken to be zero.

$$\theta_1 = \tilde{\theta}_1 + a_2\xi_1^2 + a_4\xi_1^4 + a_6\xi_1^6 \qquad (1a)$$

$$-\rho_1 = \quad b_2\xi_1^2 + b_4\xi_1^4 + b_6\xi_1^6\,, \qquad (1b)$$

where $\tilde{\theta}_1$ denotes the value of $\theta_1$ for orbits with $\zeta_z = 0$ and $\xi_1$ and $\rho_1$ represent the axial and radial coordinates of the exit slit. Typical results are shown in table 4, in which $\Delta\rho$ is the displacement relative to the exit slit for the initial conditions $\xi_0$, $\sin\zeta_r$, and $\sin\zeta_z$ listed; $D$ is the dispersion as given by eq. (5) of ref.[1]); and $\omega$ is the fractional solid angle determined by the

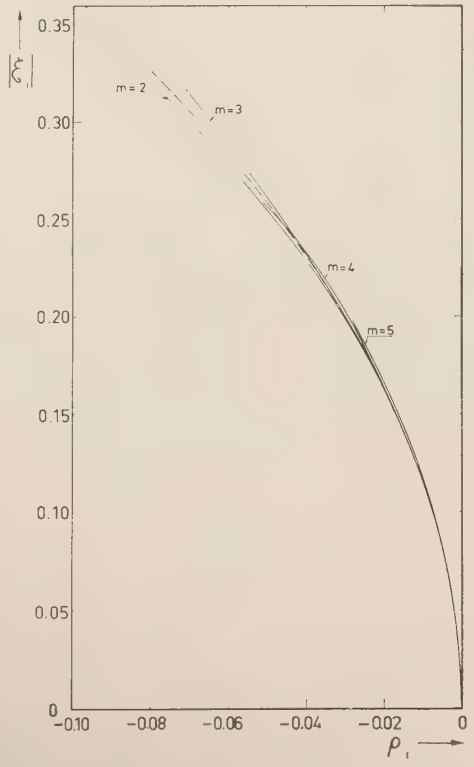


Fig. 2. Axial coordinate, $\xi_1$, of the exit slit as a function of the radial coordinate, $\rho_1$. The result of the second-order approximation[1]) is indicated by the dashed line.

entrance diaphragm. Concurrently $|\Delta\rho/D|$ is of the order of the resolution width (full width at half maximum) for the $\omega$-value listed. It has been assumed that $|\Delta\rho/D|$ does not differ strongly for orbits with the same $|\sin\zeta_r \sin\zeta_z|$. Table 5 contains, for the model $m = 2$, data which show the variation of the exit slit coordinates $\rho_1, \theta_1$ with the electron momentum $p$ (in units of the momentum $p_0$ for the stationary orbit) in the case $\xi_0 = \zeta_z = 0$, this result being of interest for spectrographic application.

Fig. 1 shows as an example the deviation of the orbit determined with the computer from the orbit calculated by second-order theory[1]). Fig. 2 depicts the $\rho$-dependence of the $\xi$-coordinate of the exit slit and fig. 3 shows the $\theta$-dependence of the $\xi$-coordinate of the exit slit.

As can be seen from table 4, the resolution

TABLE 2
Coordinates of several points of the exit slit

| $m$ | $\sin\zeta_z$ | $\zeta_z$ | $\theta_1$ | $-\rho_1$ | $\xi_1$ |
|---|---|---|---|---|---|
| 2 | 0 | 0 | 324.4999° | 0 | 0 |
| 2 | 0.0500 | 0.0500 | 324.5930° | 0.0027096 | — 0.0600478 |
| 2 | 0.1000 | 0.1001 | 324.8542° | 0.0108560 | — 0.1198944 |
| 2 | 0.1500 | 0.1506 | 325.2340° | 0.0244797 | — 0.1793385 |
| 2 | 0.2000 | 0.2014 | 325.6643° | 0.0436105 | — 0.2381783 |
| 2 | 0.2500 | 0.2527 | 326.0787° | 0.0682150 | — 0.2962113 |
| 2 | 0.3000 | 0.3047 | 326.4402° | 0.0981331 | — 0.3533301 |
| 3 | 0 | 0 | 484.660° | 0 | 0 |
| 3 | 0.0500 | 0.0500 | 484.816° | 0.0021754 | 0.0538343 |
| 3 | 0.1000 | 0.1001 | 485.102° | 0.0086960 | 0.1075417 |
| 3 | 0.1500 | 0.1506 | 485.000° | 0.0194868 | 0.1609914 |
| 3 | 0.2000 | 0.2014 | 483.792° | 0.0342415 | 0.2141134 |
| 3 | 0.2500 | 0.2527 | 480.536° | 0.0521590 | 0.2666664 |
| 3 | 0.3000 | 0.3047 | 474.401° | 0.0714774 | 0.3171561 |
| 4 | 0 | 0 | 655.209° | 0 | 0 |
| 4 | 0.0500 | 0.0500 | 655.407° | 0.0020287 | — 0.0519840 |
| 4 | 0.1000 | 0.1001 | 655.475° | 0.0080765 | — 0.1038533 |
| 4 | 0.1500 | 0.1506 | 653.947° | 0.0179476 | — 0.1556196 |
| 4 | 0.2000 | 0.2014 | 648.524° | 0.0308293 | — 0.2061902 |
| 4 | 0.3000 | 0.3047 | 617.047° | 0.0513132 | — 0.2589 |
| 5 | 0 | 0 | 829.74° | 0 | 0 |
| 5 | 0.0500 | 0.0500 | 830.06° | 0.001965 | 0.051201 |
| 5 | 0.1000 | 0.1001 | 829.86° | 0.00779 | 0.10230 |
| 5 | 0.1500 | 0.1506 | 825.9° | 0.0171 | 0.1531 |
| 5 | 0.2000 | 0.2014 | 813.5° | 0.0281 | 0.1976 |

TABLE 3
Coefficients for the interpolation polynominals

| $m$ | $a_2$ | $a_4$ | $a_6$ | $b_2$ | $b_4$ | $b_6$ |
|---|---|---|---|---|---|---|
| 2 | 26.228 | — 113.1 | 228 | 0.75000 | 0.366 | — 0.62 |
| 3 | 58.87 | — 1812 | 1880 | 0.75000 | 0.24 | — 6.6 |
| 4[a] | 89.8 | — 6075 | 8400 | 0.75000 | — 0.08 | — 11.9 |
| 5[b] | 160 | — 14460 | 27500 | 0.75000 | — 0.1 | — 43 |

[a]) Coefficients for $|\xi_1| < 0.21$.
[b]) Coefficients for $|\xi_1| < 0.16$.

TABLE 4
Typical results

| $m$ | $\xi_0$ | $\sin \zeta_r$ | $\sin \zeta_z$ | $\Delta p/D$ | $\omega(\%)$ |
|---|---|---|---|---|---|
| 2 | 0 | 0.06 | 0.1 | $1.0 \times 10^{-6}$ | 0.4 |
| 2 | 0 | 0.1 | 0.2 | $-7.3 \times 10^{-6}$ | 1.3 |
| 2 | 0 | 0.14 | 0.3 | $-4.0 \times 10^{-4}$ | 2.7 |
| 2 | 0.02 | 0.14 | 0.3 | $-5.3 \times 10^{-4}$ | 2.7 |
| 3 | 0 | 0.06 | 0.1 | $4.8 \times 10^{-5}$ | 0.4 |
| 3 | 0 | 0.08 | 0.2 | $4.4 \times 10^{-4}$ | 1.0 |
| 3 | 0 | 0.1 | 0.3 | $5.9 \times 10^{-4}$ | 1.9 |
| 3 | 0.02 | 0.1 | 0.3 | $8.7 \times 10^{-4}$ | 1.9 |
| 4 | 0 | 0.03 | 0.1 | $1.9 \times 10^{-5}$ | 0.2 |
| 4 | 0 | 0.05 | 0.2 | $3.0 \times 10^{-4}$ | 0.6 |
| 5 | 0 | 0.02 | 0.05 | $1.4 \times 10^{-6}$ | 0.06 |
| 5 | 0 | $-0.02$ | 0.05 | $-1.0 \times 10^{-6}$ | 0.06 |
| 5 | 0 | 0.02 | 0.1 | $1.0 \times 10^{-5}$ | 0.1 |
| 5 | 0 | $-0.02$ | 0.1 | $-1.5 \times 10^{-5}$ | 0.1 |

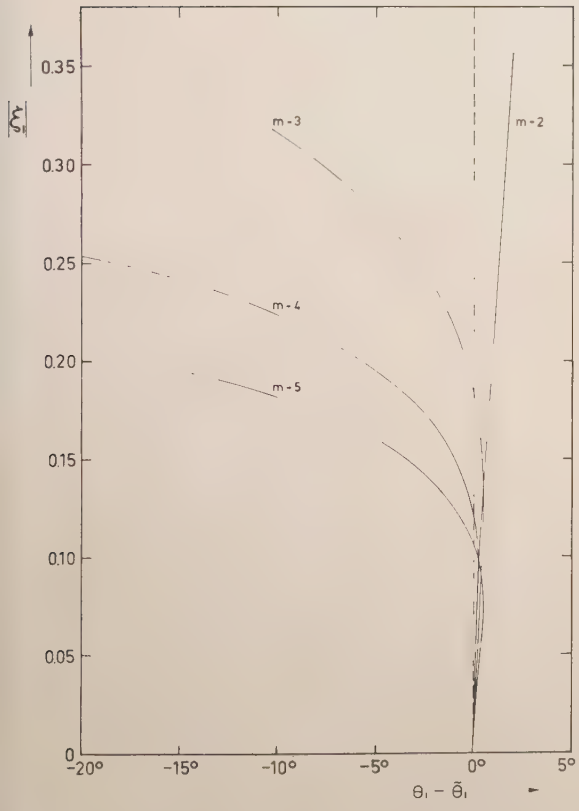


Fig. 3. Axial coordinate, $\xi_1$, of the exit slit as a function of the azimuthal angle difference, $\theta_1 - \tilde{\theta}_1$. The result of the second-order approximation[1]) is indicated by the dashed line.

TABLE 5
Exit-slit coordinates as a function of $p_0/p$ in the case $m = 2$

| $p_0/p$ | $\rho_1$ | $\theta_1$ |
|---|---|---|
| 1 | 0 | 324.4999° |
| 1.02 | $-0.1199$ | 316.5697° |
| 1.04 | $-0.2223$ | 309.5836° |

width increases rapidly with increasing fractional solid angle $\omega$, as well as with increasing $m$-value. In any case, however, the resolution is very good for $\omega$-values which are not too large. As discussed in ref.[1]) the models with the higher $m$-values have a high dispersion, which means that a larger source may be used and that source positioning is less critical. Such designs require, however, special arrangements to prevent electrons of undesired momenta from hitting the detector. A source shift was proposed for this purpose[1]). It has been shown[3]), in the case of a high-dispersion double-focusing spectrometer, that a source shift as great as 20% from the stationary orbit does not alter the electron-optical properties significantly. It may be expected that the same is true for the spectrometer with a curved exit slit. Therefore no calculations

for a displaced source were performed, although it cannot be expected that the shape of the exit slit will be exactly the same.

**Acknowledgments**

It is a pleasure to thank Mr. M. Storm and the staff of the MURA Computer Section for kindly performing the computations. The authors are indebted to Mr. B. McDaniel and Mr. C. Engler for their help in evaluating the data.

**Appendix**

THE CASE $m = 1$

The special case $m = 1$, $n = 1$, for which one would have $\alpha = -\frac{1}{6}$, has been omitted throughout this paper as well as in ref.[1]). In this case the perturbation theory is not applicable, as indicated by the vanishing of certain denominators in the orbit equations [eqs. (3) and (4) of ref.[1])]. It might be expected, however, that the actual orbits would behave "regularly" and a suitable spectrometer would be possible, so computer work also was performed for this case.

Unfortunately, the coupling between radial and axial oscillations was found to be so strong, not only for small oscillation amplitudes but also for large, that the spectrometric efficiency of this model is rather poor. The computational results indicated that the correct shape of the exit slit is, in second order, that given by the perturbation theory[1]). Orbits for which $\zeta_z$ and/or $\xi_0$ differ from zero, and for which $\zeta_r$ differs from zero, however, pass the exit surface at a height very different from that for an orbit with the same $\zeta_z$ and $\xi_0$ but with vanishing $\zeta_r$. Accordingly, because of the curvature of the exit slit, a large displacement, $\Delta\rho$, results—thus, for example, with $\omega \approx 0.6\%$, $\Delta\rho/D$ was found to be $6.5 \times 10^{-3}$.

NUCLEAR INSTRUMENTS AND METHODS 10 (1961) 53–65; NORTH-HOLLAND PUBLISHING CO.

# A $dE/dx$ — $E$ COUNTER TELESCOPE FOR CHARGED PARTICLES PRODUCED IN REACTIONS WITH 14 MeV NEUTRONS

L. G. KUO, M. PETRAVIĆ and B. TURKO

*Institute Ruder Bošković, Zagreb, Yugoslavia*

Received 11 October 1960

A $dE/dx$ — $E$ counter has been constructed for measuring angular distributions of charged particles produced in reactions with 14 MeV neutrons. Several requirements on such an instrument are considered with regard to particle selection efficiency, background, angular definition, and counting rate. Optimum design with a given angular definition is discussed. Actual performance of the counter is presented and possible improvements suggested especially as regards to background.

## 1. Introduction

In studying nuclear reactions and especially angular distributions of reaction products, it is very often necessary to be able to distinguish between various kinds of charged particles. In other words, one often has to measure the energy spectrum of one kind of charged particles against the background of other charged particles. A method that is commonly used for charged particle discrimination is the method of simultaneous measurement of energy and specific ionization. Information afforded by these two may be used in different ways to select the desired particles and the most important methods will be discussed later in this paper. The method was first developed for medium energy work by Wolfe, Silverman and De Wire[1]) and Aschenbrenner[2]). They used two scintillation counters in coincidence. A thin plastic scintillator, whose thickness is much smaller than the range of particles measured, is used as $dE/dx$ counter, followed by a thick scintillation crystal for the $E$-counter. Later improvements included an additional "thin" counter which served to define the direction of the charged particles uniquely and to reduce background by triple coincidence. In neutron work, an anticoincidence counter was introduced in front of the target to eliminate the background arising from materials such as counter wall which is invariably present between the target and the neutron source. Owing to the presence of large quantities of hydrogen in plastic scintillators, and the difficulty of making uniform and thin inorganic scintillators, the thin scintillation counter is generally replaced by gas proportional counters or ionization chambers in neutron work.

In constructing the present $dE/dx$—$E$ counter telescope, the existing designs[3,4,5,6]) were considered in the light of our requirement which is the measurement of angular distributions and energy spectra of protons and deuterons in the range 3 MeV–14 MeV, with an overall discrimination efficiency for protons against deuterons and vice versa of better than 90%.

## 2. Construction of the Counter

A drawing of the counter is shown in fig. 1. It is similar in design to the counter of Marcazzan, Sona and Pignanelli[5]), the essential difference being in the method of defining the active volume of the $dE/dx$ proportional counter and in the

[1]) B. Wolfe, A. Silverman and J. W. De Wire, Rev. Sci. Instr. **26** (1955) 504.

[2]) F. A. Aschenbrenner, Phys. Rev. **98** (1955) 657.

[3]) F. L. Ribe and J. D. Seagrave, Phys. Rev. **94** (1954) 934.

[4]) C. H. Johnson and C. C. Trail, Rev. Sci. Instr. **27** (1956) 468.

[5]) G. Marcazzan, A. M. Sona and M. Pignanelli, Nuovo Cimento **10** (1958) 155.

[6]) W. Jack and A. Ward, Proc. Phys. Soc. **75** (1960) 833.

design of the target chamber which presents the same wall thickness to the incoming neutrons up to the scattering angle of 125°.

The counter consists essentially of two brass cylindrical chambers soldered at right angles to each other. The first chamber, 7.4 cm in diameter and 15.2 cm in height, contains the target wheel with four targets up to 3 cm in diameter and the anticoincidence proportional counter. It has two detachable lids. The one on the top carries the lead for the anticoincidence proportional counter and the glass filling tube, while the one on the side (not visible on the drawing) enables the target wheel to be removed. The target wheel is held in position by a catch and may be rotated from the outside by means of a magnet. The second cylindrical chamber which is 4 cm in diameter houses the two proportinal counters and the scintillation counter. The first (No. 1) short proportional counter is not required to have good energy resolution since it serves only to define the direction of the beam and hence to reduce the random coincidence rate. However, it is important that its walls are not seen by the scintillation counter for that would then give rise to true coincidences. This is achieved by placing a graphite aperture between counters 1 and 2. The second (No. 2) coincidence proportional counter is the $dE/dx$ counter. It has an active volume 12.7 cm in length and 3.6 cm in diameter. The active volume is defined by means of two tubes 0.045 cm in diameter and 2 cm long at each end of the counter. These tubes, at the same potential as the counter wire, while not producing a strong enough field for gas

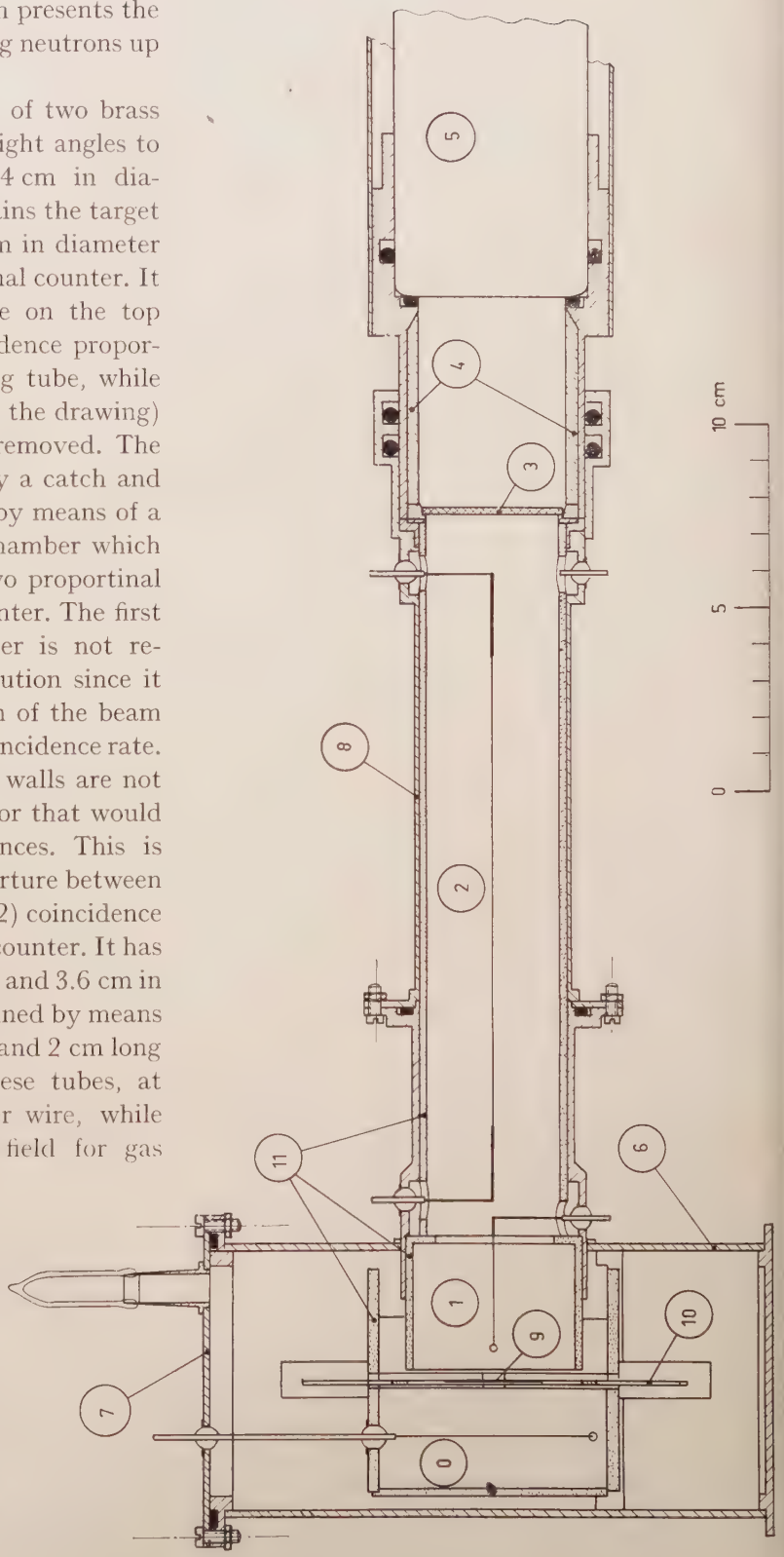


Fig. 1. Vertical cross section of the $dE\ dx$ — $E$ counter telescope. (0) Anticoincidence proportional counter. (1) Proportional counter. (2) The $dE/dx$ proportional counter. (3) CsI(Tl) scintillation crystal. (4) MgO light guide. (5) RCA 6342 photomultiplier. (6) The brass cylindrical chamber for housing the target and the anticoincidence counter. (7) The top lid with gas filling tube. (8) The brass cylindrical chamber for the coincidence counters. (9) The target. (10) The target wheel. (11) Graphite lining of the counters.

multiplication, ensure that the lines of force of electric field remain almost perpendicular to the counter wire at the active volume boundary thus ensuring a sharp definition of the latter.

The counter wires in all three counters are of tungsten 0.015 cm in diameter. The counters are filled with purified dry $CO_2$ at 80 mm Hg and operate at voltages between 1400–1700 volts. All the counters and the target chamber are lined with 2 mm thick graphite (99.5% purity) to reduce proton and deuteron background.

The $E$ counter (No. 3) is a scintillation counter consisting of a 3.8 cm diameter and 0.2 cm thick CsI(Tl) crystal combined with a RCA 6342 photomultiplier. An aluminium cylinder, painted with 0.5 cm thick MgO serves as light guide to distribute light evenly over the photocathode surface.

In order to measure angular distributions the counter can be mounted on a rotatable arm enabling the counter to cover an angular range from 0° to 145°.

## 3. Particulars of the Counter Design

### 3.1. GEOMETRY

A detailed study of the geometry, which involves target and crystal detector size, source to target, and target to detector distances, was made in order to determine how well the energy and the scattering angle of the reaction products may be defined. There is no best choice in the sense that one could always improve on the angular and energy definition if one is prepared to have lower counting rate. For that reason our choice was arbitrary except that the crystal size was made as large as possible in relation to the target in order to have a smaller angular spread for the same solid angle. The same applies to the target size with respect to the neutron source although the target size could be varied to some extent from one experiment to another.

Our final choice was as follows: neutron source size (fixed): 0.5 cm diameter, target size: 2 cm diameter, detector size: 3.6 cm diameter, source to target distance: 10 cm, target to crystal distance: 23.4 cm. With these figures, the maximum angular spread is $\pm$ 12.5° at 0° and less at other angles.

The counting rate can be given only for a particular case. Assuming a target of mass number 30 and thickness of 10 mg/cm², a cross section of 10 mb/sterad and a flux of $10^9$ neutrons/sec in $4\pi$ (all characteristic values), the counting rate is 5.4 counts/min.

### 3.2. PARTICLE DISCRIMINATION

This is obtained by a measurement of $\Delta E$ over a fixed path $\Delta x$ in No. 2 counter which then gives the value of $dE/dx$. In order to obtain a good measurement of $dE/dx$ and to avoid producing large distortions in the energy spectrum, $\Delta x$ has to be small compared to the range of the particles. This however introduces another difficulty. If $\Delta x$ is small, the average energy loss $\Delta E$ can become comparable or smaller than the maximum energy loss possible in a single collision of the charged particle with an electron. In this case, as has been shown theoretically by Landau[7]), and Symon[8]), $\Delta E$ has a large statistical spread which can make a discrimination by this method rather ineffective.

In designing a $dE/dx - E$ counter, one then has to calculate what $\Delta x$ is needed to obtain the required difference in energy loss $\Delta E$ for different charged particles. The calculation is facilitated by the extensive numerical calculations of Symon which have been summarized by Rossi[9]). For the most probable energy loss $\Delta E_{mp}$, which is the relevant quantity here as the distribution of energy loss is asymmetric, Symon gives the following formula:

$$\Delta E_{mp} = \frac{C m_e M c^4 x}{E}\left[\ln \frac{4 C m_e^2 c^4 x}{(1-\beta^2)\, I^2(Z)} - \beta^2 + j\right] \qquad (1)$$

where

$M$ = mass of the particle
$E$ = energy of the particle
$x$ = absorber thickness in g/cm²
$C$ = a constant depending on the absorber
$m_e$ = electron mass

[7]) L. Landau, J. Phys. U.S.S.R. **8** (1944) 201.
[8]) K. R. Symon, Harvard University Thesis (1948).
[9]) B. B. Rossi, High Energy Particles (Prentice-Hall, New York, 1952).

$Z$ = atomic number of the absorber nucleus
$c$ = velocity of light
$I(Z)$ = mean excitation potential of the absorber nucleus
$j$ = a correction factor which is composed of density effect and shell corrections.

It may be noted that the ratio of the most probable energy loss for deuterons and protons of the same energy is approximately a factor of 2 since $\Delta E_{\mathrm{mp}} \propto M/E$, just as in the Bethe-Bloch theory[10,11]). This fact enables a simultaneous separation to be made for deuterons and protons over a range of energies. Fig. 2 shows a theoretical calculation of the distribution of energy loss for protons and deuterons at 12.2 MeV. The mean excitation potential $I$, used in the calculation, was taken as $I = 13\,Z$ eV. This value of $I/Z$ is generally used instead of earlier lower values after the extensive measurements of Bichsel *et al.*[12]) and Burkig *et al.*[13]).

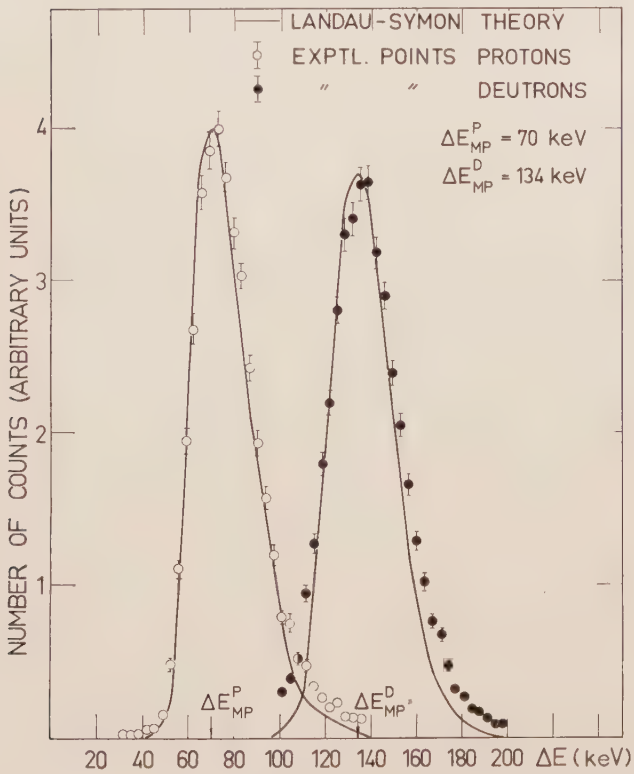


Fig. 2. The distribution of energy loss in the $\mathrm{d}E/\mathrm{d}x$ counter for 12.2 MeV protons and deuterons. The theoretical curves have been calculated from ref.[9]) using $I = 13Z$ eV. The proton experimental points have been obtained with protons having an energy spread from 10.2 MeV to 14.2MeV. The deuteron experimental points are obtained with deuteron energies ranging from 11.6 MeV to 12.8 MeV. The absolute values of $\Delta E_{\mathrm{mp}}$ for protons and deuterons have not been measured. The areas under the theoretical proton and deuteron curves have been made equal. The errors shown are statistical errors.

It is clear that even with a counter of ideal resolution, it is not possible to obtain a 100% separation efficiency for the $\Delta x$ given. Such a $\Delta x$ can, however, be quite adequate in many cases since for reactions with 14 MeV neutrons, most deuterons come off at lower energies where the separation gets better. Fig. 2 also shows that one needs a $\mathrm{d}E/\mathrm{d}x$ counter of fairly good resolution in order not to widen the proton and deuteron distributions. Even a small increase in width of the distribution would result in considerable worsening of the discrimination efficiency. It is interesting to note that for $\Delta E$ larger than the maximum energy loss in a single collision, as in our case, the method of Igo *et al.*[14]), which consists of splitting the counter into two counters of equal length and selecting the smaller of the two $\Delta E$'s, does not represent a significant improvement.

As has been noted, we have chosen a proportional counter for the $\mathrm{d}E/\mathrm{d}x$ counter because it is capable of giving better resolution and, most important of all, it can be hydrogen-free and be made very uniformly thin. Also its thickness can be easily varied to suit a particular experiment. A good energy resolution implies a well defined active volume in the counter. This cannot be achieved by the use of thin windows because they would unduly increase the total energy loss of the particles and would also (in the case of neutron reactions) increase the background. This problem was solved by the thick to thin wire transition (see section 2) which has the merit of avoiding the use of field tubes and insulators which would only increase the background

[10]) H. A. Bethe, and M. S. Livingston, Rev. Mod. Phys. **9** (1937) 261.

[11]) F. Bloch, Z. Physik **81** (1933) 363.

[12]) H. Bichsel, R. F. Mozley and W. A. Aron, Phys. Rev. **105** (1957) 1788.

[13]) V. C. Burkig, and K. R. MacKenzie, Phys. Rev. **106** (1957) 848.

[14]) G. Igo, and R. M. Eisberg, Rev. Sci. Instr. **25** (1954) 450.

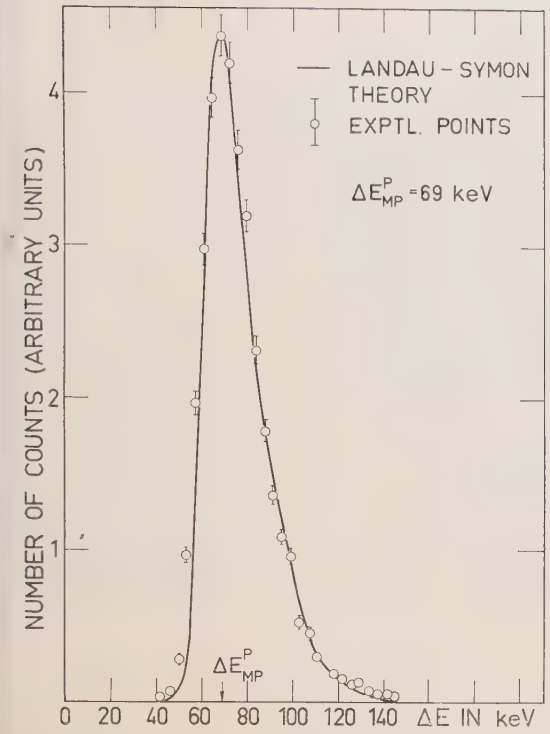


Fig. 3. The distribution of energy loss in the $dE/dx$ counter for 13.8 MeV protons. The theoretical curve has been calculated from ref.[9]) using $I = 13Z$ eV. The experimental points have been obtained with proton energies ranging from 13.2 MeV to 14.4 MeV. The absolute value of $\Delta E_{mp}$ has not been measured. The errors shown are statistical errors.

and produce a large shadow. The small counter which results has the advantage over the Johnson type[4]) in that it is a much faster counter for the same operating conditions, and has less background troubles (see section 3.3).

The performance of the counter was first tested with 6.2 MeV and 8.94 MeV $\alpha$'s from a ThC source. The distribution of energy loss $\Delta E$ in the counter was found to be symmetric and its width at half maximum was 6%. Taking into account noninstrumental effects such as Landau effect, the counter resolution was found to be of the order of 4%. The performance was further tested in the neutron flux by measuring the energy loss of protons and deuterons knocked-on by 14.4 MeV neutrons. Fig. 3 shows a comparison of experimental points with Landau-Symon theory for protons of 13.8 MeV. The energy of 13.8 MeV is an average between 13.2 MeV and 14.4 MeV, the energy spread being produced by the target thickness and the finite angular definition of the counter. As may be seen, the agreement with theory is satisfactory. This has been found by other workers[14,4]) at higher energies and for different energy losses. As for the separation efficiency, the results are shown and compared with theory in fig. 2. Here the proton energy ranges from 10.2 MeV to 14.2 MeV because of the target thickness and because of the rapid variation of proton energy with angle as the counter was set at 18°. For the deuteron curve, a 10 mg/cm² thick deuterated paraffin target was used and the counter was set at 0°. The deuteron energy ranges from 11.6 MeV to 12.8 MeV. The agreement with theory is still quite good in this case owing to the slow variation of $\Delta E$ with energy. These curves give then the lower limit for the efficiency of discrimination between protons and deuterons. Theoretically one could count 97.4% of protons with 1.2% of deuterons. Experimentally one obtains 95% of protons with 3% of deuterons, all for the same number of protons and deuterons going through the counter.

### 3.3. BACKGROUND PROBLEMS

Since there is no possibility of neutron collimation with the existing geometry of the experiment, every part of the counter is irradiated by neutrons and so those parts which are viewed by the scintillation counter would contribute many more counts than the target itself if extreme care were not taken in the design. The background may be reduced by lining the whole of the counter and in particular the parts viewed by the scintillation counter with a suitable material which gives the least number of protons and deuterons in the energy region of interest. Graphite was chosen for this purpose for it has the following relevant $Q$ values: $C^{12}(n,p)B^{12}$, $Q = -12.58$ MeV; $C^{12}(n,d)B^{11}$, $Q = -13.4$ MeV; $C^{12}(n,\alpha)Be^{9}$, $Q = -5.7$ MeV. A large number of $\alpha$ particles may be expected although these may not reach the scintillation counter. The use of triple coincidence also reduces the background although chance coincidences must still be considered. There exist chance coincidences between

all three counters and chance coincidences between real coincidences of a pair of counters and the third counter. Let us denote the number of counts/sec in the counters 1, 2, and 3 by $N_1$, $N_2$ and $N_3$ respectively and the number of real coincidences between pairs of counters by $N_{12}$, $N_{23}$, and $N_{13}$, then the number of chance coincidences/sec is given by:

$$N = 3N_1N_2N_3\,\tau^2 + 2(N_{12}N_3 + N_{13}N_2 + N_{23}N_1)\,\tau \quad (2)$$

for

$$N_1,\ N_2,\ N_3 >> N_{12},\ N_{13},\ N_{23}$$

where $\tau$ is the coincidence resolving time.

The resolving time $\tau$ was made as short as possible. Unfortunately, the present type of counters cannot be made very fast. Firstly, the CsI(Tl) crystal has a decay time of 1.1 $\mu$sec, and secondly, a more serious limitation, there is a delay in the proportional counter pulse due to the finite time the initial electrons take to reach the central wire. This time may be longer than 1 $\mu$sec and the resolving time should be made longer than the maximum delay occurring when the particle passes near the wall of the counter. The drift velocity of the electron varies greatly between different gases and gas mixtures. Carbon dioxide was chosen for the present counter mainly because of the large negative $Q$-values for (n,p) and (n,d) reactions on carbon and oxygen, and because of its relative insensitivity to impurities. It is also a reasonably fast gas compared to other simple gases. Although certain admixtures of gases may be faster, they were not used because of their sensitivity to the presence of impurities. It has been found that the counter once filled with $CO_2$ does not change its characteristics over a period of 30 days.

The electron collection time in $CO_2$ may be calculated using the known dependence of electron velocity $v$ on $E/p$, where $E$ is the electric field and $p$ the gas pressure. We have found that the experimental values of $v$ given by Fulbright[15]) as a function of $E/p$ may be well approximated in the region of interest ($1.5 < E/p < 6.5$) by a parabola:

$$v = c\left(\frac{E}{p}\right)^2 + d\,. \quad (3)$$

The constants $c$ and $d$ giving the best fit with the data have been determined as 0.17 and 0.57 respectively for $E$ in volts/cm, $p$ in mm Hg, and $v$ in cm/$\mu$sec. With this the calculated parabola does not deviate from the experimental values for more than 5%. Now for cylindrical geometry

$$E = \frac{V}{r \ln b/a} \quad (4)$$

where

$r$ = radial distance from the central wire
$a$ = wire radius
$b$ = counter cylinder radius
$V$ = potential difference across the counter.

Substituting (4) in (3) one obtains $v$ as a function of distance $r$:

$$v = -\frac{\mathrm{d}r}{\mathrm{d}t} = \frac{K}{r^2} + d \quad (5)$$

where

$$K = \frac{cV^2}{p^2 \ln^2 (b/a)}\,.$$

Upon integration, one obtains the electron collection time as a function of the position $r_0$ where the electron is released:

$$t = -\frac{1}{d}\sqrt{\frac{K}{d}}\left(\operatorname{arctg}\sqrt{\frac{d}{K}}\,r_0 - \operatorname{arctg}\sqrt{\frac{d}{K}}\,a\right) + \frac{r_0 - a}{d}\,. \quad (6)$$

The electron collection time was calculated for a range of potential differences, wire diameters, and pressures, using formula (6). Of these, the upper limit of $V$ was set at 1800 volts, the pressure was set around 80 mm Hg for reasons of energy resolution, and the wire diameter had to be chosen so as to give the shortest collection time compatible with a reasonable gain.

To be able to calculate the gain, we measured it on a model of the counter for a certain pressure, wire diameter, and for several voltages using ThC' $\alpha$ particles. In this way, the two empirical constants of the formula of Rose and Korff[16]) giving the multiplication factor in a gas as a function of $V$, $p$, $b$, and $a$ were determined.

[15]) H. W. Fulbright, Encyclopedia of Physics Vol. **45** (Springer-Verlag, 1958) 24.

[16]) M. E. Rose, and S. A. Korff, Phys. Rev. **59** (1941) 850.

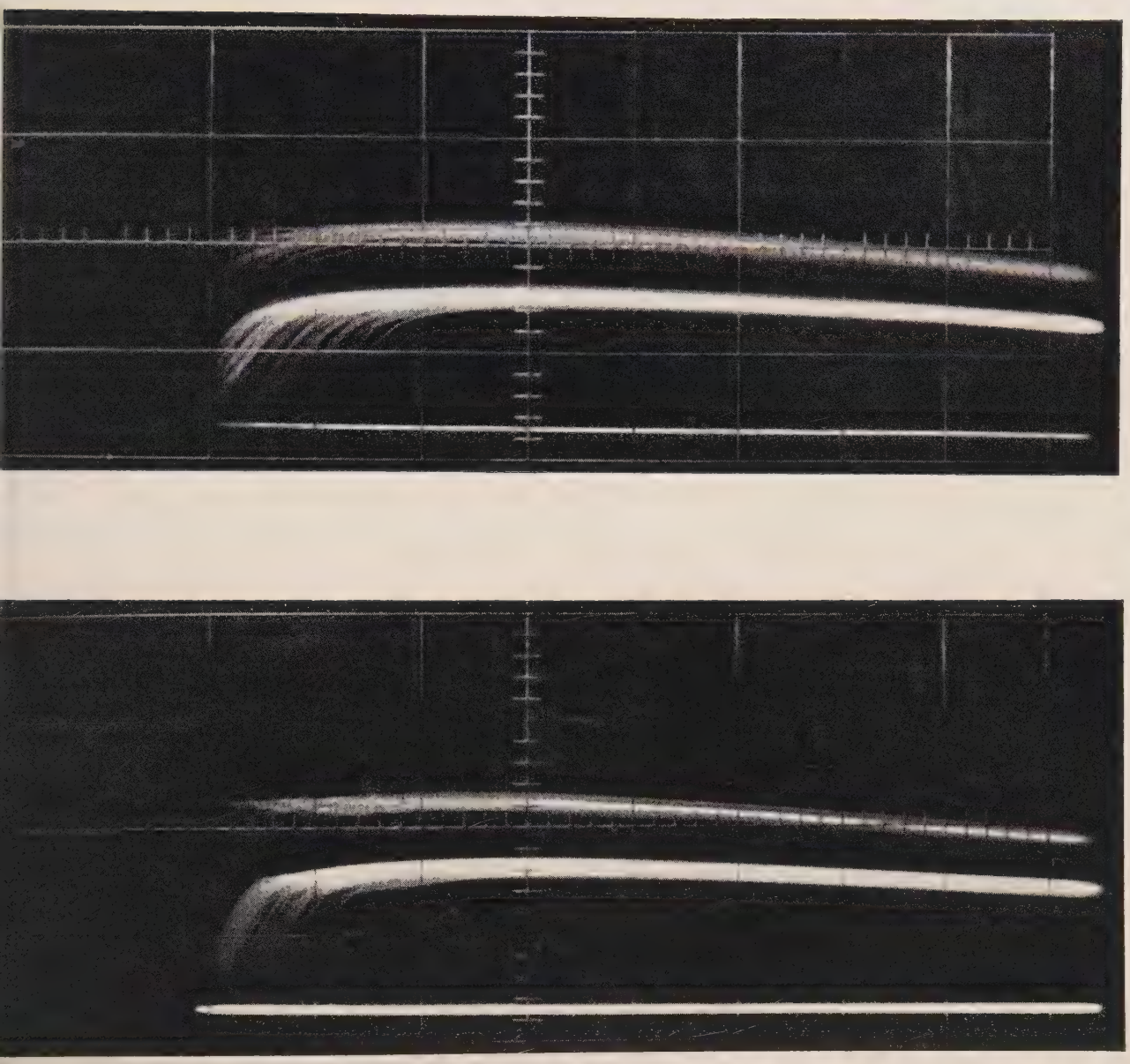


Fig. 4. Two examples of oscilloscope photograph measuring electron collection time in the proportional counter as a function of counter voltage. The cm scale is visible on the photograph and the time base is 0.5 $\mu$s/cm.

(a) Counter voltage = 1000 volts. The upper curve corresponds to $\alpha$'s of 6.2 MeV and the lower curve $\alpha$'s of 8.94 MeV

(b) Counter voltage = 1300 volts. The shape of the curves here is due to saturation in the preamplifier.

On the basis of the above calculations of gain and electron collection time, we chose a wire diameter of 0.015 cm. With this wire at 1500 V, we obtained a gain of a few hundreds and a collection time $< 1$ $\mu$sec. Actually it would have been better to use slightly higher voltages and a correspondingly thicker wire.

Before choosing the resolving time, the electron collection time was measured by a very simple method. Pulses from the proportional counter produced by a ThC $\alpha$ source at the target position are displayed on a Tektronix 545 oscilloscope whose time base was triggered by pulses from the scintillation counter produced by the same $\alpha$ particles. The pulses from the scintillation counter are amplified to maximum so as to trigger the oscilloscope as soon as possible after the instant of arrival of the pulse. This precaution is not absolutely necessary as may be seen in fig. 4, where two examples of oscilloscope photos are shown for two voltages. A measurement of the separation between the first and the last pulse gives the maximum delay due to electron drift irrespective of the delays introduced by the electronics in the measurement.

The calculated and measured electron collection times are compared in table 1.

TABLE 1
Experimental and calculated values of electron collection time as a function of counter voltage

| Counter voltage | 1000 V | 1100 V | 1200 V | 1300 V |
|---|---|---|---|---|
| $(t)_{\text{cal.}}$ | 0.91 $\mu$s | 0.82 $\mu$s | 0.72 $\mu$s | 0.64 $\mu$s |
| $(t)_{\text{measured}}$ | 0.80 $\mu$s | 0.75 $\mu$s | 0.64 $\mu$s | 0.58 $\mu$s |

The experimental values may be expected to have an error of 10% due to statistics. The calculated values may be too high by a maximum of 0.06 $\mu$sec from the fact that formula (6) is only accurate for $r$ larger than about 0.4 cm for the voltages considered. Hence the agreement between measured and calculated values may be considered satisfactory. On this basis, a coincidence resolving time variable between 1.5 and 2.5 $\mu$s was chosen. This resolving time was thought to be quite adequate to make the first term in eq. (2) negligible. Since it was believed that it was the most important term no precautions were taken in the design to keep the other term small.

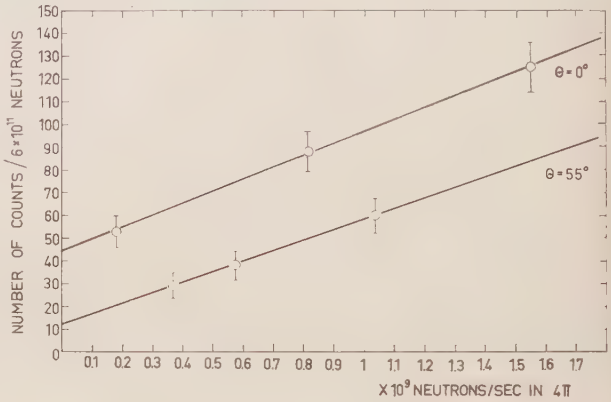


Fig. 5. The variation of background with neutron flux. The ordinate gives the total number of background counts above 1.5 MeV for a total number of $6 \times 10^{11}$ neutrons in $4\pi$. The abscissa gives the total neutron flux in $4\pi$. $\theta$ denotes the counter angle.

The first background measurements, however, gave considerably larger values than expected. When $N_1$, $N_2$ and $N_3$ were separately measured, the product $3\,N_1N_2N_3\tau^2$ was found in no way sufficient to account for the observed background. $N_{12}$, $N_{23}$, and $N_{13}$ were then separately measured which gave us the result that $N_{12}N_3\tau$ was mainly responsible for the background. Moreover, as may be seen from fig. 5, the total background above 1.5 MeV measured for a given number of neutrons from the source is a linear function of the neutron flux. This again may be explained by assuming that a term like $N_{12}N_3\tau$ is the main term. This may be readily seen by writing down eq. (2) in a different form:

$$n = 3n_0n_1n_2n_3\,\tau^2 f^2 + 2n_0(n_{12}n_3 + n_{13}n_2 + n_{23}n_1)\,\tau f \quad (7)$$

where $n$ is the total number of background counts for a total number $n_0$ of neutrons from the neutron source, $f$ is the neutron flux in number of neutrons/sec in $4\pi$, and $n_1$, $n_2$ and $n_3$ are defined by $N_i = n_i f$, $i = 1$, 2, and 3. At fluxes higher than $10^9$ neutrons/sec in $4\pi$, the quadratic term would also come into play.

Fig. 5 shows also that for the counter angle of 0° there is a part of the background which is independent of the flux. This part must come from parts of counter No. 1 such as the counter wire, the glass bead at the end of the wire etc. It is also possible that a few particles coming from the wall of the target chamber fail to be noticed by the anticoincidence counter. The angular distribution of this part of the background must be rather anisotropic as may be seen by comparison with the background at 55° where this part is very small. At 0°, this part represents about a half of the total background at the flux of $\approx 10^9$ neutrons/sec in $4\pi$.

As for the $n_{12}n_3$ term, it was found that it mainly comes from $\alpha$ particles from the $C^{12}(n,\alpha)Be^9$ reaction which start from the walls of counter No. 1 and the target chamber and traverse counters No. 1 and No. 2. This background could be eliminated by particle discrimination in the case the $\alpha$ particles produce big pulses in counter No. 2. There is, however, quite a fraction of small pulses in counter No. 2 which are coincident with No. 1. These cannot be eliminated in the same way. An obvious improvement would be to make the walls of No. 1 counter invisible to No. 2 counter. This is in practice difficult to realize. While this refinement may not be necessary for (n,p) and (n,d) reactions, it may be imperative if (n,$\alpha$) reactions were to be studied.

The background of the counter measured at a total neutron flux of $8 \times 10^8$ neutrons/sec in $4\pi$ in the region 1.5 MeV–15 MeV and without particle discrimination is as follows:

Counter: No. 3: 106000 counts/min

Counter No. 3 in coincidence with No. 2 and anticoincidence with No. 0: 240/min

Counter No. 3 in coincidence with No. 1 and 2, and anticoincidence with No. 0: 7/min

Counter No. 3 in coincidence with No. 1 and 2 but without anticoincidence counter: 20/min.

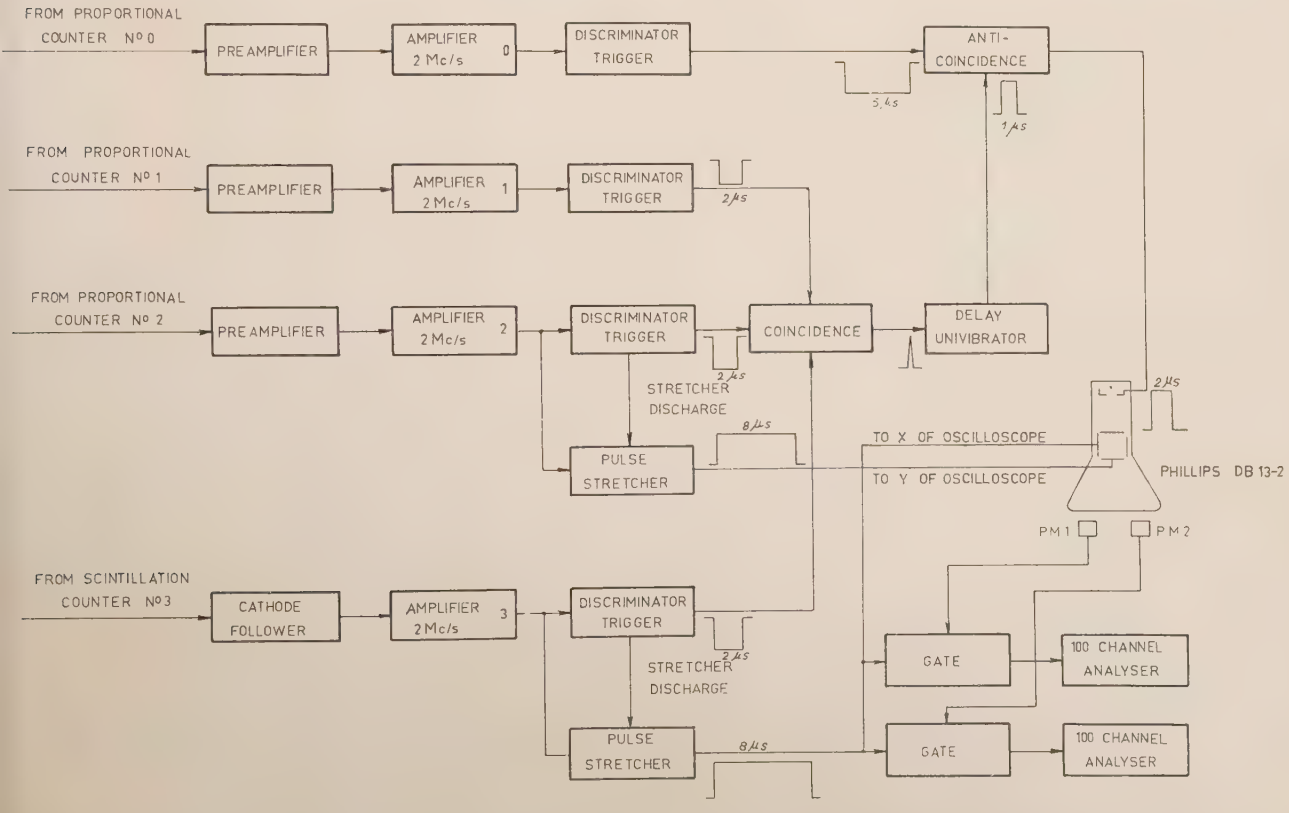


Fig. 6. Block diagram of the electronics using oscilloscope for particle discrimination.

However, when the apparatus is set to measure only deuterons in the energy range 3.5 MeV–12 MeV, the background measured for counter No. 3 in coincidence with No's 1 and 2 and anti-coincidence with No. 0 is 0.04 counts/min, which corresponds to a cross section of 75 microbarns for the example of section 3.1.

due to the slow drift of positive ions towards the cathode is almost preserved. However, to prevent pile-up and to obtain maximum signal to noise ratio, differentiation and integration time constants of 1 $\mu$s are used at the inputs of the amplifiers. Thus only the very fast rise of the proportional counter pulse is used for coinci-

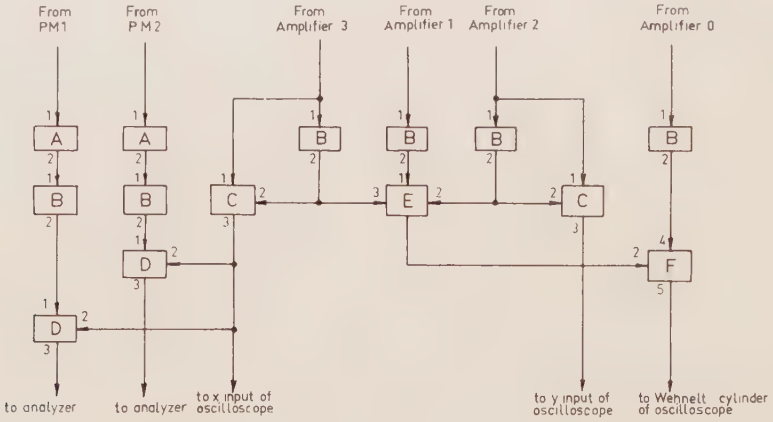


Fig. 7. Circuit diagram.

## 4. Electronics

As has been seen in section 3.2, $\Delta E$ is approximately proportional to $M/E$. An electronic multiplier can be used to give the product $\Delta E \cdot E$. This product, being twice for deuterons as for protons, can then be used to gate the $E$-spectrum. Another electronically simpler method, although perhaps not so easy to handle, is to plot $\Delta E$ and $E$ on an $X$–$Y$ oscilloscope. Spots corresponding to deuterons and protons will lie on distinct near-hyperbolas. The gating may be achieved by masking parts of the oscilloscope and setting photomultipliers to view the hyperbolas. This method has been adopted for the present system. Fig. 6 shows a block diagram of the electronics used, and fig. 7 some details of the circuitry.

Pulses from the proportional counters which are of the order of a few millivolts are transmitted through preamplifiers of gain 50 to the non-overloading amplifiers. The relevant time constants in the preamplifiers are fairly long, $\approx 20\ \mu$s, such that the original shape of the proportional counter pulse with its long decay

dence. Pulses from amplifiers 1, 2, and 3 are fed into pulse shapers with variable discrimination levels. For this purpose, 6BN6 tubes are used for triggering and their negative grid bias serve to

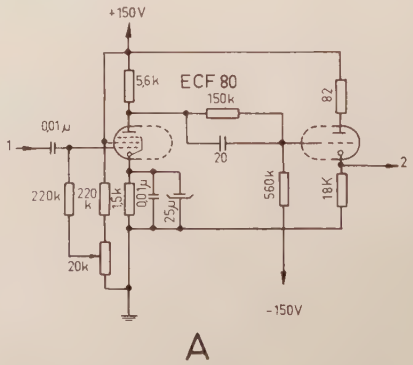


(A) Amplifier for the gating pulse.

define the discriminator levels. Univibrators following the 6BN6 provide pulses of standard amplitude and variable length between 1.5 $\mu$s and 2.5 $\mu$s. This length defines the resolving time $\tau$ of the coincidence system. Owing to the variable delay in the time of arrival of pulses in

ounters 0, 1, and 2 due to electron drift, it is ecessary to make the anticoincidence pulse om pulse shaper No. 0 5 $\mu$s long, and to in- roduce a delay between the coincidence and univibrator is then always delayed by a time $\tau$ with respect to the time of arrival of the first pulse in the coincidence circuit. After passing through the anticoincidence, the pulse is shaped to the

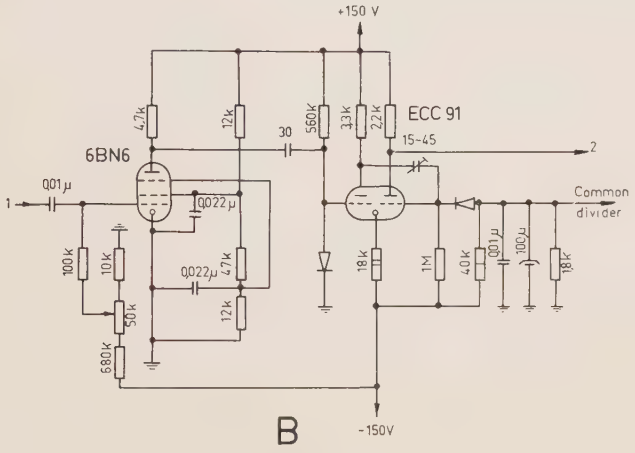


(B) Discriminator trigger.

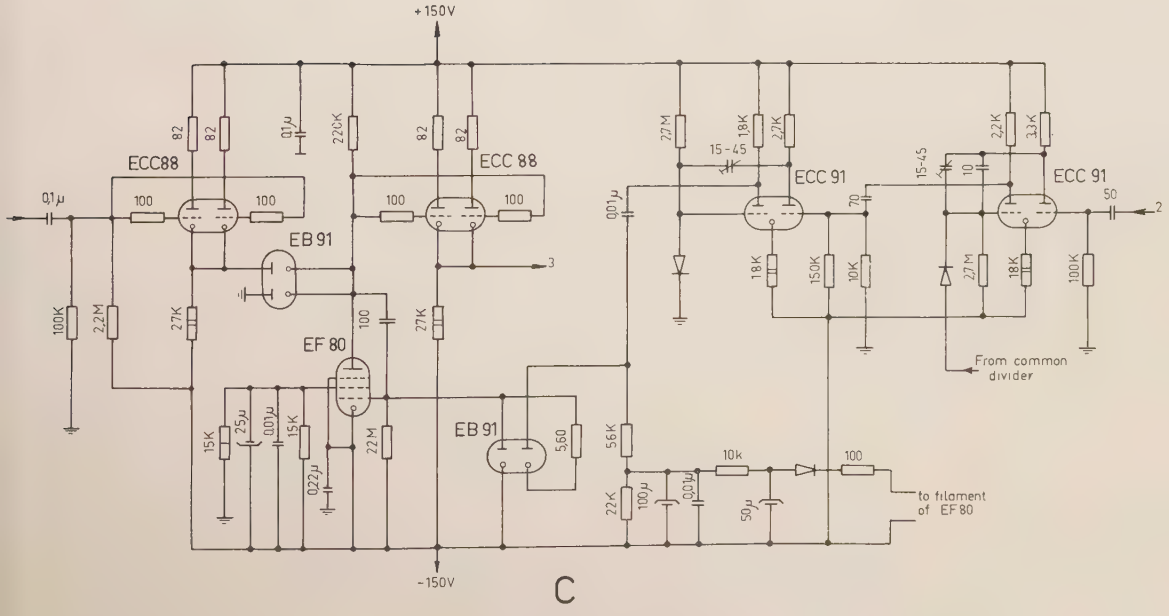


(C) Pulse stretcher.

nticoincidence circuit such that the anti- oincidence gating pulse always arrives before ne coincidence pulse and covers its entire length. his delay is realized by a univibrator which triggered by the trailing edge of the pulse om the coincidence circuit. The output of this required amplitude and length ($\sim$ 45 V, and 2 $\mu$s) and fed to the Wehnelt cylinder of a Phillips DB13–2 cathode ray tube.

Two stretchers based on the Miller circuit stretch the pulses from amplifiers 2 and 3 into 8 $\mu$s long pulses and these are sent to the $X$ and

$Y$ plates of the oscilloscope where they await the arrival of the coincidence-anticoincidence pulse on the Wehnelt cylinder before the spot corresponding to a certain $dE/dx$ and $E$ can be

loscope was used with a mask such that only protons above 1.5 MeV were detected. It may be noted that the background is extremely small. The resolution of the scintillation counter, in-

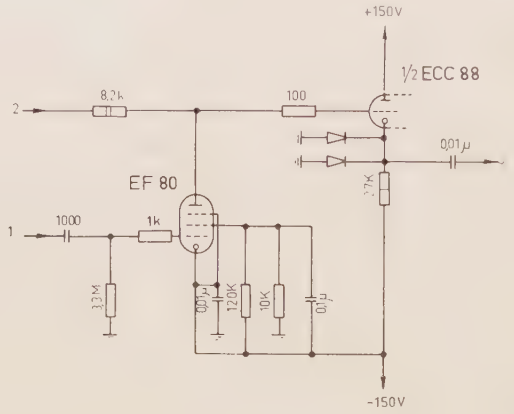


(D) Gate.

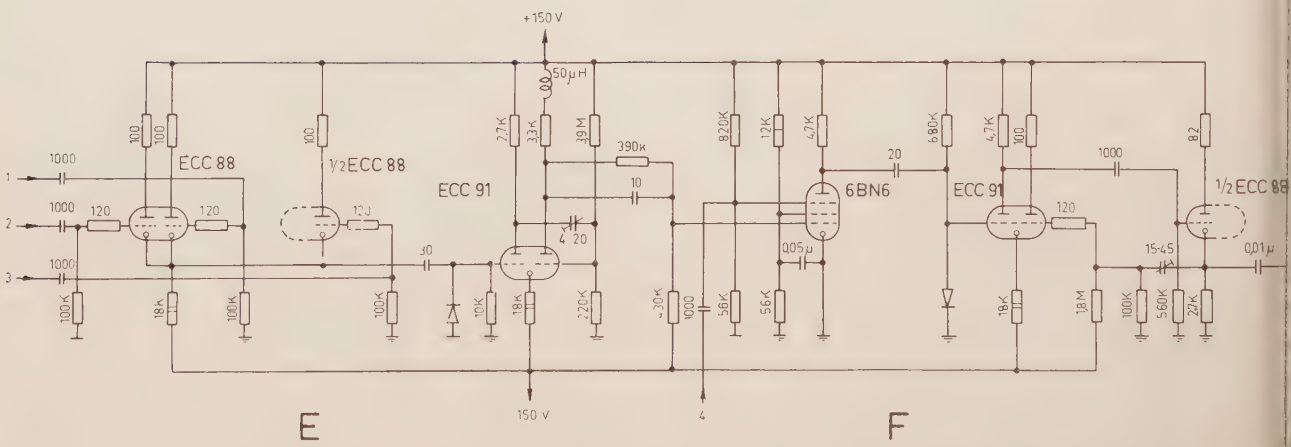


(E) Coincidence.

(F) Anticoincidence. All capacitors and resistors are in $\mu\mu$F and $\Omega$ respectively if not otherwise specified. All diodes are 0A85 type.

brightened. Two DuMont 6292 photomultipliers are placed in such a way that they view separately the regions where spots corresponding to protons and deuterons are expected to lie. Pulses from the two photomultipliers are amplified and used to gate the inputs to two 100-channel pulse height analysers. In this way spectra of protons and deuterons may be analysed simultaneously.

Fig. 8 shows a spectrum of knock-on protons produced by 14.4 MeV neutrons at 0°. The oscil-

cluding effects like target thickness (16 mg/cm² of polythene) and angular definition, is 6.7%.

## 5. Conclusion

The method of charged particle discrimination by $dE/dx$ and $E$ has recently been challenged by the scintillation pulse shape discrimination method[17]). However, in neutron work it is necessary to have some coincidence telescope

[17]) M. Forte, Private Communication; also F. Brooks, Nucl. Instr. and Meth. **4** (1959) 151.

vhich means that one cannot avoid proportional ounters or thin scintillators. Moreover, the cintillation pulse-shape discrimination for pro-ons and deuterons becomes only effective for

counter is fast enough to keep the background small at $10^9$ neutrons/sec in $4\pi$, it is not fast enough to deal with higher fluxes. In future designs, one should look for faster counters

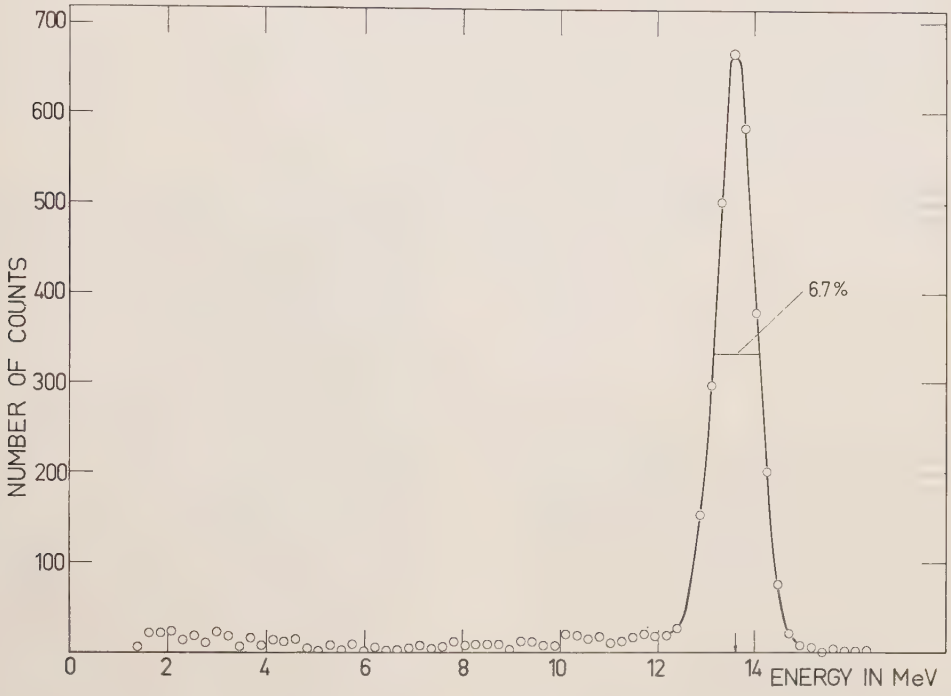


Fig. 8. The energy spectrum of knock-on protons (average energy 13.6 MeV) produced at 0° by 14.4 MeV neutrons.

igher energies and at low energies the separa-ion is incomplete. From this point of view, the $E/dx - E$ system, whose performance is im-roved as far as in our case, retains its merits. Iowever, the system has severe limitations, for hough the background is very low and cross ections of the order of 1 mb/sterad may be neasured without difficulty, the counting rates re very low. Since the solid angle subtended by he counter is already large, the counting rate nay be increased only by increasing the neutron ux. With the present counter, a flux of $2 \times 10^9$ eutrons/sec in $4\pi$ is about the limit. The dead me correction due to random anticoincidence eaches 10% and there is also danger of pile-up the proportional counters with consequent ss of resolution. Therefore, although the such as gas scintillation counters and silicon n–p junction detectors both of which would permit nanosecond resolving times. However, problems such as signal to noise ratios make the adoption of these counters not immediately obvious.

**Acknowledgement**

We would like to thank Ing. H. Babić for building the amplifiers, preamplifiers and the $X$–$Y$ oscilloscope. We are also indebted to Professors Colli and Facchini for helpful discussions and to Professor M. Paić and Dr. K. Ilakovac for constant encouragement, and for providing the facilities making the investigation possible. We would like to thank Mr. J. Tudorić for doing some of the numerical calculations.

NUCLEAR INSTRUMENTS AND METHODS **10** (1961) 66–67; NORTH-HOLLAND PUBLISHING CO.

LETTERS TO THE EDITOR

# A CONVENIENT METHOD OF CONSTRUCTING ACCELERATOR TUBES

K. R. CHAPMAN and S. GOWARIKER

*Physics Department, Birmingham University*

Received 25 September 1960

A method for the construction of constant gradient accelerator tubes is described. The advantages of this method are stated and details given of the performance.

## 1. Introduction

In an earlier paper[1]) a method was described for the construction of short accelerator sections having an overall voltage of approximately 40 kV and it was stated that tests were proceeding to extend this technique with some modifications to produce a complete accelerator tube. Tubes of this type have been constructed and the performance of these tubes can now be given.

## 2. Method of construction

It was decided to produce a tube for use at 200 kV. This voltage being chosen as giving a convenient unit capable of being coupled together to give 400 kV or 600 kV tubes, it was also a tube that we could test conveniently as a 250 kV electrostatic generator with vacuum plant was available which would enable the tube to be tested above its operating conditions.

The internal construction may be seen from fig. 1 which shows a complete core ready for encapsulation. It consists of aluminium electrodes and ceramic rings bonded together to give a stack 10.5 inches long. The bonding is achieved using Araldite, taking care that none is allowed to spread onto the internal surface of the ceramic rings. The electrodes are "dished" to protect the internal surface of the ceramic from bombardment. Grading resistors each of 50 M$\Omega$ are assembled between the rings in such a manner that, when encapsulation is complete, they have several millimetres of the resin covering them in every direction.

The mould in which the encapsulation was completed presented an interesting problem. As the tube had an external length of only 10.5 inches and was intended for use in air it was necessary to have the external surface corrugated

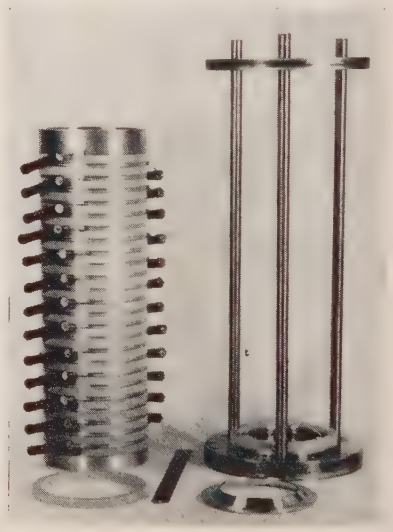

Fig. 1.

to increase the surface path between the two ends. To produce such a mould cheaply necessitated using novel methods, as orthodox turning or milling would have required special cutters and been a long and expensive task.

The problem was solved by having a pattern made that was just the thickness of one corrugation, from this a number of light alloy

[1]) K. R. Chapman and S. Gowariker, Nucl. Instr. and Meth. **7** (1960) 215.

castings having good surface finish were made. These after simple surfacing and polishing were screwed together to produce the required length and the mould then split on a milling machine with a splitting saw.

This produced a very satisfactory mould (fig. 2) which gave a good clean encapsulation free from excessive "flash".

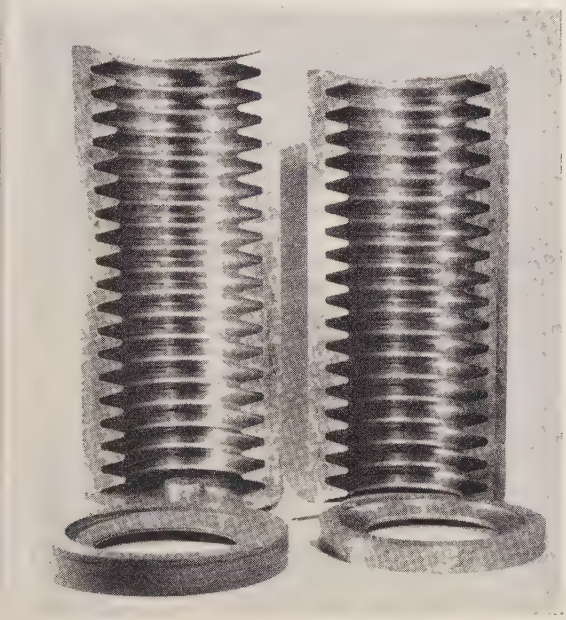

Fig. 2.

much more cheaply than by any glass sealing technique and also has the advantage that, as the resistances are included in the encapsulation, the tube is self grading. Whilst possessing these advantages over a conventional tube for a pressurized application it has for normal use in air the very considerable additional advantage that the whole construction is enclosed in a material little affected by atmospheric conditions and easily cleaned.

Such 200 kV units may be used to build a higher voltage tube by simply screwing an intermediate plate complete with corona spinning between the sections. The vacuum seal being made by "O" rings as are the seals at each end of the tube. If at any time one such unit should need replacement it is simply a matter of unscrewing it and screwing in a replacement. The tubes are constant gradient type and may easily be constructed with sufficient accuracy to ensure that such replacement shall have negligable effect on the beam position at the emergent end.

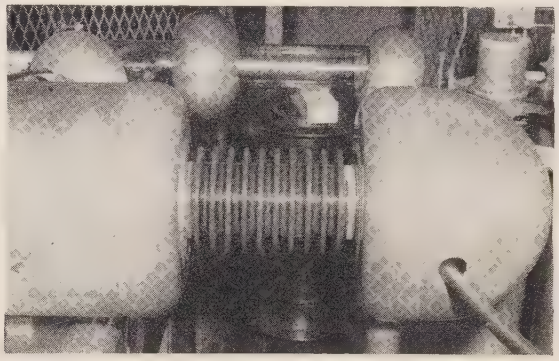

Fig. 3.

## 3. Performance

A tube to this design has been constructed and is shown in fig. 3 under test. It has been tested at 200 kV for considerable periods and has proved completely satisfactory. If the voltage is increased to approximately 230 kV the air insulation between the end spinnings breaks down but the tube itself gives every indication that it could operate at still higher voltages. The breakdown always occurs between spinnings well away from the surface of the tube and there are no indications of tube failure or flash-over along the surface.

## 4. Conclusions

This method of construction enables a constant gradient tube to be constructed very

A tube is being constructed to determine the effect of replacing the ceramic rings by Areldite ones at these voltages.

## Acknowledgements

We should like to thank Professor P. B. Moon for his encouragement in this work and also Dr. J. Walker and his reactor-physics group for considerable practical assistance and the use of their 250 kV generator and test plant.

NUCLEAR INSTRUMENTS AND METHODS **10** (1961) 68-69; NORTH-HOLLAND PUBLISHING CO.

# WIDE BAND DETECTION OF SMALL ION BEAM CURRENTS

A. N. JAMES and C. M. P. JOHNSON†

*Cavendish Laboratory, Cambridge*

Received 20 September 1960

The ion beam of the Cavendish Laboratory's 1.4 MV. Cockcroft-Walton generator has been pulsed using the radiofrequency sweeping method before the main acceleration[1]). The length of the accelerating tube was sufficient for the voltage ripple from the generator to cause large phase

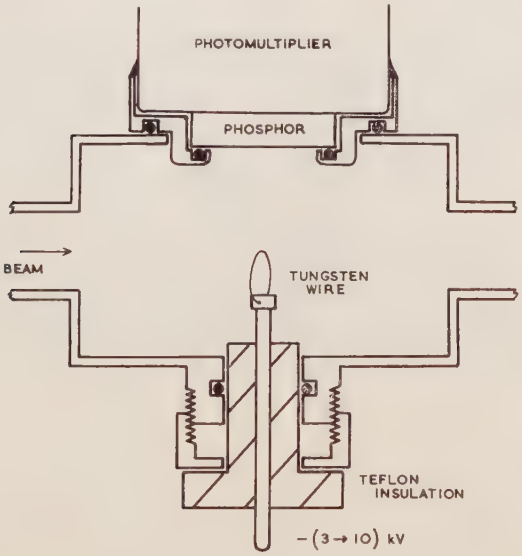


Fig. 1.

variations between the arrival of the beam pulses at the target and the radio frequency sweeping field, which therefore could not be used in timing experiments[1]). Although direct pick up of the target current (time average 0.05 to 2.0 $\mu$ amps) could be used to provide timing signals, the wide band amplification required ($\sim 10^4$) was inconveniently sensitive when obtained with distributed amplifiers. A more versatile system was sought using the wide band amplification of electron multiplying systems.

† Now at the Clarendon Laboratory, Oxford.

Several schemes were tried including multiplying the secondary electrons from the target, and inserting phosphors, optically coupled to photomultipliers, into the beam[2]). The apparatus shown in the figure was the most successful, the idea for this apparatus was based on the design of a counter for single ions built by B. W. Ridley[3]). Secondary electrons formed by a beam striking the wire were accelerated into the plastic phosphor to produce a flash of light, the photomultiplier producing an output current proportional to the number of electrons entering the phosphor.

The fine tungsten wire (chosen to give the smallest background reaction rate with a deuteron beam) intersected the beam where it was widest, near the exit aperture of the final focussing electrostatic lens, ensuring the minimum loss of beam current on the target and an almost linear relation between pulse height and beam current. The plastic phosphor was Nuclear Enterprise N.E. 102 and was coated with an evaporated film of aluminium to exclude light. The photomultiplier could be of any type consistent with the requirements for time spread and mean dynode current; mean output currents of 1 mA (i.e. a gain of $10^3$ or more) were used without damage to the photomultiplier.

By changing the potential of the wire, the same size of output could be obtained for a ten-to-one variation in beam current. Larger changes in the gain of the system could be made by varying the voltage on the photomultiplier or

[1]) S. D. Bloom, C. M. Turner, Rev. Sci. Instr. **29** (1958) 480.

[2]) K. G. Malmfors, J. Kjellman, A. Nilsson, Nucl. Instr. **1** (1957) 186.

[3]) B. W. Ridley, Ph. D. Thesis, University of Cambridge (1957).

by varying the number of multiplying stages used.

The apparatus has been used with an R.C.A. 6655 photomultiplier to give timing signals at the rate of $5 \times 10^6$ per second. Over a period of two years no loss in phosphor efficiency or photomultiplier gain has been observed.

**Acknowledgements**

The authors are grateful to C. W. McCutchen and B. W. Ridley for helpful discussions. One of us (A.N.J.) is indebted to the Department of Scientific and Industrial Research for a maintenance allowance during the course of this work.

# BOOK REVIEWS

*Traveaux Pratiques de Physique Nucléaire et de Radiochimie* M. DUQUESNE, R. GRÉGOIRE, M. LEFORT et R. DEVORET. 324 pages, 321 figures (Masson et Cie, Paris) Prix 39 NF.

L'introduction contient une récapitulation des notions fondamentales de la physique atomique et une exposition semblable sur la structure du noyau.

La première partie concerne la détection et la mesure des rayonnements. Les chambres d'ionisation y sont décrites en détail ainsi que l'appareillage auxiliaire pour l'enregistrement du courant ou des impulsions. Les fluctuations statistiques sont discutées dans un chapitre consécutif. Le fonctionnement du compteur Geiger-Müller et du compteur proportionnel est expliqué sans trop de détails sur le processus d'avalanche. Un chapitre concernant les compteurs à scintillations contient une analyse très claire des bases théoriques du spectre $\gamma$. Cette première partie contient en outre une description d'expérience utilisant les émulsions nucléaires.

La deuxième partie du livre comporte d'abord une discussion des problèmes purement physiques, rattachés à l'investigation de la structure nucléaire: mesures de périodes, mesures de spectres $\beta$ et $\gamma$ et de conversion, mesures de corrélations angulaires et méthode de mesures en coïncidence (les deux derniers points étant principalement discutés à propos d'expériences). Deux chapitres, enfin, l'un sur l'excitation coulombienne, l'autre sur les réactions nucléaires terminent cette discussion des problèmes purement physiques.

Les auteurs abordent ensuite les effets chimiques des rayonnements nucléaires et l'utilisation des radioisotopes pour divers problèmes de chimie.

En appendice sont exposés les effets biologiques ainsi que des questions de protection.

Cet ouvrage est remarquable, tant par la clarté de l'exposition, que par le choix judicieux des exemples numériques et des expériences, et la simplicité suggestive des figures. Le livre s'adresse surtout aux étudiants de physique et de chimie nucléaires des universités, mais il peut aussi bien servir d'introduction pour les ingénieurs qui s'occuperont de l'application industrielle de la radioactivité.

GUNNAR BÄCKSTRÖM

*Physique Nucléaire*, M. BAYET, 404 pages, 169 figures, (Masson et Cie Paris) Prix 65 NF

Ce cours de physique nucléaire est destiné à compléter l'enseignement de la physique classique. La lecture suppose la connaissance de la physique générale et des mathématiques. Les notions de mécanique ondulatoire, spin, statistiques etc. sont exposées dans le livre, qui s'adresse non seulement aux futurs spécialistes en la matière, mais aussi à tous ceux qui désirent étendre leurs connaissances au delà de ce que renferment les ouvrages élémentaires.

La première partie (85 pages) traite quelques compléments de physique théorique. La deuxième partie (113 pages) est consacrée à la constitution de la matière et à la radioactivité. La dernière partie (166 pages) expose l'intéraction des particules élémentaires avec la matière (ionisation, diffusion, Bremsstrahlung, interactions des photons, réactions nucléaires etc.) Les principles de fonctionnement des détecteurs de particules et des circuits électroniques fréquemment utilisés sont présentés d'un point de vue plutôt théorique.

En somme, le livre correspond à peu près à l'ouvrage américain bien connu, "Evans, The Atomic Nucleus", mais il semble plus concis et peut-être plus précis que ce dernier.

GUNNAR BÄCKSTRÖM

S. E. LIVERHANT: *Elementary Introduction to Nuclear Reactor Physics*. John Wiley & Sons, Inc. New York, N.Y., USA, 1960. Price: US $ 9.75.

The rapidly expanding field of nuclear engineering, like so many other fields of technology, is suffering from a severe lack of qualified personnel. The people required are largely engineers with conventional training but with some insight into the special problems of chain-reacting systems. In the last few years more and more colleges and universities have responded to these requirements by offering courses in reactor physics, often on an elementary level and intended primarily for non-physicists. The book "Elementary Introduction to Nuclear Reactor Physics" by S. E. Liverhant is based on the author's experience from teaching such a course. The title of the book is slightly misleading, since only about one third of it deals with the physics of chain-reacting systems. In the first five chapters are reviewed the basic ideas of nuclear physics, with particular emphasis on the concepts that are important in connection with neutron reactions. When written in a simple yet logical way, as is the case here, such a survey of the fundamental principles no doubt greatly facilitates the understanding of reactor physics. Also, in this way the treatment of radioactive decay is given a natural background. The subsequent six chapters are devoted to an elementary and conventional treatment of reactor physics. The last three chapters, finally, deal with radiation, its interaction with matter and radiation protection.

The book is written throughout with commendable clarity. A mathematical treatment is generally accompanied by a descriptive interpretation of the result, and the problems at the end of each chapter further elucidate the text (answers are provided). Although the book is elementary, the reader is constantly kept in touch with technology by means of exemplifying descriptions of actual reactors. The figures and illustrations are of high quality, and, in particular, the student will appreciate the drawings that clarify geometrical problems.

Those who wish to penetrate the subject further will find the extensive bibliographies very helpful. Finally, the excellent lay-out of the book deserves mentioning.

EVELYN SOKOLOWSKI

Zucker, E. C. Halbert and F. T. Howard (Editors), *ceedings of the Second Conference on Reactions between Complex clei, held in Gatlinburg, Tennessee, May 2–4, 1960.* John ley & Sons, Inc., New York N.Y.

This book contains all forty papers presented at the Second nference on Reactions between Complex Nuclei in Gatlin- g, Tenn., May 1960, by scientists from the United States, nada, Great Britain, and Switzerland. One Soviet paper was d by title at the conference and is included in full in the book. luded also is the discussion which followed each paper and summary of the whole conference given by E. P. Wigner. The book is divided into five sections, each corresponding to session at the conference, namely Transfer reactions, ulomb excitation, Scattering, Transuranium and fission, and mpound nuclear reactions.

Naturally, the experimental papers are in majority and deal stly with particular experimental set ups. Since the heavy- technique is a very rapidly growing field with applications widely separated branches of nuclear physics, it will certainly of great value to the workers in the field to have all these scriptions collected in a single volume. In this connection, wever, some readers will probably miss papers of more general aracter with wider aspects on the various experimental oblems.

The theoretical papers, on the other hand, are more re- ewing, particularly those by G. Breit on Nucleon transfer eory and by K. Alder and A. Winter on The theory of multiple ulomb excitation. These articles together with the excellent mmary by Wigner can be recommended also to those who are t directly in the field but want to get some insight into its rious applications.

INGVAR LINDGREN

*roceedings of the International Conference on Nuclear Structure ingston, Canada, Aug. 29–Sept. 3, 1960,* University of Toronto ess, Toronto and North-Holland Publishing Company, msterdam, 1960, 990 pages.

This report is divided into ten sections, each corresponding one session at the conference. Each section contains several view articles of outstanding physicists together with a small mber of research contributions. Included are also the dis- ssions which followed each paper.

Of the survey papers the following may be mentioned more examples than as a representative selection. R. E. Peierls scusses some open problems in nuclear structure, which will obably not be solved within the next few years, such as the igin of nuclear forces and the possibility of many-body forces. ther unsolved questions, e.g. those connected with the nuclear rface, are taken up by D. H. Wilkinson. The new treatment of e nuclear models, which orginates from the works of K. A. ueckner, is reviewed by Brueckner, de Shalit and C. Bloch in chapter called Physical foundations of nuclear models. In a apter on gross properties of nuclear matter G. E. Brown gives review of the optical model and its astonishing success in plaining scattering data, and the physical interpretation of is model is discussed by D. S. Saxon. The rapidly expanding field of heavy-ion physics (which was recently given its own conference in Gatlinburg, Tennessee) is briefly reviewed by A. Zucker and the mechanism for reactions with light nuclei by D. A. Bromley. Two chapters are devoted to the properties of individual levels, a field where a tremendous amount of experimental and theoretical data has now been collected. Here most interest seems nowadays to be given to regions of deformed nuclei, which is reflected by the fact that very few shell-model calculations were submitted to the conference. The new trend to describe collective effects in terms of independant-particle motions is reviewed in an interesting article by B. R. Mottelson. Systematics of nuclei in various regions are also given in these chapters. The last chapters are devoted to neutron resonances and fission phenomena.

Finally, there is a summary of the whole conference by V. F. Weisskopf, where he points out the surprisingly great success of the various nuclear models in explaining experimental data but also our failure to get much deeper insight into such basic problems as the nature of nuclear forces.

The arrangement and balance of the different chapters are in general good. Particularly valuable for the average reader is the fact that only a few representative research contributions from each field are included in full, while the rest is summarized into 60-word abstracts so that more room could be given to survey articles. He will also acknowledge the inclusion of the discussions, which will help to clarify many obscure points.

The editors are to be complemented for the very rapid publication of this volume.

INGVAR LINDGREN

G. P. Barnard, G. H. Aston and A. R. S. Marsh: *Effects of Variation in the Ambient Air on the Catibration and Use of Ionization Dosemeters* (Her Majesty's Stationary Office, 1960. 31 pages, 2 s 6 d.)

The roentgen has been defined in terms of the air-ionization produced by the high-speed electrons released by the ionizing radiation per 0.001293 g of dry air. It has been difficult to use this definition since ambient air is never dry. When correcting to the reference state one has previously tried to apply corrections for humidity e.g. on a gravimetric basis. Also one has taken account of the different electron densities of dry air and water vapour and calculated the dividing factor solely on the basis of electron density.

The authors have pointed out, that one has to take account of relative total energy losses for electron-electron collisions in dry air and water vapour. The final correction for pressure, temperature and humidity can be performed by calculating the difference between two terms, the first written as a function of pressure and temperature and the second as a function of humidity and temperature. The values for the temperature range 10 to 40° C and for the pressure range 600 to 845 mm Hg are given in one table. In another table the correction term for temperature and humidity is given. The factors are given to four figures. The photon absorption is also discussed and tabulated for different energies.

INGRID OLSSON

# NEWS ITEM

## IMEKO CONFERENCE

JUNE 26 — JULY 1, 1961

BUDAPEST

---

**Scientific Program (preliminary communication)**

1.1 PLENARY SESSIONS: papers of general character in the field of measurement and instrument technology; papers of special importance concerning fundamental questions; integrating papers.

1.2. SECTION-MEETINGS:

21. *Sections on general subjects.*

211. Theory and practice of instrument design.

212. Technology and organization in instrument manufacture.

213. Electronic measuring instruments for general application.

214. Border-questions related to measurement and automation (to be prepared jointly with the Technical Committee on "Components" of IFAC).

22. *Specialized Sections:*

221. Instruments and methods for measuring geometrical and mechanical quantities, including geodetic measurements.

222. Instruments and methods for measuring time and frequency.

223. Instruments and methods for measuring thermal quantities.

224. Instruments and methods for measuring physicochemical measurements (such as photometry, spectroscopy, colorimetry, electrochemical measurements, gas-analysis, etc.).

225. Instruments and methods for measuring electrical and magnetic quantities.

226. Instruments and methods for measuring radioactive radiation.

Detailed information and invitation may be obtained from the IMEKO Secretariat (Budapest, 5. P.O.B. 3.).